

6752

NATIONAL LIBRARY
OTTAWA



BIBLIOTHÈQUE NATIONALE
OTTAWA

NAME OF AUTHOR.....KENNETH REED.....

TITLE OF THESIS.....ORIENTATION DEPENDENCE
OF THE ²³Na QUADRUPOLE
RELAXATION IN NaNO₃.....

UNIVERSITY.....ALBERTA.....

DEGREE FOR WHICH THESIS WAS PRESENTED.....Ph.D.....

YEAR THIS DEGREE GRANTED.....1970.....

Permission is hereby granted to THE NATIONAL LIBRARY
OF CANADA to microfilm this thesis and to lend or sell copies
of the film.

The author reserves other publication rights, and
neither the thesis nor extensive extracts from it may be
printed or otherwise reproduced without the author's
written permission.

(Signed).....*Kenneth Reed*.....

PERMANENT ADDRESS:
#5 10743 - 85 AVE
AUGUST LAVERGNE
EDMONTON

DATED.....AUGUST 21st.....1970.....

THE UNIVERSITY OF ALBERTA

ORIENTATION DEPENDENCE OF THE ^{23}Na
QUADRUPOLE RELAXATION IN NaNO_3

by

© KENNETH REED

A THESIS

SUBMITTED TO THE FACULTY OF GRADUATE STUDIES
IN PARTIAL FULFILMENT OF THE REQUIREMENTS FOR THE DEGREE
OF DOCTOR OF PHILOSOPHY

DEPARTMENT OF PHYSICS

EDMONTON, ALBERTA

FALL, 1970

UNIVERSITY OF ALBERTA

FACULTY OF GRADUATE STUDIES

The undersigned certify that they have read, and recommend to the Faculty of Graduate Studies for acceptance, a thesis entitled ORIENTATION DEPENDENCE OF THE ^{23}Na QUADRUPOLE RELAXATION IN NaNO_3 , submitted by Kenneth Reed, in partial fulfilment of the requirements for the degree of Doctor of Philosophy.

DC Hughes
Supervisor

Frank
Abbott

W. J. Donald
R. E. Melnyk

Myer Bloom
External Examiner

Date May 22nd 1970

ACKNOWLEDGEMENTS

I wish to express my sincere gratitude to Dr. D.G. Hughes, my research supervisor, for suggesting this project and for his continual help, interest and encouragement throughout the whole project.

I also wish to thank Dr. R.E. Snyder for assistance with computing and for many helpful discussions during this latter part of the work.

The cooperative attitude of members of the technical staff, in particular Mr. D. Gerritsen and Mr. A. O'Shea, is gratefully acknowledged.

Also, I wish to thank my wife, Carol, for her patience and encouragement during the course of this research.

It is a pleasure to acknowledge the National Research Council's financial support of this work in particular the award of a Graduate Scholarship. I wish to thank the University of Alberta for the award of a Dissertation Fellowship.

Finally, I would like to thank Mrs. Marilyn Wahl for her work in typing this thesis.

Abstract

This thesis describes an investigation of the orientation dependence of the ^{23}Na quadrupole relaxation in a single crystal of NaNO_3 at room temperature. Nuclear quadrupole relaxation occurs via transitions where the magnetic quantum number m changes by ± 1 or ± 2 , the respective probabilities of these allowed transitions being W_1 and W_2 . The ratio W_2/W_1 was measured as a function of the crystal orientation with respect to the external magnetic field using a steady-state nuclear magnetic resonance technique.

The technique is an extension of the double-resonance method devised by Pound where the intensity changes of one of the quadrupole-split ^{23}Na resonance components caused by severe simultaneous saturation of another component is measured. By measuring the intensity changes as a function of the spectrometer observing power, the effect of the observing power was corrected for using a linear extrapolation. In order to make accurate measurements for a range of crystal orientations, a sensitive flux-balance system was developed. This enabled the coupling between the spectrometer and the saturating signals to be eliminated. The final resonances obtained with the equipment were such that their intensities

could be measured with an accuracy of 0.2% giving the value of W_2/W_1 accurate to 2.0%.

The quadrupole relaxation is characterized by a fourth rank tensor, the so-called M-tensor. Theoretical expressions for the orientation dependence of W_2/W_1 for triad symmetry have been developed in terms of the M-tensor components by Pietila. Our experimental values of W_2/W_1 were fitted by a least squares technique to this equation resulting in a very good fit when the M-components in the equations for W_2 and W_1 were considered equal. This implies that the predominant relaxation mechanism is an indirect process. The results obtained were $M_{1313}/M_{1111} = 0.850 \pm 0.015$, $M_{3333}/M_{1111} = 0.822 \pm 0.016$, $M_{1113}/M_{1111} = -0.115 \pm 0.018$ and $M_{1123}/M_{1111} = 0.147 \pm 0.017$ where the z axis is along the triad axis and the x axis is along the projection of a rhombohedral unit cell edge on a plane perpendicular to the triad axis. Using symmetry arguments it is shown that M_{1123} should equal zero in NaNO_3 . This is in marked contrast with our experimental value, indicating that at room temperature the crystal structures of NaNO_3 is not as presently accepted.

Previous measurements of the W_2/W_1 orientation dependence of ^{23}Na in monocrystalline NaNO_3 at 77°K by

Niemela using pulse techniques are reanalyzed. It is shown that agreement between experiment and theory is satisfactory and that the relaxation mechanism at 77°K is again via an indirect mechanism.

In an attempt to interpret the experimental values of the M-tensor components, a calculation using a point charge model is presented. The calculated values of the ratios of the M-components are in surprisingly good agreement with experiment.

TABLE OF CONTENTS

	Page
SECTION I, Introduction	1
SECTION II, Theory	7
SECTION III, Apparatus and Experimentation	53
SECTION IV, Results and Discussion	124
References	216

SECTION I Introduction

Nuclear spin-lattice relaxation in solids occurs through the coupling of the magnetic dipole moment and the electric quadrupole moment with the lattice. For nuclei having a nuclear spin number $I = 1/2$, the quadrupole interactions are absent, but for $I > 1/2$, both of these interactions contribute to the relaxation. In the magnetic case, the magnetic dipole is coupled to the fluctuating magnetic field at the nuclear site. In the electric quadrupole case, the electric quadrupole moment couples with the fluctuating electric field gradient at the nuclear site.

The allowed nuclear spin transitions in the magnetic case are governed by the selection rule $\Delta m = \pm 1$ (Bloembergen, Purcell and Pound, 1948). In the quadrupole case on the other hand, transitions corresponding to $\Delta m = \pm 1$ and $\Delta m = \pm 2$ can occur (Pound, 1950).

If the nucleus is situated in a crystal at a site possessing less than cubic symmetry, the time-average electric field gradient will be non-zero. This interacts with the electric quadrupole moment (for $I > 1/2$) to modify the nuclear magnetic energy levels. In sodium salts the static quadrupole interactions of the ^{23}Na nuclei, for which $I = 3/2$, are usually

much smaller than the Zeeman interaction of the nuclear magnetic moment with magnetic fields $\sim 10^4$ G generally available in the laboratory. This situation is usually referred to as the 'high-field' case and we shall be concerned with this case throughout this thesis. Since the static quadrupole interactions depend on the m value of the Zeeman levels, the $2I+1$ levels become unequally spaced. For nuclei located in identical sites in a single crystal, the resonance spectrum will therefore consist of $2I$ components.

Spin-lattice relaxation via quadrupole interactions was first investigated by Pound (1950) who studied the ^{23}Na spin system in a pure single crystal of NaNO_3 at room temperature. Pound showed theoretically that by severely saturating one component of the three-line resonance spectrum the intensity of other components would be significantly changed if the relaxation mechanism is quadrupolar. On the other hand, severely saturating one component would produce no effect on the intensity of the other components if the relaxation mechanism is magnetic. By assuming that the quadrupole transition probabilities corresponding to $\Delta m = \pm 1$ and $\Delta m = \pm 2$ were equal, Pound showed that severe saturation of the central component of the spectrum (the so-called centre line) should cause an enhancement of the other components, the so-called satellites,

by a factor of $3/2$. Similarly, Pound showed that severe saturation of a satellite should depress the other satellite by a factor of $2/3$ and enhance the centre line by a factor of $5/3$.

To check this, Pound performed a double resonance experiment in which one component of the spectrum was severely saturated and the intensities of the other components were measured using a marginal oscillator spectrometer (Pound and Knight, 1950, Watkins and Pound, 1951). Although the signal-to-noise ratios were poor, approximate agreement with the expected intensity changes was obtained. The indication therefore was that the dominant relaxation mechanism was quadrupolar. This was later confirmed by Andrew and Swanson (1957), by observing the saturation behaviour of the centre line and satellites.

Abragam (1961) generalized the Pound theory taking into account the fact that the transition probabilities corresponding to $\Delta m = \pm 1$ and $\Delta m = \pm 2$ are not necessarily equal. Abragam pointed out that Pound's data implies that W_2/W_1 is approximately 1.5 rather than unity, where W_1 and W_2 are the respective probabilities of the transitions $\Delta m = \pm 1$ and ± 2 (Yosida and Moriya, 1956).

In addition to assuming that W_1 and W_2 were equal,

Pound assumed that the effect of the spectrometer (observing) power was negligible. By taking into account the spectrometer power and lifting the restriction that $W_1=W_2$, Hughes (1966) derived expressions for the double resonance behaviour of an $I = 3/2$ spin system. In particular, Hughes showed that the enhancement of a component should be linearly dependent on the spectrometer observing power when the observing power is small. It should therefore be possible to correct for the effect of the spectrometer observing power in the Pound experiment by measuring the enhancement as a function of the spectrometer observing power and using a linear extrapolation procedure.

The first experimental measurement of W_2/W_1 in the high-field case was made by Goldberg (1959) for the ^{23}Na spin system in monocrystalline NaNO_3 at 77°K . Whereas Pound measured the enhancement using a steady-state technique, Goldberg employed a pulse method. The crystal was orientated such that its triad symmetry axis was directed along the externally applied magnetic field and W_2/W_1 was found to be 0.90 ± 0.05 .

The aim of the work discussed in this thesis is to investigate experimentally the orientation dependence of W_2/W_1 in a solid. The investigation was carried out on the ^{23}Na spin system in NaNO_3 at room temperature.

A steady state method was chosen in preference to a pulse method (Hahn, 1949) because of the danger of interference with other components of the spectrum when the 90° pulse is applied to a given component. The quadrupole splitting is a function of the crystal orientation with respect to the external magnetic field and at certain orientations the resonance separation is so small that pulse methods can no longer be used.

The double resonance method cannot be used for a quadrupole study of ^{23}Na in NaNO_3 if the radio-frequency fields interfere with each other. We describe the design and construction of a sensitive flux-balance system that enabled the coupling between the radio-frequency fields to be reduced to very small values. If this had not been done, the measurements that we describe could not have been carried out.

During the course of the work described in this thesis, the results of the orientation dependence of W_2/W_1 for ^{23}Na in NaNO_3 at 77°K were given by Niemela (1967) and compared to the theoretical dependence given by Pietila (1968). This work is criticized in detail in Section IV.

It was necessary for us to extend the theory in order to analyze our data and this is done in Section II. The equipment and experimental procedure is given in Section III.

Some auxiliary data concerned with the equipment is also given in Section III. The main body of the experimental data is presented and discussed in Section IV.

SECTION II Theory

a) Introduction

The application of a steady magnetic field H_0 to a system of nuclei with nuclear spin number I and magnetic dipole moment μ gives rise to $2I+1$ nondegenerate Zeeman energy levels. These energy levels are given by

$$E_m = \frac{-m\mu H_0}{I} \quad (\text{II } 1)$$

where m is the magnetic quantum number. In a state of thermal equilibrium, the ratio of the populations of adjacent levels is given by the Boltzmann factor $\exp\left|\frac{\Delta E}{kT}\right|$ where ΔE is the energy separation of adjacent levels, k is the Boltzmann constant and T is the temperature of the spin system. For a spin system at room temperature in an applied field of a few thousand gauss, the Boltzmann factor is of the order of 10^{-6} . So to an excellent approximation the Boltzmann factor can be written as $1 + \frac{\Delta E}{kT}$. It follows that if N is the total number of spins then the population of the m th energy level is given by

$$N_m = \frac{N}{(2I+1)} \left[1 + \frac{m\mu H_0}{IkT} \right]. \quad (\text{II } 2)$$

NMR occurs when photons of frequency ν given by the expression E/h interact with the spin system. A quantum of energy will excite transitions between the energy levels if it has the same value as the level spacings.

Let us consider an alternative picture. The application of a steady magnetic field will result in a precessional motion of the spin about the direction of the applied magnetic field. Such a motion will be characterized by the Larmor frequency of precession that is given by the equation

$$\omega_0 = \gamma_n H_0 \quad (\text{II } 3)$$

where γ_n is the nuclear gyromagnetic ratio for the particular species. Let us suppose that a circularly polarized field is applied such that its plane is perpendicular to the steady magnetic field H_0 . The frequency of the polarized field can be adjusted until the rotation rate of the radial vector representing the field is equal to the precessional rate of the spin about the field H_0 and in the correct sense. In this case there will be a sustained interaction between the spin and the circularly polarized field resulting in the re-orientation of the spin into another energy state. Such an interaction is the basis of the Nuclear Magnetic Resonance phenomenon and this description is equivalent to the energy

level picture given in the preceding paragraph.

The magnetic transitions resulting from absorption of energy by the spin system and resulting in the redistribution of the spin population is governed by the selection rule $\Delta m = \pm 1$. The probability for such a transition takes the form (Bloembergen, Purcell and Pound, 1948 henceforth referred to as BPP, 1948)

$$P_{m \rightarrow m-1} = P_{m-1 \rightarrow m} = \left(\frac{1}{4}\right) \gamma_n^2 H_1^2 g(\nu) [I+m] [I-m+1] \quad (\text{II } 4)$$

where $g(\nu)$ is the normalized lineshape function and H_1 is the magnitude of the circularly-polarized applied field. The net absorption of energy by the spin system occurs because of the slight excess of population in the lower energy levels and the intensity of the nuclear absorption is directly proportional to the population difference between the two levels between which the spin transition takes place.

For an isolated nuclear spin system, devoid of interactions with another system, the continued presence of the appropriate radiation would in time lead to equal population of the Zeeman levels and there would be no further net energy absorption by the spin system. In such a state, the characteristic spin temperature will be infinite and the spin system is described as being completely saturated.

In practice the spin system is not isolated but in fact interacts with the lattice. Such an interaction, the so-called spin-lattice interaction, has a finite probability of inducing transitions. However, in this case the probability of downward transitions exceeds that of upward transitions (Andrew, 1955). Clearly such spin-lattice interactions will form the basis of the relaxation mechanisms for the particular nuclear spin system.

To illustrate this let us consider the simple case of a spin system with $I = 1/2$. Using equation (II 4) we write the transition probability as

$$\frac{P_{\frac{1}{2} \rightarrow -\frac{1}{2}}}{2} = \frac{P_{-\frac{1}{2} \rightarrow \frac{1}{2}}}{2} = P_0 = \frac{(1)}{4} \gamma^2 H_1^2 g(\nu). \quad (\text{II } 5)$$

Defining the upward transition probability arising from the spin-lattice interaction as W we can write the downward transition probability as $W(1+\Delta)$ (Andrew, 1955) where $\Delta = h\nu/kT$, $h\nu$ being the energy separation between the two levels. By probability arguments we can then write rate equations for the populations of the two levels as

$$\dot{N}_{\frac{1}{2}} = N_{\frac{1}{2}} W(1+\Delta) + N_{-\frac{1}{2}} P_0 - N_{\frac{1}{2}} W - N_{-\frac{1}{2}} P_0 \quad (\text{II } 6)$$

and

$$\dot{N}_{-\frac{1}{2}} = N_{\frac{1}{2}} W + N_{\frac{1}{2}} P_0 - N_{-\frac{1}{2}} W(1+\Delta) - N_{-\frac{1}{2}} P_0 \quad (\text{II } 7)$$

where the N's are the populations of the particular levels.

Since $\Delta \ll 1$ and $N_{\frac{1}{2}} - N_{-\frac{1}{2}} = N_0 \ll N$, it follows that

$$\dot{N}_{\frac{1}{2}} = -WN_0 + N_{-\frac{1}{2}} W\Delta - N_0 P_0 \quad (\text{II } 8)$$

and

$$\dot{N}_{-\frac{1}{2}} = WN_0 - N_{-\frac{1}{2}} W\Delta + N_0 P_0. \quad (\text{II } 9)$$

Hence, it follows that

$$\dot{N}_0 = -2WN_0 - 2N_{-\frac{1}{2}} W\Delta - 2N_0 P_0 \quad (\text{II } 10)$$

Now using equation (II 2), $N_{\frac{1}{2}}\Delta$ is the equilibrium value of N_0 which we denote as n_0 and $-\frac{1}{2}$ therefore

$$\dot{N}_0 = 2W(n_0 - N_0) - 2N_0 P_0. \quad (\text{II } 11)$$

For $P_0=0$ the solution for this type of equation is of the form $N_0 = n_0 [1 - C \exp(-2Wt)]$ where C is a constant that is determined

by the initial conditions. The time constant for the exponential return to equilibrium is $(2W)^{-1}$ which is defined as the spin-lattice relaxation time T_1 .

In the presence of a radiation field, it follows from equation (II 4) that the steady-state solution of equation (II 11) is

$$N_0 = \frac{n_0}{1 + \frac{1}{2} \gamma_n^2 H_1^2 T_1 g(\nu)} \quad (\text{II } 12)$$

If the applied radiation field is sufficiently large such that $\gamma_n^2 H_1^2 T_1 g(\nu) \gg 1$ then the spin system is said to be severely saturated. This derivation of equation (II 12) was first given by BPP (1948). However, for NMR, in solids equation (II 12) is only valid for small values of H_1 except at the centre of the resonance where it is true for large H_1 . This was demonstrated by Goldburg (1961) for ^{23}Na in NaCl.

For the case $I = 1/2$, spin-lattice relaxation is due to the magnetic dipole moment of the nucleus interacting with the time-dependent magnetic field produced at the nuclear site. However, measurements by BPP (1948) indicated another type of relaxation process. In water doped with deuterium, T_1 for a proton is approximately 3 seconds whereas T_1 for a deuteron

is approximately 0.5 seconds. Since the magnetic dipole for the deuteron is much less than that of the proton, it is clear that another relaxation mechanism is involved. The deuteron has an electric quadrupole moment and it was proposed by BPP (1948) that it was this interacting with the time-dependent electric field gradient that caused the short T_1 . In the case of heavier nuclei which have large quadrupole moments, broad linewidths have been found that indicate relaxation times as short as 10^{-5} seconds in liquids.

In the case of liquids, the quadrupole interaction, although broadening the resonance line, does not result in any additional structure of the line. Such structural changes would arise from the interaction of the quadrupole moment with the time-average electric field gradient in the crystal. However, in the liquid the local configuration time is sufficiently short that such an interaction is averaged out. In the case of a solid, however, the local configuration does not fluctuate so rapidly, and a non-zero time-average electric field gradient may exist at the nuclear site. Thus, the interaction of the electric quadrupole moment with this field gradient may result in fine structure of the resonance (Pound, 1950). In passing, we mention that the time-averaged electric field gradient at the nuclear site is zero if the

nucleus is in a site possessing cubic symmetry. On the other hand electric quadrupole relaxation may still occur.

Let us now consider in detail the quadrupole interaction in a solid and the subsequent effect that such an interaction will have on the Zeeman energy levels arising from the application of the steady field H_0 to the system. Consider a nucleus with atomic number Z whose total electric charge is distributed over the nuclear volume with a density $\rho(\vec{r})$. Let $V(\vec{r})$ be the electric potential arising from all the other charges in the environment excluding that of the nuclei under consideration. The electrostatic interaction H is given, over the nuclear volume, by

$$H = \int \rho(\vec{r}) V(r) dV. \quad (\text{II } 13)$$

The term $V(\vec{r})$ can be expanded over the nuclear volume about the nuclear centre of mass by a Taylor series giving

$$H = \int d^3x \rho(\vec{x}) \left[V_0 + \sum_j \left[\frac{\partial V}{\partial x_j} \right] x_j + \frac{1}{2} \sum_{jk} \left[\frac{\partial^2 V}{\partial x_j \partial x_k} \right] x_j x_k + \dots \right] \quad (\text{II } 14)$$

where the components of \vec{x} in the Cartesian representation are $x_1=x$, $x_2=y$ and $x_3=z$ with the summation over each of the subscripts extending over 1, 2 and 3. Thus one obtains the ex-

pression

$$H = ZeV_0 + \sum_j P_j \left[\frac{\partial V}{\partial x_j} \right]_0 + \frac{1}{2} \sum_{jk} Q'_{jk} \left[\frac{\partial^2 V}{\partial x_j \partial x_k} \right]_0 + \dots \quad (\text{II } 15)$$

where

$$P_j = \int d^3x \rho(\vec{x}) x_j \text{ is the nuclear electric dipole moment and} \quad (\text{II } 16)$$

$$Q'_{jk} = \int d^3x \rho(\vec{x}) x_j x_k \text{ is the nuclear electric quadrupole moment.} \quad (\text{II } 17)$$

The first term in equation (II 15) represents the electrostatic energy of the point charge nucleus and since it is independent of the nuclear shape or orientation it is of no interest in this work. The electric dipole interaction term vanishes by virtue of a parity argument. The basis of the argument is that the ground state wave function ψ_{1m} has a definite parity such that $\psi_{1m} \psi_{1m}'$ is unchanged if all nuclear coordinate signs are reversed. Thus, it follows that $\rho_{mm}(-\vec{r}) = \rho_{mm}(\vec{r})$, but since the term x_j in equation (II 16) has different signs in the different octants then the term P_j vanishes. This argument also holds true for the case of the electric octupole term so that in fact the next non-zero term in the expansion is the electric hexadecapole term. One can therefore write

the interaction Hamiltonian in the form

$$H = \frac{1}{2} \sum_{jk} Q_{jk} V_{jk} + \text{hexadecapole terms} + \dots \quad (\text{II } 18)$$

where

$$V_{jk} \equiv \left[\frac{\partial^2 V}{\partial x_j \partial x_k} \right].$$

Looking at the approximate orders of magnitude of the interaction terms in equation (II 15), the electrostatic energy Ze^2/r_e is $\sim 10^5 \text{ cm}^{-1}$ having taken r_e to be typically one Angstrom. The quadrupole term is $\sim e r_n^2 (e/r_e^3) = e V_0 (r_n/r_e)^2$ where r_n , the nuclear radius is $\sim 10^{-12}$ cms. It follows that the quadrupole interaction $\sim 10^{-8}$ of the monopole interaction. The hexadecapole interaction is some 10^{-8} of the quadrupole interaction ruling it out for all intents and purposes.

We shall henceforth be concerned with the so-called "high field" case where the quadrupole interactions are small compared to the Zeeman interaction. The effect of the quadrupole interactions can therefore be treated by perturbation theory. A first-order perturbation treatment was carried out by Pound (1950) and results in the nuclear energy levels being given by the equation

$$E_m = \frac{-m\mu H_0}{I} + \frac{eQ}{4I(2I-1)} \left[3m^2 - I(I+1) \right] \overline{V}_{zz}. \quad (\text{II } 19)$$

where eQ is the nuclear electric quadrupole moment and \overline{V}_{zz} is the time-average zz component of the field gradient at the nuclear site and z is the direction of the applied magnetic field. In the absence of quadrupole interactions, the Zeeman splitting produces $2I+1$ equally-spaced energy levels. As can be seen from equation (II 19), quadrupole perturbation results in a degree of perturbation that depends on the magnetic quantum number m of the nuclear level with the result that the energy levels are no longer equally spaced. If the environment has axial symmetry then the field gradient term is given by (Pound 1950)

$$\overline{V}_{zz} = \left[\frac{1}{2} \right] eq \left[3 \cos^2 \theta - 1 \right] \quad (\text{II } 20)$$

where θ is the angle between the symmetry axis of the crystal and the external field H_0 . Also, eq is a scalar descriptive of the electric environment defined as

$$eq = \int \sigma [3 \cos^2 \phi - 1] r^{-3} dV \quad (\text{II } 21)$$

where the integral is taken over all the charges outside of the nucleus, r is the vector joining the nucleus to the

volume element dV , σ is the charge density and ϕ is the angle between r and the symmetry axis. From equation (II 19) it follows that the component lines have frequencies

$$\nu_{m \rightarrow m-1} = \nu_0 + \frac{3e^2 Qq}{8I(2I-1)h} (2m-1) (3\cos^2\theta - 1) \quad (\text{II } 22)$$

where ν_0 is the unperturbed Zeeman frequency.

For a single crystal of NaNO_3 , all the ^{23}Na nuclei are in environments possessing axial symmetry and identical $\overline{V_{zz}}$. Since $I=3/2$ for the ^{23}Na nucleus, and since the symmetry of the crystal is lower than cubic, the ^{23}Na nuclear magnetic resonance will consist of three lines. These are the so-called centre line arising from the transition $m=\frac{1}{2} \rightarrow -\frac{1}{2}$ and the satellites corresponding to the transitions $m=\frac{3}{2} \rightarrow \frac{1}{2}$ and $m=-\frac{3}{2} \rightarrow -\frac{1}{2}$. The first-order perturbation treatment of Pound has been extended to higher orders by Bersohn (1952). The frequency ν_c of the centre line and the frequencies ν_{\pm} of the satellites are given by

$$\frac{\nu_{\pm}}{\nu_0} = 1 \pm \frac{\rho}{4} (3\cos^2\theta - 1) + \frac{3\rho^2}{32} \sin^2 2\theta \pm \frac{\rho^3}{512} \sin^2\theta (3\cos^2\theta - 1) \times$$

$$(3 - 5\cos^2\theta) + O(\rho^4)$$

$$\frac{\nu_c}{\nu_0} = 1 - \frac{3\rho^2}{64} (9\cos^2\theta - 1) \sin^2\theta + O(\rho^4) \quad (\text{II } 23)$$

where ρ is the dimensionless parameter $e^2 Qq/h\nu_0$. The first-order term in ρ give the equations as expressed by Pound (1950). To this approximation, quadrupole interactions affect only the satellite frequencies, with each satellite being affected the same degree. Second-order and higher even-order perturbation terms affect the centre line and also the satellites shifting the satellites with respect to the frequency ν_0 whilst maintaining a constant satellite separation. For ^{23}Na in NaNO_3 , the third-order term is of the order of 10Hz and for most purposes can be ignored.

The frequency separation of the satellite components as a function of the orientation of the symmetry axis of the crystal with respect to the direction of the applied field H_0 , is to first order given by

$$\frac{\nu_+ - \nu_-}{\nu_0} = \frac{1}{2} \left[\frac{e^2 Qq}{h\nu_0} \right] \left[3\cos^2 \theta - 1 \right] \quad (\text{II } 24)$$

where the quantity $e^2 Qq/h$ is usually referred to as the quadrupole coupling constant.

b) Population dynamics for a spin system with $I=3/2$

We consider a system of nuclear spins with $I=3/2$

situated in a single crystal on sites which have identical and non-zero $\overline{V_{zz}}$. The resonance spectrum therefore consists of three lines. Furthermore, we shall suppose that the relaxation of the spin system is due to homogeneous quadrupole interaction. The allowed spin transitions are governed by the selection rules $\Delta m = \pm 1$ and $\Delta m = \pm 2$.

We shall suppose further that the spin system is subject to a double resonance experiment of the type carried out by Pound (1950) in which one resonance is severely saturated whilst another is simultaneously observed using a much weaker signal. In his experiments Pound investigated the ^{23}Na spin system in NaNO_3 at room temperature and showed that the relaxation mechanism was predominantly quadrupolar. This was later confirmed by Andrew and Swanson (1960) who studied the saturation behaviour of various components of the spectrum. By assuming the probability of the two possible quadrupole transitions were equal, and that the observing power of the spectrometer measuring the component undergoing the intensity variation was having no effect on the spin system, Pound showed that the intensity of the satellite should be enhanced by a factor of $3/2$ when the centre line transition is severely saturated. Similarly, Pound showed that when a satellite is severely saturated the centre line should be en-

hanced by 5/3 and the other satellite depressed by a factor of 3/2. Experimentally, Pound obtained enhancement values in rough agreement with these values.

We now generalize the Pound theory to take into account other considerations which are necessary to carry out accurate double resonance experiments. The quadrupole induced spin-lattice transitions probabilities are given by (Yosida and Moriya, 1956)

$$W_{m \rightarrow m-1} = \frac{W_1 (2m-1)^2 (I-m+1) (I+m)}{2I (2I-1)^2} \quad (\text{II } 25)$$

and

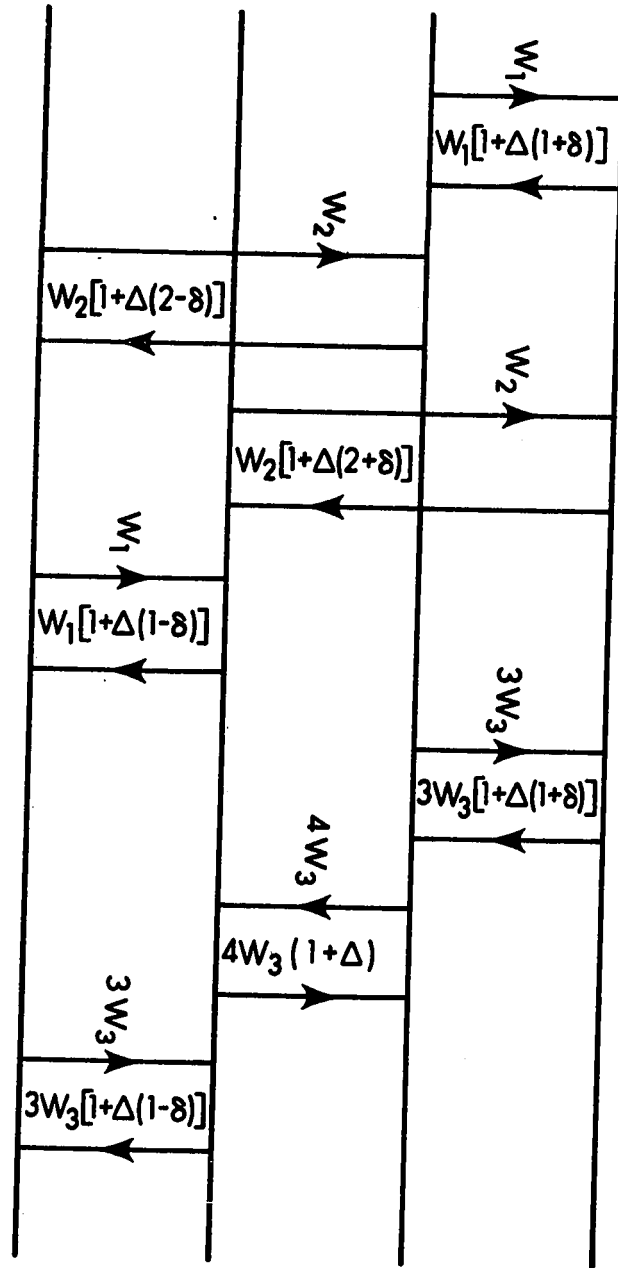
$$W_{m \rightarrow m-2} = \frac{W_2 (I+m) (I+m-1) (I-m+1) (I-m+2)}{2I (2I-1)^2} \quad (\text{II } 26)$$

The downward quadrupole transition probability by the same selection rules are given by the above equations multiplied by the appropriate Boltzman factor.

From examination of the unit cell of NaNO_3 , it is apparent that for relaxation purposes there are in general two different Na sites though they both have the same $\overline{V_{zz}}$ and therefore the same quadrupole splitting. The quadrupole

Caption II a

Figure II a shows the nuclear transitions considered in the setting up of the population rate equations for the $I = 3/2$ spin system. Transitions resulting from the interaction of the electric quadrupole moment with the time-dependent electric field gradient are labelled in terms of the quadrupole transition probabilities W_1 and W_2 . Transitions resulting from the interaction of the magnetic dipole moment with the time dependent magnetic field are labelled in terms magnetic transition probability W_3 .



transition probabilities W_1 and W_2 given by equations (II 25) and (II 26) are therefore in general different for both sites and our theory must take this into account.

We shall consider the general case where W_1 and W_2 are unequal. We shall further introduce into our calculations of the population dynamics the refinement that the ^{23}Na energy levels are not equally spaced. Ignoring second-order frequency shifts, we express the frequencies of the components of the ^{23}Na spectrum in monocrystalline NaNO_3 as ν_0 for the centre line, $\nu_0(1+\delta)$ for the high frequency satellite and $\nu_0(1-\delta)$ for the low frequency satellite. The two spin systems, say A and B, will be coupled by spin-exchange interactions since corresponding ^{23}Na resonance frequencies are equal (Andrew and Swanson, 1960). We label the intrinsic spin-exchange transition probabilities as α for $m = -\frac{3}{2} \rightarrow -\frac{1}{2}$, β for the transition $m = -\frac{1}{2} \rightarrow \frac{1}{2}$ and γ for $m = \frac{3}{2} \rightarrow \frac{1}{2}$. We now develop the rate equations for the various levels of the A spin system, and calculate the enhancement of the high frequency satellite where a saturating power P' is applied to the centre line, P' being given by $\frac{1}{4} \gamma_n^2 H_1^2 g(\nu)$. This will correspond to the experimental case where the observing power of the spectrometer is zero. The allowed transitions are shown schematically in Figure II a.

i) $m = -3/2$

Using $N_{-3/2}^A$ for the population of the $m = -3/2$ level of the A spin system and similar labelling for the other levels, the time-dependent population of the $m = -3/2$ level is

$$\begin{aligned} \dot{N}_{-3/2}^A &= N_{-1/2}^A W_1^A + N_{1/2}^A W_2^A - N_{-3/2}^A W_1^A (1 + \Delta) - N_{-3/2}^A W_2 (1 + 2\Delta) \\ &+ \frac{\alpha}{N^B} \left[N_{-1/2}^A N_{-3/2}^B - N_{-3/2}^A N_{-1/2}^B \right]. \end{aligned}$$

This can be rewritten (c.f. Andrew and Swanson 1960)

$$\begin{aligned} \dot{N}_{-3/2}^A &= N_{-1/2}^A W_1^A + N_{1/2}^A W_2^A - N_{-3/2}^A W_1^A (1 + \Delta) - N_{-3/2}^A W_2 (1 + 2\Delta) \\ &+ \frac{\alpha}{4} \left[N_{-1}^A - N_{-1}^B \right]. \end{aligned} \quad (\text{II } 27)$$

where $N_{-1} = N_{-3/2} - N_{-1/2}$, $N_0 = N_{1/2} - N_{-1/2}$ and $N_1 = N_{1/2} - N_{-3/2}$.

ii) $m = -1/2$

Using a similar notation we can write

$$\dot{N}_{-1/2}^A = N_{-3/2}^A W_1^A (1 + \Delta) + N_{3/2}^A W_2^A - N_{-1/2}^A W_1^A - N_{-1/2}^A W_2^A (1 + 2\Delta)$$

$$\begin{aligned}
& + 4P' N_0 + \frac{\alpha}{N_B} \begin{bmatrix} N_3^A & N_1^B \\ -\frac{3}{2} & -\frac{1}{2} \end{bmatrix} - \begin{bmatrix} N_1^A & N_3^B \\ -\frac{1}{2} & -\frac{3}{2} \end{bmatrix} \\
& + \frac{\beta}{N_B} \begin{bmatrix} N_1^A & N_1^B \\ \frac{1}{2} & -\frac{1}{2} \end{bmatrix} - \begin{bmatrix} N_1^A & N_1^B \\ -\frac{1}{2} & \frac{1}{2} \end{bmatrix}
\end{aligned}$$

which can be reexpressed as

$$\begin{aligned}
\dot{N}_{\frac{1}{2}}^A &= N_{\frac{3}{2}}^A W_1^A (1 + \Delta) + N_{\frac{3}{2}}^A W_2^A - N_{\frac{1}{2}}^A W_1^A - N_{\frac{1}{2}}^A W_2^A (1 + 2\Delta) \\
& + 4P' N_0 + \frac{\alpha}{4} \begin{bmatrix} N_1^B \\ -1 \end{bmatrix} - \begin{bmatrix} N_1^A \\ -1 \end{bmatrix} + \frac{\beta}{4} \begin{bmatrix} N_0^A \\ -N_0^B \end{bmatrix}. \quad (\text{II } 28)
\end{aligned}$$

iii) $m = 1/2$

Similarly $\dot{N}_{\frac{1}{2}}^A$ is given by

$$\begin{aligned}
\dot{N}_{\frac{1}{2}}^A &= N_{\frac{3}{2}}^A W_1^A + N_{\frac{3}{2}}^A W_2^A (1 + 2\Delta) - N_{\frac{1}{2}}^A W_1^A (1 + \Delta) \\
& - N_{\frac{1}{2}}^A W_2^A - 4P' N_0 + \frac{\gamma}{4} \begin{bmatrix} N_1^A \\ -1 \end{bmatrix} - \begin{bmatrix} N_1^B \\ -1 \end{bmatrix} + \frac{\beta}{4} \begin{bmatrix} N_0^B \\ -N_0^A \end{bmatrix} \quad (\text{II } 29)
\end{aligned}$$

iv) $m = 3/2$

Similarly $\dot{N}_{\frac{3}{2}}^A$ is given by

$$\dot{N}_{\frac{3}{2}}^A = N_{\frac{1}{2}}^A W_1^A (1 + \Delta) + N_{\frac{1}{2}}^A W_2^A (1 + 2\Delta) - N_{\frac{3}{2}}^A W_1^A$$

$$-N_3^A W_2^A + \frac{\gamma}{4} [N_1^B - N_1^A]. \quad (\text{II } 30)$$

Using equations (II 27), (II 28), (II 29) and (II 30) we get following expressions for the population differences

$$\begin{aligned} \dot{N}_1^A = & N_0^A (4P') + N_1^A (-2W_1^A - W_2^A) + N_1^A (W_2^A) + \frac{\Delta N^A}{4} (2W_1^A) \\ & + \frac{\Delta N^A \delta}{4} (2W_1^A + 2W_2^A) + \frac{\gamma}{2} (N_1^B - N_1^A) + \frac{\beta}{4} (N_0^A - N_0^B), \quad (\text{II } 31) \end{aligned}$$

$$\begin{aligned} \dot{N}_1^A = & N_0^A (4P') + N_1^A (W_2^A) + N_1^A (-2W_1^A - W_2^A) + \frac{\Delta N^A}{4} (2W_1^A) \\ & + \frac{\Delta N^A \delta}{4} (-2W_1^A - 2W_2^A) + \frac{\beta}{4} (N_0^A - N_0^B) + \frac{\alpha}{2} (N_1^B - N_1^A) \quad (\text{II } 32) \end{aligned}$$

and

$$\begin{aligned} \dot{N}_0^A = & N_0^A (-8P' - 2W_2^A) + N_1^A (W_1^A - W_2^A) + N_1^A (W_1^A - W_2^A) \\ & + \frac{\Delta N^A}{4} (4W_2^A - 2W_1^A) + \frac{\alpha}{4} (N_1^A - N_1^B) + \frac{\beta}{2} (N_0^B - N_0^A) + \frac{\gamma}{4} (N_1^A - N_1^B). \quad (\text{II } 33) \end{aligned}$$

We wish to find the steady state solution where $\dot{N}_1^A = \dot{N}_1^B = \dot{N}_0^A = 0$. The term P' can be eliminated from these expressions to simplify obtaining the solution. Multiplying (II 31) by 2 and adding to (II 33) we get

$$\begin{aligned}
0 = & N_0^A (-2W_2^A) + N_1^A (-3W_1^A - 3W_2^A - \frac{3\gamma}{4}) + N_1^A (W_2^A + W_1^A + \frac{\alpha}{4}) \\
& + N_1^B (\frac{3\gamma}{4}) + N_1^B (\frac{-\alpha}{4}) + 2n_0 [W_1^A + 2W_2^A + 2\delta(W_1^A + W_2^A)]. \quad (\text{II } 34)
\end{aligned}$$

Likewise multiplying (II 32) by 2 and adding to (II 33) we have the form

$$\begin{aligned}
0 = & N_0^A (-2W_2^A) + N_1^A (W_1^A + W_2^A + \frac{\gamma}{4}) + N_1^A (-3W_1^A - 3W_2^A - \frac{3\alpha}{4}) \\
& + N_1^B (\frac{-\gamma}{4}) + N_1^B (\frac{3\alpha}{4}) + 2n_0 [W_1^A + 2W_2^A - 2\delta(W_1^A + W_2^A)]. \quad (\text{II } 35)
\end{aligned}$$

A similar set of rate equations will exist for the spin system B and by similar manipulation they can be put into the form

$$\begin{aligned}
0 = & N_0^B (-2W_2^B) + N_1^B (-3W_1^B - 3W_2^B - \frac{3\gamma}{4}) + N_1^B (W_2^B + W_1^B + \frac{\alpha}{4}) \\
& + N_1^A (\frac{3\gamma}{4}) + N_1^A (\frac{-\alpha}{4}) + 2n_0 [W_1^B + 2W_2^B + 2\delta(W_1^B + W_2^B)] \quad (\text{II } 36)
\end{aligned}$$

and

$$\begin{aligned}
0 = & N_0^B (-2W_2^B) + N_1^B (W_2^B + W_1^B + \frac{\gamma}{4}) + N_1^B (-3W_1^B - 3W_2^B - \frac{3\alpha}{4}) \\
& + N_1^A (\frac{-\gamma}{4}) + N_1^A (\frac{3\alpha}{4}) + 2n_0 [W_1^B + 2W_2^B - 2\delta(W_1^B + W_2^B)]. \quad (\text{II } 37)
\end{aligned}$$

If we assume that the power P' applied to the centre line is sufficiently large to cause complete saturation, then we can set the term $N_0^A = N_0^B = 0$ thereby giving four steady-state equations:

$$\begin{aligned}
0 &= N_1^A \left(-3W_1^A - 3W_2^A - \frac{3\gamma}{4} \right) + N_1^A \left(W_2^A + W_1^A + \frac{\alpha}{4} \right) + N_1^B \left(\frac{3\gamma}{4} \right) \\
&+ N_1^B \left(\frac{-\alpha}{4} \right) + 2n_0 \left[W_1^A + 2W_2^A + 2\delta (W_1^A + W_2^A) \right], \\
0 &= N_1^A \left(3W_1^A + 3W_2^A + \frac{3\gamma}{4} \right) + N_1^A \left(-9W_1^A - 9W_2^A - \frac{9\alpha}{4} \right) + N_1^B \left(\frac{-3\gamma}{4} \right) \\
&+ N_1^B \left(\frac{9\alpha}{4} \right) + 2n_0 \left[3W_1^A + 6W_2^A - 6\delta (W_1^A + W_2^A) \right], \\
0 &= N_1^A \left(\frac{3\gamma}{4} \right) + N_1^A \left(\frac{-\alpha}{4} \right) + N_1^B \left(-3W_1^B - 3W_2^B - \frac{3\gamma}{4} \right) \\
&+ N_1^B \left(W_2^B + W_1^B + \frac{\alpha}{4} \right) + 2n_0 \left[W_1^B + 2W_2^B + 2\delta (W_1^B + W_2^B) \right], \\
0 &= N_1^A \left(\frac{-3\gamma}{4} \right) + N_1^A \left(\frac{9\alpha}{4} \right) + N_1^B \left(3W_2^B + 3W_1^B + \frac{3\gamma}{4} \right) \\
&+ N_1^B \left(-9W_1^B - 9W_2^B - \frac{9\alpha}{4} \right) + 2n_0 \left[3W_1^B + 6W_2^B - 6\delta (W_1^B + W_2^B) \right]. \quad (\text{II } 38)
\end{aligned}$$

We now solve these equations in order to obtain the value N_1^A and N_1^B which will be directly proportional to the enhanced intensity of the high frequency satellite due to the

spin systems A and B. The total intensity of the enhanced satellite component is written as N_1^{sat} , the sum of N_1^{A} and N_1^{B} . Assuming $\alpha, \beta, \gamma \gg W_1^{\text{A}}, W_1^{\text{B}}, W_2^{\text{A}}, W_2^{\text{B}}$, the solution takes the form

$$N_1^{\text{sat}} = \frac{2n_0 \left[(W_1^{\text{A}} + 2W_2^{\text{A}}) + (W_1^{\text{B}} + 2W_2^{\text{B}}) + \delta(W_1^{\text{A}} + W_2^{\text{A}}) + \delta(W_1^{\text{B}} + W_2^{\text{B}}) \right]}{\left[W_1^{\text{A}} + W_2^{\text{A}} + W_1^{\text{B}} + W_2^{\text{B}} \right]} \quad (\text{II } 39)$$

Since the unsaturated intensity is given by

$$N_1^{\text{unsat}} = 2n_0 (1 + \delta), \quad (\text{II } 40)$$

the enhancement is given by

$$E = \frac{\left[(W_1^{\text{A}} + 2W_2^{\text{A}}) + (W_1^{\text{B}} + 2W_2^{\text{B}}) + \delta(W_1^{\text{A}} + W_2^{\text{A}}) + \delta(W_1^{\text{B}} + W_2^{\text{B}}) \right]}{(1 + \delta) \left[W_1^{\text{A}} + W_2^{\text{A}} + W_1^{\text{B}} + W_2^{\text{B}} \right]} \quad (\text{II } 41)$$

It is now convenient to introduce mean transition probabilities W_1 and W_2 defined by

$$W_1 = \frac{W_1^{\text{A}} + W_1^{\text{B}}}{2} \quad \text{and} \quad W_2 = \frac{W_2^{\text{A}} + W_2^{\text{B}}}{2} \quad (\text{II } 42)$$

Equation (II 41) then reads

$$E = \frac{W_1 + 2W_2 + \delta(W_1 + W_2)}{(1 + \delta) (W_1 + W_2)} \quad (\text{II } 43)$$

When $\delta = 0$, this reduces to the single spin expression (Abragam 1961, Hughes, 1966). We can therefore treat the ^{23}Na spin system in NaNO_3 as a single spin species with transition probabilities W_1 and W_2 .

Let us now develop the equations for a single spin species allowing for unequal energy level spacings and assuming that radio-frequency power is applied to all three resonances simultaneously (Hughes, 1966). In this case the spin-exchange interactions need not be considered since we exclude the crystal orientation where the resonances overlap.

The rate equations for the various levels now take the form:

i) $m = -3/2$

$$\begin{aligned} \dot{N}_{-\frac{3}{2}} = & 3P'_1 N_{\frac{1}{2}} - 3P'_1 N_{\frac{3}{2}} + W_1 N_{\frac{1}{2}} - W_1 \left(\frac{\Delta}{2}\right) N_{\frac{1}{2}} + W_1 \left(\frac{\Delta\delta}{2}\right) N_{\frac{1}{2}} - W_1 N_{-\frac{3}{2}} \\ & - W_1 \left(\frac{\Delta}{2}\right) N_{-\frac{3}{2}} + W_1 \left(\frac{\Delta\delta}{2}\right) N_{-\frac{3}{2}} + W_2 N_{\frac{1}{2}} - W_2 \Delta N_{\frac{1}{2}} + W_2 \left(\frac{\Delta\delta}{2}\right) N_{\frac{1}{2}} \\ & - W_2 N_{-\frac{3}{2}} - W_2 \Delta N_{-\frac{3}{2}} + W_2 \left(\frac{\Delta\delta}{2}\right) N_{-\frac{3}{2}} \end{aligned} \quad (\text{II } 44)$$

$$\text{ii) } m = -\frac{1}{2}$$

$$\begin{aligned} N_{-\frac{1}{2}} &= 4P'_0 N_{\frac{1}{2}} - 4P'_0 N_{-\frac{1}{2}} + W_1 N_{-\frac{3}{2}} + W_1 \left(\frac{\Delta}{2}\right) N_{-\frac{3}{2}} - W_1 \left(\frac{\Delta\delta}{2}\right) N_{-\frac{3}{2}} + W_2 N_{\frac{3}{2}} \\ &\quad - W_2 \Delta N_{\frac{3}{2}} - W_2 \left(\frac{\Delta\delta}{2}\right) N_{\frac{3}{2}} - W_3 N_{-\frac{1}{2}} - W_2 \Delta N_{-\frac{1}{2}} - W_2 \left(\frac{\Delta\delta}{2}\right) N_{-\frac{1}{2}} \\ &\quad - W_1 N_{-\frac{1}{2}} + W_1 \left(\frac{\Delta}{2}\right) N_{-\frac{1}{2}} - W_1 \left(\frac{\Delta\delta}{2}\right) N_{-\frac{1}{2}} + 3P'_{-1} N_{-\frac{3}{2}} - 3P'_{-1} N_{-\frac{1}{2}} \end{aligned} \quad (\text{II } 45)$$

$$\text{iii) } m = 1/2$$

$$\begin{aligned} N_{\frac{1}{2}} &= 4P'_0 N_{-\frac{1}{2}} - 4P'_0 N_{\frac{1}{2}} + W_1 N_{\frac{3}{2}} - W_1 \left(\frac{\Delta}{2}\right) N_{\frac{3}{2}} - W_1 \left(\frac{\Delta\delta}{2}\right) N_{\frac{3}{2}} - W_1 N_{\frac{1}{2}} \\ &\quad - W_1 \left(\frac{\Delta}{2}\right) N_{\frac{1}{2}} - W_1 \left(\frac{\Delta\delta}{2}\right) N_{\frac{1}{2}} + W_2 N_{-\frac{3}{2}} + W_2 \Delta N_{-\frac{3}{2}} - W_2 \left(\frac{\Delta\delta}{2}\right) N_{-\frac{3}{2}} \\ &\quad - W_2 N_{\frac{1}{2}} + W_2 \Delta N_{\frac{1}{2}} - W_2 \left(\frac{\Delta\delta}{2}\right) N_{\frac{1}{2}} + 3P'_1 N_{\frac{3}{2}} - 3P'_1 N_{\frac{1}{2}} \end{aligned} \quad (\text{II } 46)$$

$$\text{iv) } m = 3/2$$

$$\begin{aligned} N_{\frac{3}{2}} &= 3P'_1 N_{\frac{1}{2}} - 3P'_1 N_{\frac{3}{2}} + W_1 N_{\frac{1}{2}} + W_1 \left(\frac{\Delta}{2}\right) N_{\frac{1}{2}} + W_1 \left(\frac{\Delta\delta}{2}\right) N_{\frac{1}{2}} - W_1 N_{\frac{3}{2}} \\ &\quad + W_1 \left(\frac{\Delta}{2}\right) N_{\frac{3}{2}} + W_1 \left(\frac{\Delta\delta}{2}\right) N_{\frac{3}{2}} + W_2 N_{-\frac{1}{2}} + W_2 \Delta N_{-\frac{1}{2}} \\ &\quad + W_2 \left(\frac{\Delta\delta}{2}\right) N_{-\frac{1}{2}} - W_2 N_{\frac{3}{2}} + W_2 \Delta N_{\frac{3}{2}} + W_2 \left(\frac{\Delta\delta}{2}\right) N_{\frac{3}{2}} \end{aligned} \quad (\text{II } 47)$$

where P'_0 , P'_1 and P'_{-1} is the power applied to the N_0 , N_1 and N_{-1} resonances respectively. It then follows that

$$\begin{aligned} \dot{N}_1 = & N_0 (4P'_0) + N_1 (-6P'_1 - 2W_1 - W_2) + N_{-1} (W_2) \\ & + \frac{\Delta N}{4} (2W_1) + \frac{\Delta N \delta}{4} (2W_1 + 2W_2), \end{aligned} \quad (\text{II } 48)$$

$$\begin{aligned} \dot{N}_{-1} = & N_0 (4P'_0) + N_1 (W_2) + N_{-1} (-6P'_{-1} - 2W_1 - W_2) \\ & + \frac{\Delta N}{4} (2W_1) + \frac{\Delta N \delta}{4} (-2W_1 - 2W_2), \end{aligned} \quad (\text{II } 49)$$

and

$$\begin{aligned} \dot{N}_0 = & N_0 (-8P'_0 - 2W_2) + N_1 (3P'_1 + W_1 - W_2) \\ & + N_{-1} (3P'_{-1} + W_1 - W_2) + \frac{\Delta N}{4} (4W_2 - 2W_1). \end{aligned} \quad (\text{II } 50)$$

We now normalize the rate equations with respect to W_1 , putting the ratio $W_2/W_1 = x$, $P'_0/W_1 = P_0$, $P'_1/W_1 = P_1$ and $P'_{-1}/W_1 = P_{-1}$. Thus the equations take the form.

$$\begin{aligned} \dot{N}_1/W_1 = & N_0 (4P_0) + N_1 (-6P_1 - 2W_1 - W_2) + N_{-1} (W_2) + n_0 (2W_1) \\ & + n_0 \delta (2W_1 + 2W_2), \end{aligned} \quad (\text{II } 51)$$

$$\begin{aligned} \dot{N}_{-1}/W_1 &= N_0 (4P_0) + N_1 (W_2) + N_{-1} (-6P_{-1} - 2W_1 - W_2) + n_0 (2W_1) \\ &+ n_0 \delta (-2W_1 - 2W_2) \end{aligned} \quad (\text{II } 52)$$

and

$$\begin{aligned} \dot{N}_0/W_1 &= N_0 (-8P_0 - 2W_2) + N_1 (3P_1 + W_1 - W_2) + N_{-1} (3P_{-1} + W_1 - W_2) \\ &+ n_0 (4W_2 - 2W_1). \end{aligned} \quad (\text{II } 53)$$

Let us now consider the situation where $P_0 = P_{-1} = 0$. Such a situation covers the experimental case where the high frequency satellite is observed using the spectrometer. The population difference N_1^{unsat} which determines the intensity of the N_1 resonance is given by

$$N_1^{\text{unsat}} = n_0 (1 + \delta) \left[1 + P_1 \frac{3(2+x)}{2(1+x)} \right]^{-1}. \quad (\text{II } 54)$$

Let us now consider the situation where, in addition, the centre line transition has power applied to it such that $P_0 \gg 1, P_1$. This will correspond to the double resonance situation where the high frequency satellite is being observed while the centre line is simultaneously severely saturated. The population difference N_1^{sat} which determines the

enhanced intensity of the N_1 resonance is given by

$$N_1^{\text{sat}} = n_0 \left[(2x + 1) + \delta(1+x) \right] (1+x+3P_1)^{-1} \quad (\text{II } 55)$$

The enhancement E of the high frequency satellite is therefore given by

$$E = \frac{\left[(2x+1) + \delta(1+x) \right] \left[2(1+x) + P_1 \cdot 3(2+x) \right]}{\left[2(1+x) (1+\delta) \right] \left[1 + x + 3P_1 \right]} \quad (\text{II } 56)$$

Expanding equation (II 56) to first order in P_1 as allowed for $P_1 \ll 1$ corresponding to low observing powers of the spectrometer, the enhancement becomes

$$E = \left[\frac{1+2x}{1+x} \right] \left[1 + \frac{3(2+x)P_1}{2(1+x)} \right] \left[1 - \frac{\delta x}{1+2x} \right] \left[1 + \frac{3P_1}{1+x} \right]^{-1} \quad (\text{II } 57)$$

Similarly, the enhancement of the low frequency satellite as a result of severe saturation of the centre line transition can obviously be expressed to first order in the power P_{-1} as

$$E = \left[\frac{1+2x}{1+x} \right] \left[1 + \frac{3(2+x)P_{-1}}{2(1+x)} \right] \left[1 + \frac{\delta x}{1+2x} \right] \left[1 + \frac{3P_{-1}}{1+x} \right]^{-1} \quad (\text{II } 58)$$

Similar expressions can be obtained for the enhance-

ment of the various components due to the saturation of any other component. However, those of interest to us are the two given above in equations (II 57) and (II 58) and a third case corresponding to the enhancement of the centreline due to severe saturation of the high frequency satellite. The enhancement for this case expanded to first order in the observing power is given by

$$E = \left[\frac{3+2x}{2+x} \right] \left[1 + \frac{2(1+x)P_0}{x} \right] \left[1 + \frac{\delta(1+x)}{3+2x} \right] \left[1 + \frac{4(1+x)}{x(2+x)} \right]^{-1} \quad (\text{II } 59)$$

For simplicity we shall henceforth refer to the three enhancements given by (II 57), (II 58) and (II 59) as Case I, Case II, and Case III respectively.

In all three cases the enhancement, for low values of the observing power, has a linear dependence on the observing power. In the limit of zero observing power, the enhancements for the three cases, I, II, and III are respectively

$$E = \left[\frac{1+2x}{1+x} \right] \left[1 + \frac{\delta x}{1+2x} \right], \quad (\text{II } 60)$$

$$E = \left[\frac{1+2x}{1+x} \right] \left[1 - \frac{\delta x}{1+2x} \right] \quad (\text{II } 61)$$

and

$$E = \left[\frac{3+2x}{2+x} \right] \left[1 + \frac{\delta(1+x)}{3+2x} \right]. \quad (\text{II } 62)$$

The value δ can be found from measuring the resonance frequencies using the relationship $\nu_+ - \nu_- = 2\nu_0 \delta$. If the enhancement at zero power is found by extrapolating the linear portion of the enhancement/observing power curve, the value of $W_2/W_1 = x$ can be found from equations (II 60), (II 61) and (II 62).

This is the basis of our proposed double resonance experiment, namely to measure the enhancement of a component due to severe saturation of another component as a function of the spectrometer power.

It has been pointed out by Snyder and Hughes (1970) that for the case of quadrupole interaction of an indirect nature, such as harmonic and anharmonic Raman processes, $W_{m \rightarrow m-1}$ and $W_{m \rightarrow m-2}$ are independent of m . If, however, the relaxation is caused by a direct process such a one-phonon interaction then $W_{m \rightarrow m-1}$ and $W_{m \rightarrow m-2}$ will depend on m . We, therefore consider the possibility that W_1 and indeed W_2 will be different for the different transitions. Using a notation in keeping with that developed previously, we define \bar{W}_1^\ddagger for the transition $m = -\frac{3}{2} \rightarrow -\frac{1}{2}$ and \bar{W}_2^\ddagger for the case $m = -\frac{3}{2} \rightarrow \frac{1}{2}$ with \bar{W}_1 and \bar{W}_2 for the transitions $m = \frac{3}{2} \rightarrow \frac{1}{2}$ and $m = \frac{3}{2} \rightarrow -\frac{1}{2}$ respectively. Further we define the relationship between them as

$$\bar{W}_1^\ddagger = \bar{W}_1 (1+\phi) \quad \text{and} \quad \bar{W}_2^\ddagger = \bar{W}_2 (1+\theta) \quad (\text{II } 63)$$

where θ and ϕ are small quantities. The appropriate rate equations can be set up in the manner described earlier. To first order in P_1 , the enhancement of the high frequency satellite caused by severe saturation of the centre line transition has the form

$$\begin{aligned}
 E &= \left[\frac{2W_2 + W_1}{W_1 + W_2} \right] \left[1 - \frac{W_1 W_2 \phi}{(W_1 + 2W_2)(W_1 + W_2)} - \frac{(5W_2^2 - 2W_2 W_1) \theta}{2(W_1 + W_2)(W_1 + 2W_2)} - \frac{W_2 \delta}{(2W_2 + W_1)} \right] \\
 &\times \left[1 + \frac{P_1 3(W_2 + 2W_1)}{2W_1(W_1 + W_2)} \left[1 - \frac{(W_2 + 2W_1) \phi}{2(W_1 + W_2)} - \frac{W_1 W_2^2 \theta}{2(W_1 + W_2)(W_2^2 + 2W_1 W_2)} \right] \right] \\
 &\times \left[1 + \frac{P_1 3}{W_1 + W_2} \left[1 - \frac{W_2 \theta}{W_1 + W_2} \right] \left[1 - \frac{W_1 \phi}{W_1 + W_2} \right] \right]^{-1} \quad (\text{II } 64)
 \end{aligned}$$

For the direct phonon interaction mentioned above, the phonon density of states should increase monotonically with frequency and therefore \bar{W}^\dagger the quadrupole transition probability for the high frequency satellite should be greater than \bar{W} , the quadrupole transition probability for the low frequency satellite. The quantities θ and ϕ defined in equation (II 63) are therefore positive. It can be seen from (II 64) that the effect of these quantities for the situation $P_1 = 0$ is to reduce the enhancement of the high frequency satellite. By symmetry

arguments the enhancement of the low frequency satellite due to severe saturation of the centre line can be obtained from equation (II 64) by changing the signs of θ , ϕ and δ . The effect of the quantities θ and ϕ in this case increases the extrapolated enhancement of the low frequency satellite.

Finally, we consider the correction that should be applied to the measured enhancement values to take account of the fact that the saturating power is not in practice infinite. (We shall see later that such a correction is necessary to obtain the required experimental accuracy). For the case where the centre line is severely saturated with a power P_0 it can be shown from the expressions presented by Hughes (1966) that the saturated enhancement of a satellite is given by

$$E = \frac{1 + 2P_0 \left[\frac{1+2x}{x} \right]}{1 + 2P_0 \left[\frac{1+x}{x} \right]}, \quad (\text{II } 65)$$

in the limit of zero observing power and for $\delta=0$. By measuring E as a function of the saturating observing power P_0 with a very small power, and fitting the data to an equation of the form given by (II 65) a correction for the non-infinite saturating power can be applied. So long as $P_0 \gg 1$

the error in such a correction factor due to the non-zero observing power used in the measurements is small.

c) Quadrupole spin-lattice interaction

The Hamiltonian for the quadrupole spin-lattice interaction can be written as

$$H = H_L + H_Z + H_Q \quad (\text{II } 66)$$

where H_L is concerned with the lattice states and H_Z is the Zeeman term. The H_Q term represents the interaction of the nuclear quadrupole moment with the electric field gradient produced by the lattice. The electric field gradient component V_{jk} at the nuclear site may be written as

$$V_{jk} = \overline{V_{jk}} + V_{jk}(t). \quad (\text{II } 67)$$

The term $\overline{V_{jk}}$ is the time-average field gradient whose interaction with the quadrupole moment determines the static quadrupole interaction. This interaction, as we discussed earlier, will result in a perturbation of the Zeeman energy levels resulting in unequally spaced energy levels giving the component structure of the spectrum. The term $V_{jk}(t)$ is the time-

dependent field gradient whose interaction with the quadrupole moment will determine the quadrupole relaxation.

Following the notation of Pietila (1968), we express the quadrupole interaction Hamiltonian in the form

$$H_Q = \sum_{\mu=-2}^2 Q^\mu (B^\mu)^* \quad (\text{II } 68)$$

where

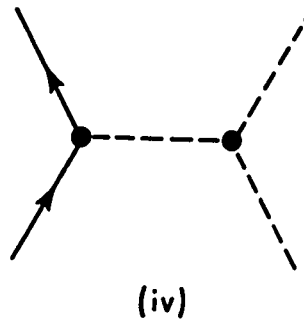
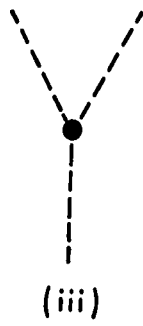
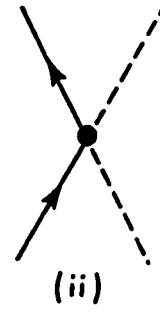
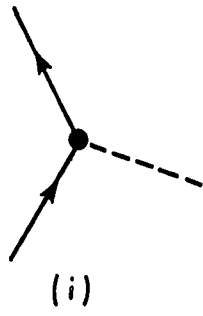
$$\begin{aligned} B^0 &= \frac{1}{2} V_{zz}, \\ B^{\pm 1} &= \pm (1/\sqrt{6}) (V_{zz} \pm V_{yz}), \\ B^{\pm 2} &= (1/\sqrt{6}) \left[\frac{1}{2} (V_{xx} - V_{yy}) \pm iV_{xy} \right], \\ Q^0 &= k [3I_z^2 - I(I+1)], \\ Q^{\pm 1} &= \pm (\sqrt{6}/2) k (I_z I_\pm + I_\pm I_z), \\ Q^{\pm 2} &= (\sqrt{6}/2) k I_\pm^2, \end{aligned} \quad (\text{II } 69)$$

and $k = eQ/[2I(2I-1)]$.

The term Q^μ involves the nuclear quadrupole moment and the nuclear spin parameters I_z and I_\pm . The subscript μ takes the five values 2, 1, 0, -1, -2 representing the five possible

Caption II b

Figure II.b shows the Feynman diagrams of the relaxation processes. The so-called direct process is shown in i), the indirect harmonic Raman process in ii), and the indirect anharmonic Raman process is shown in iv). The process indicated in iii) is a three-phonon process which, as is discussed in the text, is not an effective relaxation process.



spin transitions $\Delta m = \pm 2$, $\Delta m = \pm 1$ and $\Delta m = 0$. The term B^μ represents the electric field gradient and this can be expanded as a power series in terms of the displacement, relative to the relaxing nucleus, of the ions representing the lattice. Such a power series has the form

$$B^\mu = \overline{B^\mu} + \sum_j \frac{\partial B^\mu}{\partial x_j} u_j + \frac{1}{2!} \sum_j \sum_k \frac{\partial^2 B^\mu}{\partial x_j \partial x_k} u_j u_k + \dots \quad (\text{II } 70)$$

where u_j represents a component of the relative displacement from the equilibrium configuration.

It is convenient to categorize relaxation processes according to whether they involve the displacement u_j linearly via the second term in equation (II 70) or quadratically via the third term in (II 70), etc. (Van Kranendonk, 1954).

As an example of the first category is the direct phonon process in which each spin transition is associated with the creation or annihilation of a lattice phonon (Van Kranendonk, 1954). Such an interaction is represented by a Feynman diagram in Figure II b i. However, this process should be relatively ineffective (except at low temperatures), since the density of phonon states with frequencies equal to the nuclear resonance frequency ($\sim 10^7$ Hz) is small.

As an example of the second category is the indirect harmonic Raman process first discussed by Van Kranendonk (1954). The treatment consisted of a first-order perturbation calculation involving the interaction of the incoming phonon with a nuclear spin to produce a spin transition and an outgoing phonon of different energy. The energy difference between the incoming and outgoing phonons is equal to the energy difference between the initial and final spin states. This process is represented by the Feynman diagram in Figure II b ii. In this process all phonons are involved thereby making the process in general much more effective than the direct phonon process referred to above.

Van Kranendonk and Walker (1967,1968) have proposed another relaxation process that they have called the anharmonic Raman process. The total potential energy of a crystal can be expanded as a Taylor series in powers of the atomic displacements from the equilibrium configuration. The quadratic term in such a series is the harmonic description of the lattice and higher powers are called anharmonic terms. The first anharmonic (cubic) term gives rise to the three-phonon process, shown in Figure II b iii, which plays a role in

lattice thermal conductivity. The anharmonic process considered by Van Kranendonk and Walker (1967, 1968) is a second-order process involving the first anharmonic term in combination with the linear term in equation (II 70). Such a process therefore falls in our first category. The Feynman diagram for such a process is shown in Figure II b iv. The phonon causing the spin transition in the anharmonic Raman process is a virtual phonon as opposed to the real phonons involved in the lattice conductivity process shown in Figure II b iii. The third real phonon of Figure II b iii was proposed as a suitable phonon for spin relaxation by Kutsishvili (1967). However, Van Kranendonk and Walker (1967) have pointed out that such a process is quite ineffective as a relaxation mechanism.

The temperature dependence of the spin-lattice relaxation time T_1 associated with indirect harmonic Raman processes and anharmonic Raman processes is the same as for the magnetic relaxation processes due to lattice vibrations. If one assumes a Debye frequency spectrum, then the temperature dependence is

$$\frac{1}{T_1} \sim T^2 (a - b/T^2) \quad \text{for } T \gtrsim \frac{1}{2} \theta_D$$

$$\frac{1}{T_1} \sim T^7 \quad \text{for } T \lesssim 0.02 \theta_D \quad (\text{II } 71)$$

where a and b are constants and θ_D is the Debye temperature. Measurements of T_1 (Wikner, Blumberg and Hahn, 1960, Weber and Allen, 1962) have confirmed the T^2 dependence of T_1^{-1} . However, the T^7 dependence has not been verified because of magnetic relaxation process at the low temperatures.

d) Orientation dependence of the quadrupole spin-lattice relaxation

As is seen from equation (II 69), the B^{μ} and hence the quadrupole relaxation probabilities depend on V_{xz} , V_{xx} , V_{yy} etc., where the z axis is along the magnetic field direction. (A coordinate system where the z axis is set along the direction of the externally applied field is later referred to as the K' coordinate system). If the crystal is rotated with respect to the magnetic field, these field gradient components will be different and hence the relaxation probabilities W_1 and W_2 should be orientation dependent.

The orientation dependence of the transition probabilities was first considered by Pietila (1968), for a harmonic

lattice. Pietila considered the quadrupole relaxation due to the direct process and the indirect harmonic Raman process, for which he derived the orientation dependence for 3-fold, 4-fold and 6-fold crystal symmetry. The question arises as to whether the form of the orientation dependence for the anharmonic Raman process is the same as that calculated by Pietila. This question was considered by Snyder and Hughes (1970), who showed that the orientation form was independent of the relaxation process. The following discussion follows the notation used by Snyder and Hughes.

It is convenient to introduce a reference system, say $K(xyz)$, associated with the symmetry properties of the crystal. For example, for NaNO_3 the z axis would be set along the crystal triad axis. It is also convenient to introduce a second reference system, say $K'(x'y'z')$, with z' coinciding with the magnetic field H_0 direction. The polar angles of the z' axis with respect to the crystal reference frame K are denoted by θ and ϕ . The quantities B^μ and Q^μ in equation (II 69) can be readily transformed from one reference frame to another with the use of a suitable rotation operator, the Euler angles for such a transformation being $\alpha = \phi$, $\beta = \theta$ and $\gamma = 0$ (Edmonds, 1957). Following the usual procedure (Van Kranendonk 1954, Pietila 1968) the quadrupole Hamiltonian

can be written as

$$H_Q = \sum_{\mu\mu'} Q^{\mu'} D_{\mu'\mu}^* (\theta, \phi) (B^\mu)^* \quad (\text{II } 72)$$

The term $Q^{\mu'}$, an irreducible tensor, is in the K' reference system representing the nuclear quadrupole term in a manner that is independent of θ and ϕ . Likewise, the term B^μ is an irreducible tensor which is independent of the angular parameters and is defined in the K reference system. The angular parameters are contained in the rotation operator which transforms B^μ into the K' system, thereby putting the whole Hamiltonian into that system. The matrix elements for the spin states are given by the expressions

$$Q_{\pm 1, m} = \langle m \pm 1 | Q^{\pm 1} | m \rangle = \pm (\sqrt{6}/2) k (2m \pm 1) [(I \pm m + 1) (I \mp m)]^{\frac{1}{2}} \quad (\text{II } 73)$$

$$Q_{\pm 2, m} = \langle m \pm 2 | Q^{\pm 2} | m \rangle = (\sqrt{6}/2) k [(I \mp m) (I \mp m - 1) (I \pm m + 1) (I \pm m + 2)]^{\frac{1}{2}} \quad (\text{II } 74)$$

Considering a relaxation process due to quadrupole interactions (Pietila 1968, Van Kranendonk and Walker 1968, Snyder and Hughes 1970), the probability per unit time of a transition $m, n \rightarrow m + \mu, n'$, where n and n' are the initial and final lattice states whilst m and $m + \mu$ are the initial and final spin states, is given to first order by

$$W_{m, n \rightarrow m+\mu, n'} = \frac{2\pi}{\hbar} \left| Q_{\mu m} \right|^2 \left| \langle n' \left| \sum_{\mu'} D_{\mu' \mu}^* (B^{\mu})^* \right| n \rangle \right|^2 \delta(E_{n'} + E_{m+\mu} - E_n - E_m). \quad (\text{II } 75)$$

The δ -function imposes energy conservation constraints on the transition. If the lattice is in thermal equilibrium, then the probability of spin transitions $m \rightarrow m+\mu$ can be rewritten by replacing the phonon states by their thermal average. Thus, the spin transition probability per unit time becomes in such a case

$$W_{m \rightarrow m+\mu} = \left| Q_{\mu m} \right|^2 \sum_{\mu', \mu''} D_{\mu' \mu} D_{\mu'' \mu}^* C(\mu', \mu'', \mu, m). \quad (\text{II } 76)$$

where

$$C(\mu', \mu'', \mu, m) = \frac{2\pi}{\hbar} \sum_{n'} \langle n' | B^{\mu'} \rangle^* | n \rangle \langle n' | (B^{\mu''})^* | n \rangle \times \delta(E_{n'} + E_{m+\mu} - E_n - E_m). \quad (\text{II } 77)$$

Let us first suppose that the transition probabilities W_1 and W_2 depend on the initial spin state (Snyder and Hughes 1970). Such a consideration was discussed earlier in connection with the evaluation of the rate equations for the $I = 3/2$ spin system. We therefore rewrite W_1 and W_2 as W_1^m and W_2^m respectively. The two transition probabilities then become

$$W_{m \rightarrow m+1} = W_1^m (2m+1)^2 (I+m+1) (I-m) / [2I(2I-1)^2] \quad (\text{II } 78)$$

and

$$W_{m \rightarrow m+2} = W_2^m (I-m) (I-m-1) (I+m+1) (I+m+2) / [2I(2I-1)^2]. \quad (\text{II } 79)$$

If the transition probabilities do not depend on the m value, then the above equations reduce to the form of the expressions given by Yosida and Moriya (1956). Using equations (II 73), (II 74) and (II 76), the spin transition probability can therefore be written in the form

$$W_{\mu}^m = \frac{3e^2 Q^2}{4I} \sum_{\mu', \mu''} D_{\mu', \mu} D_{\mu', \mu}^* C(\mu', \mu'', \mu, m). \quad (\text{II } 80)$$

By substituting for B^{μ} in (II 77) it can be shown (cf. Pietilä 1968) that $W_{m \rightarrow m+\mu}$ and W_{μ}^m can be expressed as linear combinations of the quantities

$$M_{\alpha\beta\alpha'\beta'}(\mu, m) = \frac{2\pi}{\hbar} \sum_{n'} \langle n' | V_{\alpha\beta} | n \rangle^* \langle n' | V_{\alpha'\beta'} | n \rangle \delta(E_{n'} + E_{m+\mu} - E_n - E_m) \quad (\text{II } 81)$$

where $\alpha, \beta, \alpha', \beta'$ are the Cartesian coordinates x, y, z , which for future simplicity we shall label as 1, 2, 3. The quantity $M_{\alpha\beta\alpha'\beta'}$ is a component of the fourth rank-tensor representing the fluctuations in the electric field gradient. In the

general, this tensor will have 81 components. Using equation (II 80) and the symmetry properties of quadrupole interactions, it can be shown (Snyder and Hughes, 1970) that the M-tensor is real. It then follows from (II 81) that

$$M_{\alpha\beta\alpha'\beta'} = M_{\beta\alpha\alpha'\beta'} = M_{\alpha\beta\beta'\alpha'} = M_{\alpha'\beta'\alpha\beta} \quad (\text{II } 82)$$

and from Laplace's equation that

$$\sum_{\alpha} M_{\alpha\alpha\alpha'\beta'} = \sum_{\alpha'} M_{\alpha\beta\alpha'\alpha'} = 0. \quad (\text{II } 83)$$

This reduces the number of independent tensor components from 81 to 15. The number of independent components may be further reduced depending on the particular crystal symmetry and this has been carried through for the 32 point groups by Snyder and Hughes (1970). Restrictions on the sign and magnitude of the M-components can also be obtained from equation (II 81) and it can be shown that these are (Snyder and Hughes, 1970)

$$M_{\alpha\beta\alpha\beta} \geq 0$$

and

$$(M_{\alpha\beta\alpha'\beta'})^2 \leq M_{\alpha\beta\alpha\beta} M_{\alpha'\beta'\alpha'\beta'}. \quad (\text{II } 85)$$

For the indirect harmonic Raman process and the anharmonic Raman process, the energy difference ($E_{m+\mu} - E_m$) is small compared to the energy of the phonons and may be neglected in equation (II 81). It follows that the M-components and hence the transition probabilities are independent of the parameters μ and m . In the case of the direct process the change in the nuclear spin energy is equal to the phonon energy and this approximation cannot be made. The M-components and W_{μ}^m are therefore dependent on μ and m .

Other relaxation mechanisms such as diffusion and torsional oscillation of molecular groups also fall into the former category where the M-components are independent of the parameters μ and m , so long as the correlation time is sufficiently short. For those group motions where the correlation time is long, then the M-components will depend on μ and m (Snyder and Hughes, 1970). In practice, even where the M-components do depend on μ and m , the m -dependence may be negligibly small if the static quadrupole interaction is much less than the Zeeman interaction.

Finally we note that the orientation dependence of W_1 and W_2 is independent of the mechanism that produces the quadrupole relaxation. For the case of a single crystal possessing triad symmetry, the quadrupole relaxation transition prob-

abilities are given by Pietilä, 1968, Snyder and Hughes, 1970)

$$\begin{aligned}
 & (M_{1111} + 4M_{1313} + 2M_{3333}) + (6M_{1111} - 6M_{3333}) \cos^2 \theta \\
 & + (M_{1111} - 4M_{1313} + 2M_{3333}) \cos^4 \theta \\
 & + 4(M_{1113} \cos 3\phi + M_{1123} \sin 3\phi) \sin^3 \theta \cos \theta \\
 \frac{W_1}{W_2} = & \frac{\phantom{+ 4(M_{1113} \cos 3\phi + M_{1123} \sin 3\phi) \sin^3 \theta \cos \theta}}{(4M_{1111} + 4M_{1313} - M_{3333}) - (12M_{1313} - 9M_{3333}) \cos^2 \theta} \cdot \quad (\text{II } 86) \\
 & - (4M_{1111} - 16M_{1313} + 8M_{3333}) \cos^4 \theta \\
 & - 16(M_{1113} \cos 3\phi + M_{1123} \sin 3\phi) \sin^3 \theta \cos \theta
 \end{aligned}$$

SECTION III Apparatus and Experimentation

a) Spectrometer

The double resonance experiment that we wish to carry out requires power being applied simultaneously to two different frequency components of the nuclear magnetic resonance spectrum. This means therefore that the supply of power to the spin system and extraction of the information pertaining to the resonance must be achieved by a single coil, leaving the second orthogonal coil to supply power to the second spectrum component. Crossed-coil spectrometers such as the Varian Associates models are therefore unsuitable for this type of experiment. Spectrometers of the bridge network type are single coil units. However, they tend to be somewhat unstable and to respond to both the absorption and dispersive modes of the nuclear magnetic resonance signal, an undesirable complication. We initially constructed a Pound-Knight-Watkins single coil spectrometer (Watkins and Pound, 1951 and Knight, 1950). However, this unit could not be made to operate at the power levels that we required, with a sufficiently good signal-to-

noise ratio (Reed, 1967). The work reported in this thesis was carried out using a Robinson nuclear spectrometer, (Robinson, 1959) whose design was similar to that built by Howling (1966).

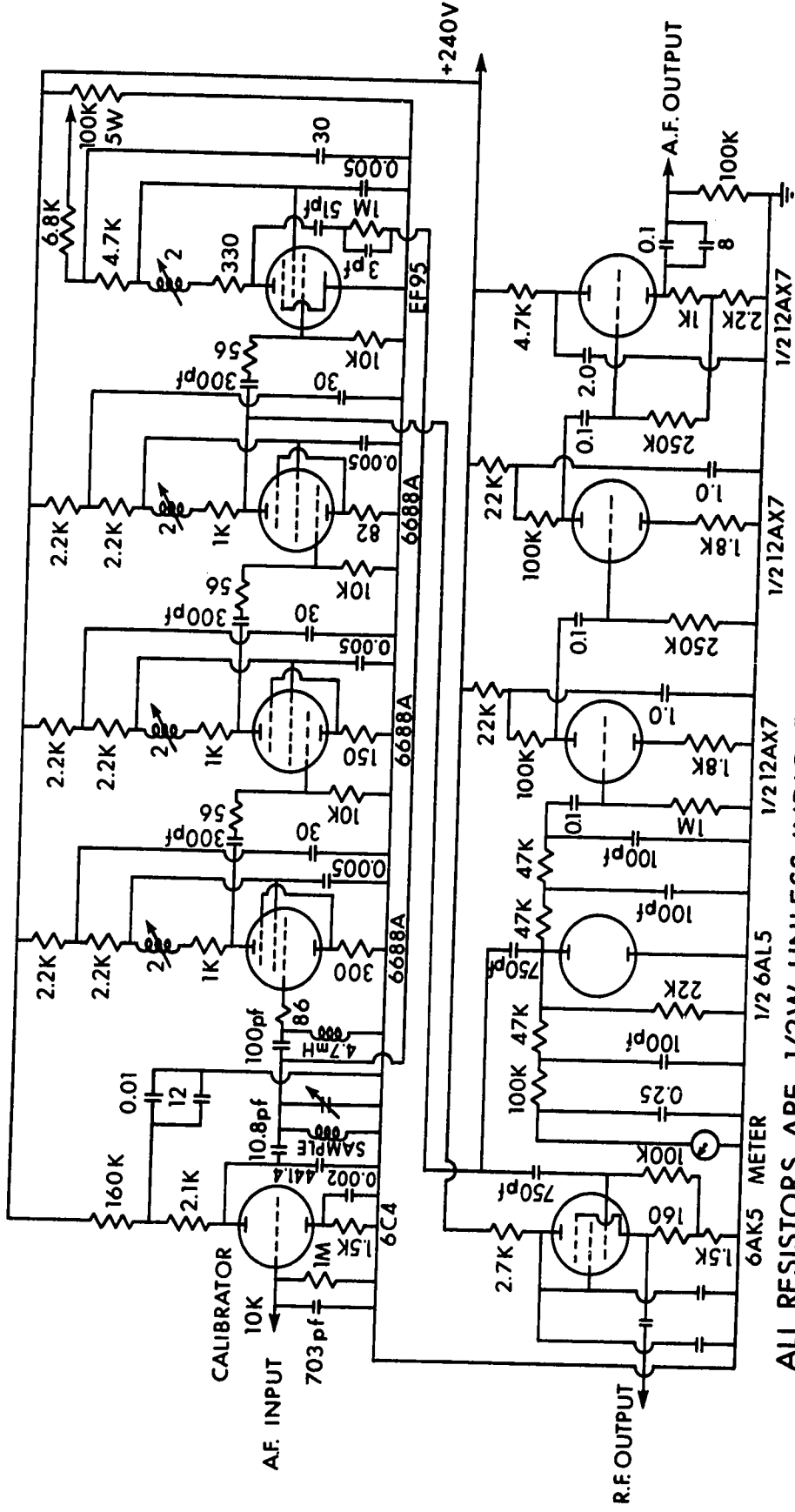
In this type of spectrometer the nuclear spin system under investigation is placed in the coil of the tank circuit of an oscillator. The energy absorbed by the spin system during resonance originates in this unit so that spin absorption will directly affect the performance of the oscillator. Therefore, by monitoring the oscillator level one can obtain information about the nuclear absorption of the spin species.

The tank circuit of the oscillator is a parallel combination of inductive and capacitative elements, plus a resistive component that may be considered to be in series with the inductive part. The sample is placed in the inductive coil therefore exposing it to the circularly polarised components of the radio-frequency field resulting from the carrier developed by the oscillator.

The absorption of energy by the spin system at resonance is equivalent to the introduction of an additional resistive component into the tank circuit. The resulting

Caption III a

Figure III a shows the circuit diagram of the Robinson nuclear magnetic resonance spectrometer (Robinson, 1959).



ALL RESISTORS ARE 1/2W UNLESS INDICATED
 ALL CAPACITORS ARE MICROFARADS UNLESS INDICATED
 ALL INDUCTORS ARE MICROHENRYS UNLESS INDICATED

change in the Q-factor of the tank circuit will then offer a means of monitoring the resonance. The Q-factor of such a parallel circuit is given by the equation

$$Q = \frac{\omega_0 L}{R}$$

(III I)

where L is the inductance, R is the resistance and ω_0 is the resonant pulsatace given by the condition $\omega_0^2 LC=1$ where C is the capacitative element. This introduction of the additional resistive term decreases the Q-factor, and the magnitude of the oscillation level falls. It is the monitoring of this amplitude change that will allow the extraction of the information from the spin system.

We shall now consider the particular design characteristics of the Robinson spectrometer whose circuit diagram is shown in Figure III a . The spectrometer may be considered as consisting of two parts, a radio-frequency oscillator section and a demodulation-audioamplification section.

Three 6688 tubes are employed in the oscillator section, which also performs the additional role of amplifying the radio-frequency oscillation by a factor of some

300. The final stage of the oscillator unit is a 6AK5 tube incorporated in a limiter circuit. The feedback is taken from the output of the limiter and coupled onto the tank circuit of the oscillator. The limiter output is a constant value that is independent of the input amplitude providing that this input is sufficiently large. Since the preceding section has a gain of 300, this condition is easily satisfied. The feedback appears to the tank circuit as a constant current source with the degree of feedback being largely independent of the gain fluctuations in the early stages of the oscillator. While the characteristics of the limiter were adjusted to have the idealised square wave response, such a situation was not achieved and a degree of ripple was always noticeable on the waveform. It is safe to say that the excellent performance of this spectrometer, particularly at the lower levels of power, is due to the inclusion and successful operation of this limiter.

Because of the signal-to-noise characteristics of the ^{23}Na NMR in NaNO_3 , one cannot observe the signal directly say by the use of an oscilloscope. Fast-passage techniques (Abragam and Proctor, 1958) are also unsuitable because of the frequency-dependence of the balance-mode system. Fast passage by variation of the magnetic field

is also ruled out since this would require the tracking of the saturation signal as the field is swept. We therefore employed phase-sensitive detection methods in conjunction with an audio-modulation of the steady magnetic field, the modulation amplitude being small compared to the linewidth. The result is an audio modulation of the radio-frequency carrier level of the order of 1 part in 10^5 which is proportional to the first derivative of the absorption line.

The audio-modulated radio-frequency carrier is taken from the last of the 6688 tubes of the oscillator section and is then fed into the demodulation-amplification unit. Here the signal is chopped, the radio-frequency components smoothed out by a series of low-pass filters, and the final audio signal is amplified by a factor of some 400. Thus the spectrometer output is an audio signal whose amplitude contains the information about the nuclear spin absorption.

Two other parts are incorporated in the spectrometer design although they are not essential to the observation of the signal. One is a circuit suitable for feeding the oscillator radio-frequency signal into a frequency counter. The other is a calibrator unit (Watkins and Pound, 1951, Watkins, 1952). This unit employs a 6C4 tube

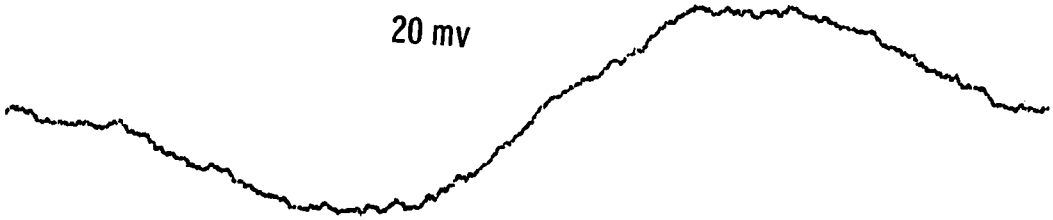
operated in a nonlinear part of its characteristic. The principle here is that, under such conditions, the plate resistance of the tube will be dependent on the instantaneous plate voltage. Therefore, if the grid voltage is varied at an audio frequency, we have introduced an audio-modulated resistance into the circuit. Furthermore, if the audio frequency is the same as that of the chosen audio field modulation frequency, then the detection and amplification units respond to it in the same way as they do to the results of the field modulation. The load of the tube is weakly coupled to the tank circuit so that we have introduced a pseudo resonance into the spectrometer. This circuit therefore offers a means of calibrating the sensitivity of the spectrometer's response to NMR and also a means of checking the linearity of the system as a whole.

Care was taken in the design and construction of the spectrometer to reduce microphonics and pick-up, both of which are of particular concern in NMR spectrometers, particularly those operating at low levels. The body of the spectrometer was made from 1/4-inch brass plate welded throughout. The body was divided into compartments each containing specific parts of the electronics of the spectrometer thereby ensuring isolation of the various stages

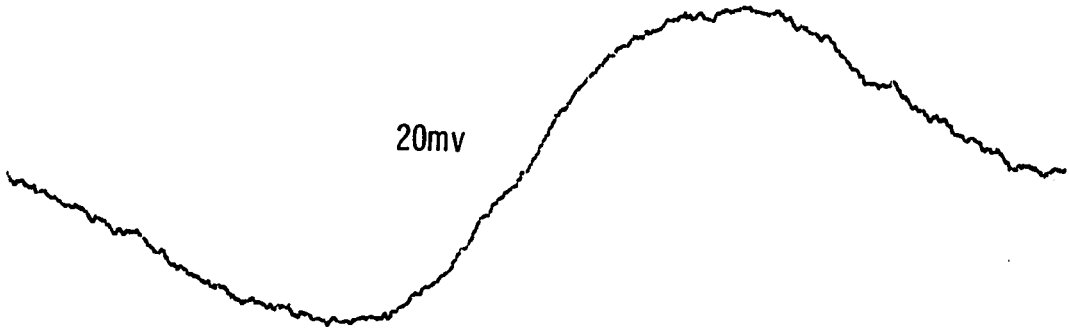
Caption III b

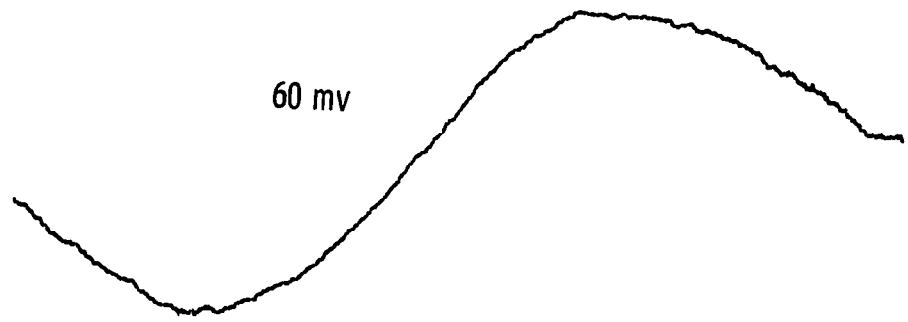
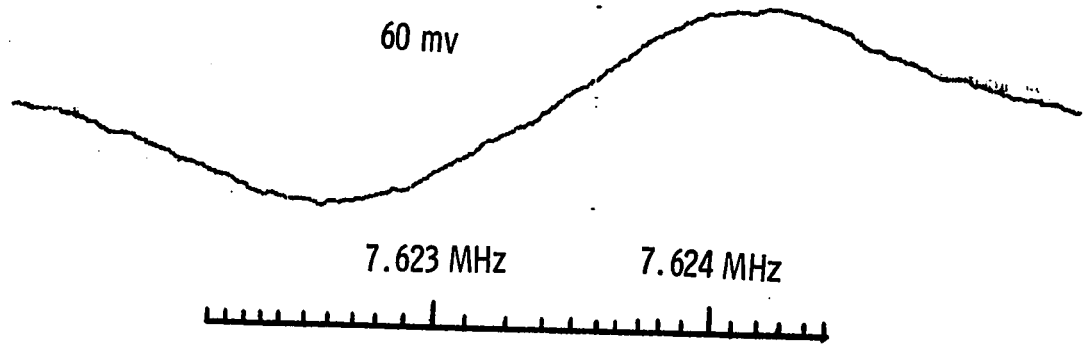
Figure III b shows typical resonances obtained during the main experiment. Those shown are for spectrometer observing powers corresponding to 20 millivolts peak-to-peak and 60 millivolts peak-to-peak measured across the sample coil. For each level we show an enhanced and an unenhanced resonance.

20 mv



20mv





from one another. The entire back plate of the spectrometer could be removed to provide accessibility to all the circuitry.

The capacitance of the tank circuit, housed in a separate part of the spectrometer away from the electronics, comprises a large variable capacitance of 50-600 μ mf and a smaller one of 5-25 μ mf. The two are arranged in a parallel, the smaller one being driven by a synchronous motor via a set of reduction gears to provide the frequency sweep of the spectrometer. By using different gears, the sweep rate could be varied, a typical sweep rate corresponding 10kHz per hour. Examples of typical resonances are shown in Figure III b.

b) The probe

In order to carry out double-resonance experiments it was necessary to construct a suitable crossed-coil probe. Such a probe must house the spectrometer and saturating coils as well as the field-modulation coils. The construction of the probe should be such that microphonics are reduced to a minimum and the components are well shielded.

The probe was therefore milled from a solid block

of aluminium and all the coils were wound on teflon formers which fitted snugly into milled cavities of the probe body. The spectrometer coil was wound into grooves machined on a cylindrical former. The internal diameter of the cylinder and the length of the coil were chosen so as to provide a good filling factor for the particular size sample that we had available. The inductance of the coaxial cable that connects this coil to the capacitance part of the tank circuit must be negligible compared to the inductance of the sample coil. There were a number of other considerations concerning the sample coil. Firstly, the Q-factor of the tank circuit must be as large as possible in order to have maximum sensitivity in detection of the NMR signal. Secondly, the inductance had to be such that the resonance frequency was around 7.5 MHz, the ^{23}Na resonance frequency in the magnetic field that we had available.

The spectrometer coil had an inductance of $2.1\mu\text{H}$, a self-capacitance of $40\mu\text{f}$ and a Q-factor of 135 at a frequency of 7.5 MHz when totally enclosed in the aluminium body of the probe.

The single crystal of NaNO_3 was housed in a cavity in the end of a teflon rod which fitted snugly into the vertically-mounted spectrometer coil. The axis of the coil and

rod coincided, and the rod was free to rotate about the common axis. The top of the rod had a 360° angular scale with the associated vernier being mounted rigidly on the body of the probe. In this way, therefore, the orientation of the crystal with respect to the horizontal steady magnetic field, could be varied and measured to within $1/4^\circ$.

The saturating coil was wound in two slots milled into a teflon former. Between these two slots a hole was drilled to take the spectrometer coil. By inserting the saturation coil into the probe in the horizontal plane, we could arrange for the steady field, the spectrometer radio-frequency field and the saturation field to be mutually orthogonal. The inductance of the saturating coil was $4.7\mu\text{H}$. This allowed a sufficiently large saturation field to be produced at the correct frequency, with the coil being part of the tuned circuit of the saturation signal amplifier unit.

The modulation field was provided by a Helmholtz coil arrangement, the coils of which were mounted on the probe such that the field was parallel to the steady magnetic field direction.

It is impossible to mount the spectrometer and saturation coils exactly orthogonal to each other to avoid direct coupling between them. In order to overcome the coupling, it

was necessary to incorporate a balance-mode system the details of which are discussed in Section III i) 6. It should be noted that the inclusion of this network will impose further constraints on the values of the inductances and Q-factors of the two coils.

The probe was mounted on rails between the pole pieces of the magnet. This allowed the probe to be moved in the gap and scales attached to the arrangement allowed the fixing of the probe's position in the field.

c) Phase-sensitive detector.

The final output from the Robinson spectrometer consists of an audio-frequency signal whose periodicity is equal to that of the field modulation so long as the modulation amplitude is small compared to the linewidth. The amplitude of this audio signal is then proportional to the first derivative of the nuclear absorption lineshape. If the spectrometer is swept through the resonance, the spectrometer output gives a representation of the first derivative of the lineshape (Andrew, 1955). The phase-sensitive detector is a device that produces a d.c. voltage proportional to $A \cos \phi$

where A is the amplitude of the Fourier component at the frequency of a predetermined reference signal and ϵ is the phase difference between the component and the reference signal. By feeding the reference signal and the modulation coils from the same audio oscillator and applying the spectrometer output to the detector input, the d.c. output will be the first derivative of the NMR signal. This output can then be displayed on a strip-chart recorder.

Our phase-sensitive detector was built according to the circuit diagram given by Schuster (1951). Preceding the mixer stage was a twin-T narrow band amplifier tuned to the 40Hz modulation frequency. This narrow band amplifier eliminates unwanted harmonics of the modulation frequency at 80Hz, etc, which will otherwise also give a d.c. output. These other harmonics will be particularly present in the output of the spectrometer if the modulation amplitude is not small compared to the linewidth of the resonance. The narrow band amplifier also cuts down the bandwidth of the noise entering the detector. The bandwidth of the amplifier depends on the Q-factor of the twin-T network. The Q-factor was chosen to be approximately 10, since a much higher Q imposes too strong a demand on the stability of the audio-oscillator frequency output. A low-pass filter with a time constant that could be

set at values from 1 to 80 seconds followed the Schuster mixer circuit.

d) Saturating equipment

The saturating signal was obtained from a Marconi radio-frequency signal generator model TF2002. The frequency stability of this unit was a few parts in 10^6 per hour. The frequency of the signal generator was monitored by a T.S.I. frequency counter, model number 385R, which had an accuracy of 3 parts in 10^7 . A vernier frequency adjustment on the signal generator enabled the frequency to be set to within 10 Hz at 7.5 MHz.

The output from the signal generator was fed into a tuned radio-frequency amplifier developing a maximum voltage of 80 volts peak-to-peak. The output from this amplifier was fed into the saturating coil of the probe and a portion was also fed into the flux-balance system as discussed in Section III g).

The Marconi generator had facilities for amplitude modulating the radio-frequency signal with known modulation depth. This facility was of great use in the initial inves-

tigation of the functioning of the spectrometer.

e) The Magnet

The large magnetic field required to lift the nuclear spin degeneracy was provided by a permanent magnet which had eight-inch pole pieces and a two-inch gap. It produced a field of 6700G and, as is usually the case with permanent magnets, its field was susceptible to thermal variations. This magnet had a temperature coefficient of approximately 1 gauss per $^{\circ}\text{C}$. In order to overcome this problem, the magnet was completely covered with one-inch thick sheets of styrofoam which were glued to the yoke of the magnet. This arrangement was then covered with a wooden box which had a removable strip to allow access to the gap. This system therefore minimized the effect of variations in the temperature of the laboratory on the magnetic field strength. Furthermore, the laboratory itself was thermostatically controlled and air-conditioned.

The magnet was situated on a concrete slab laid in the floor of the laboratory. However, as we shall see in the discussion of the flux-balance system in Section III g), the

problem of vibrations originating outside the laboratory remained an inconvenience in the final experiment.

An aluminium shelf was bolted across the magnet yoke near the magnet gap to support the flux-balance system. The Robinson spectrometer was placed on top of the magnet in order to minimize the length of the spectrometer-to-probe coaxial cable. However, care was taken to keep the spectrometer away from the fringe field of the magnet.

The homogeneity of the magnetic field was investigated using an NMR sample comprising a saturated aqueous solution of NaNO_3 . One tenth of a cc. of this solution was placed in a quartz phial. A little FeCl_3 was added to the NaNO_3 solution so that the Fe^{+++} ions would reduce the spin-lattice relaxation time T_1 of the sample. This allows the use of stronger spectrometer observing power so as to improve the signal-to-noise ratio of the resonance.

Detailed homogeneity plots were carried out in the gap of the magnet. Although the field was not symmetric in the gap, a region with a homogeneity of about 1 part in 10^5 over 1cc was found.

f) Frequency Marking System

The resonances were recorded by sweeping the spectrometer frequency as opposed to sweeping the magnetic field which would require simultaneous frequency-sweeping of the saturating signal. Since we wanted to set the saturation frequency to within 30 Hz of the centre frequency of the spectrum component being saturated, we needed to be able to measure the resonant frequency to this kind of accuracy. The spectrometer frequency sweep was not perfectly uniform. It was therefore not possible to use a frequency counter since this could not sample and display the varying frequency with enough accuracy without a substantial time lag. We now describe in some detail the frequency-marking procedure adopted, since it is our impression that such a scheme is neither widely used nor easily understood.

In essence, the system consisted of the following:
A crystal-controlled RMS frequency standard, model number M76BR, delivering a signal at 100kHz which is accurate to 1 part in 10^7 . This signal is then fed into a series of decade divider and multiplier circuits and amplifier units producing signals at 1MHz, 100kHz, 10kHz, 1kHz and 100Hz, both in the form of sinusoidal fundamentals and pulses. The 10kHz pulse

was then combined with the 1MHz or 100kHz fundamental to produce a series of signals 10kHz apart throughout the radio-frequency band. This mixing and dividing was done using an Airmec frequency-standard unit.

The spectrometer signal was picked up using a lead that was inserted into one of the oscillator tube cans on the spectrometer. The spectrometer signal and the mixer output were then fed into an Eddystone communications receiver which had a band-pass of 5kHz. Tuning the receiver to the spectrometer frequency meant that the audio output from the receiver consisted of the beat note between the spectrometer and the nearest 10kHz component marker. As the spectrometer sweeps through a range, the frequency of this beat note will change, decreasing as the spectrometer sweeps towards the pulse marker, and increasing as it sweeps away from the pulse marker. The beat note was fed into a loudspeaker and also to the X-plates of a double-beam oscilloscope. The 1kHz fundamental signal from the Airmec unit was fed to one set of the Y-plates and a 100Hz fundamental signal was fed to the other set of Y-plates. The resulting Lissajous figures indicate changes in the spectrometer frequency of 100Hz and 1kHz increments with respect to the 10kHz marker. After some practice, it was possible to identify these figures. Using an event marker

frequency markers could be put on the recorder chart.

What remains now is to identify the marker pulses which will allow the exact determination of the spectrometer frequency. This was done by first feeding a 100kHz pulse to the receiver. As the receiver tuning control is varied, the signal level meter (s-meter) on the receiver gives a large deflection each time the receiver is tuned to a 100kHz harmonic. Thus, having calibrated the receiver, it is possible to dial the receiver to within 10kHz of the desired frequency by simply reading the receiver scales since the band-pass of the instrument is only 5kHz. The tuning capacitances of the spectrometer are now adjusted to tune in the spectrometer to the frequency set on the receiver. The 100kHz pulse fed to the receiver is now replaced by a 10kHz pulse. Thus, the spectrometer is now beating against a 10kHz pulse whose frequency is known, with the resultant Lissajous kHz pattern going 5,4,3,2,1 as the spectrometer sweeps towards the marker and 1,2,3,4,5 as it passes the pulse and sweeps away. The process would of course be reversed if the spectrometer was in the frequency decreasing mode. Thus, by observing the pattern, markers can be put onto the recorder trace every 1000Hz and specifically identified. Observing the 100Hz Lissajous pattern will allow markers to be put on at 100 Hz

intervals. Finally, the 100Hz divisions can be subdivided by eye to give a final identified frequency accurate to a few tens of Hz.

g) The Flux-balance system

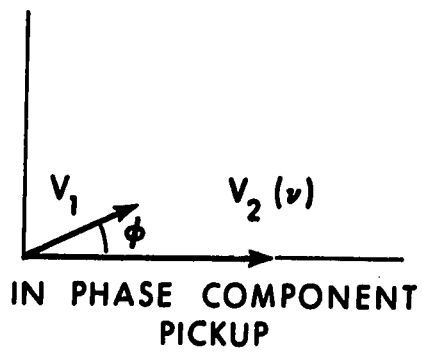
In the performance of a double resonance experiment, meaningful results can only be obtained if the direct pick-up between the saturating and spectrometer signal is negligible. This is because the NMR sensitivity of the spectrometer depends on the oscillation conditions of the spectrometer and this can be changed by an external signal, particularly if the external signal frequency and the spectrometer frequency are close.

In an idealized case of the saturating coil and the spectrometer coil being exactly orthogonal to one another, no pick-up between the coils would result. However, as was pointed out in the discussion of the probe, these coils cannot be mounted orthogonal to one another to the required accuracy. Furthermore, the coils are by necessity in a probe whose dimensions are restricted by the dimensions of the magnet gap. There will in general be a signal induced in the sample coil from the saturating coil via the body of the probe. This

Caption III c

Figure III c is a schematic representation of the orthogonal and in-phase pick-up components considered in the evaluation of the flux-balance system.

ORTHOGONAL COMPONENT
PICKUP



would in fact exist even if the two coils were exactly orthogonal, so long as the probe body is not symmetrically located with respect to the coils.

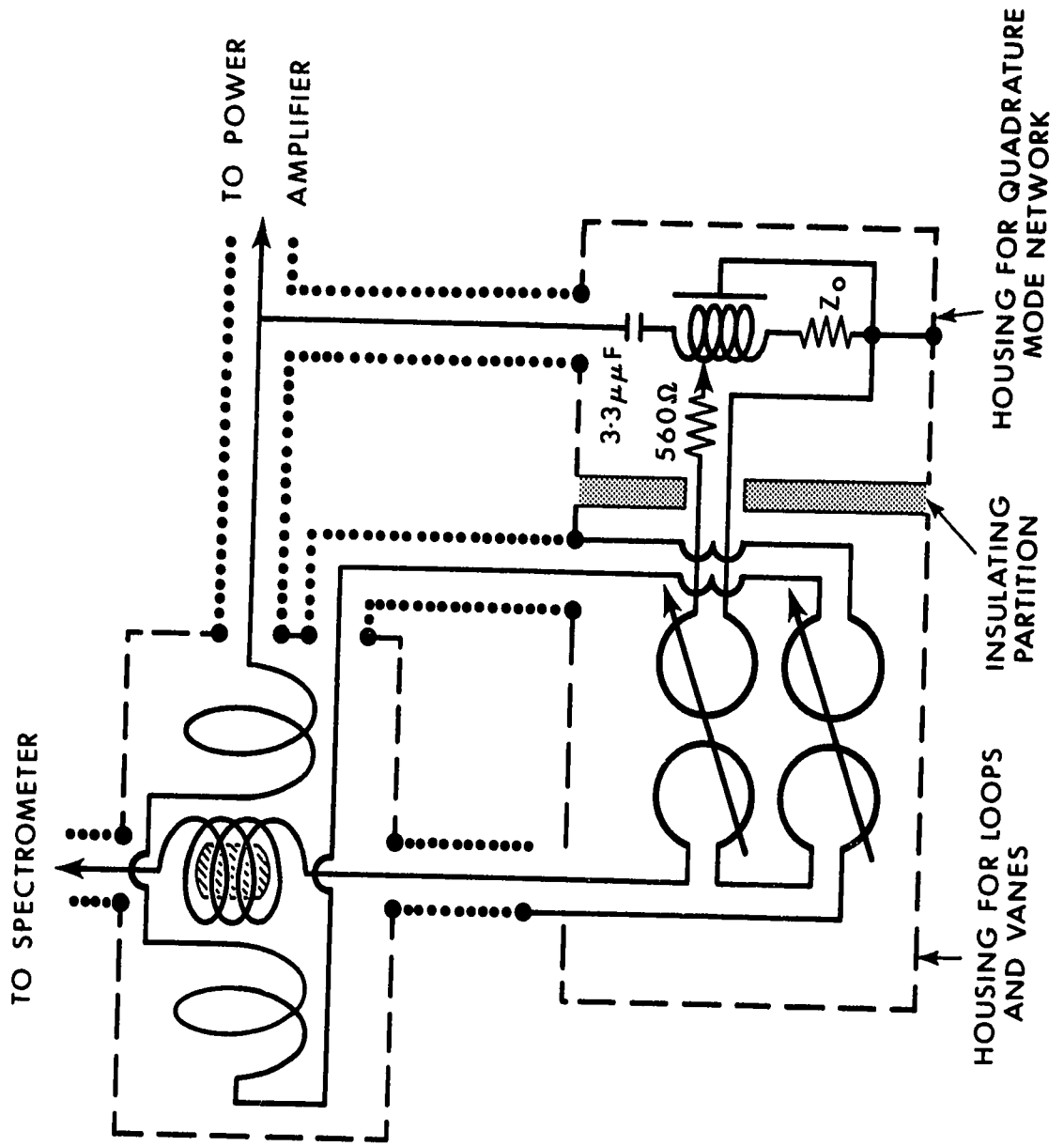
It was pointed out in Section I that the saturating signal had to be at least 40 volts peak-to-peak in order to ensure essentially complete saturation of a particular component of the spectrum. Also, the spectrometer level was in the range 10 to 100 millivolts peak-to-peak, where the enhancement is a linear function of the observing power. It is obvious from the difference between these two magnitudes and the fact that one wishes to make measurements at crystal orientations where the two frequencies are as close as 40kHz, that a sensitive flux-balance system is required.

Let us first consider the form of the voltage pick-up in the spectrometer coil due to the signal in the saturating coil. The resultant pick-up may be considered as having an amplitude coil as is illustrated in Figure III c. This pick-up can be resolved into two components one in-phase with the saturating voltage and a smaller component orthogonal to the saturating voltage. The in-phase component is due to direct coupling between the coils, and the orthogonal portion is due to induced pick-up via the resistive body of the probe.

The in-phase component is balanced out using the

Caption III d

Figure III d is a schematic diagram of the flux-balance system. Particular attention is paid in the diagram to the grounding and shielding of the units.



mutual inductance coupling between a loop inserted in the ground return of each of the two coils as shown in Figure III d . These loops are single turns thereby keeping to a minimum the additional inductance that they will introduce into their respective circuits. This is of particular importance in the case of the spectrometer coil since it is imperative that most of the inductance in this line is located at the crystal. Furthermore, the inclusion of the loop must not markedly reduce the Q-factor of the tank circuit. The two loops come within a few millimeters of each other and are supported along their whole length in the housing by styrofoam chips to minimize microphonics. The degree of coupling between the two loops is varied by means of a semi-circular vane that is rotated about an axis parallel to the common axis of the loops. This vane is made from one sixteenth brass plate and is one and a half inches long. By choosing the correct sense of the winding of these two loops, one will introduce a mutual inductance into the circuit that is opposite in sign to the mutual inductance between the spectrometer and saturating coils. Furthermore, by altering the position of the vane between the two loops, the magnitude of the coupling can be varied until complete cancellation has been achieved. The position of the vane was varied by means

of a 2000:1 reduction gear, such a reduction being necessary to provide the required fine adjustment. The use of a mutual inductance coupling introduced into the ground-returns of the two coils was first reported by Blume (1962).

In his paper, Blume also suggested a means of removing the orthogonal component. Blume's suggestion is to feed the spectrometer coil with a signal of variable phase and amplitude which is coherent with the saturating signal. This involves applying a portion of the saturating signal through a phase-shift network to the spectrometer coil via a potential divider. In our particular experiment, we require that the tank circuit has a large Q-factor and that this will not be significantly reduced by the orthogonal balance-mode. Furthermore, as was stated previously, the voltage applied to the saturating coil must be at least 40 volts peak-to-peak. These conditions could not be satisfied by the circuit suggested by Blume. Firstly, in order that the Q-factor is not significantly reduced, the orthogonal signal must be fed onto the spectrometer coil via a network whose effective resistance is much greater than the parallel resistance of the tank circuit which is of the order of 10^4 ohms. Since the output impedance of the delay line is 450 ohms, a resistance of the order of 10^5 ohms is required. The result is that the current

reaching the spectrometer coil is insufficient to cancel out the orthogonal pick-up. A further difficulty arises at the input to the delay line. The source of the coherent signal fed into the orthogonal mode is the voltage amplifier that feeds the saturating coil. If connected directly to the delay-line, whose input impedance ~ 450 ohms, the saturating coil is overloaded by the orthogonal network with the result that a sufficiently large voltage cannot be developed in the saturating coil. This difficulty could only be avoided by including a resistance of the order of 10^4 ohms in the delay line input circuit. This meant a further reduction in the magnitude of the signal that finally reaches the spectrometer coil. Therefore, it was not possible to use this arrangement in our apparatus.

The network we employed (Hughes and Reed, 1970) is schematically shown in Figure III d . The coherent signal is fed from the amplifier into the delay line via a small capacitance. The delay line is terminated by its characteristic impedance thereby providing a delay line output that is independent of the phase or delay line settings. The output is now coupled, via a 560 ohm resistance, into the tank circuit via an additional small loop introduced into the spectrometer coil ground-return lead as shown in Figure III d . The degree

of coupling can be varied again by the use of a vane as in the case of the in-phase coupling. Since the return loop is only a single coil, the effect on the Q-factor and inductance of the spectrometer coil is minimal. We found that this arrangement allowed us to cancel the orthogonal component without unduly loading the saturating coil. For the flux-balance system as a whole, we have independent control over the amplitude of the in-phase component, and independent control over both the phase and amplitude of the nominally orthogonal component. In principle, of course, one should be able to balance out the pick-up using only the orthogonal mode. However, the main component of the pick-up is the in-phase component caused by the mutual inductance coupling between the spectrometer and saturating coils. A separate mode where this component is cancelled greatly reduces the demands on the phase-shift properties of the delay-line. It is therefore a great advantage to have these two independent balance modes.

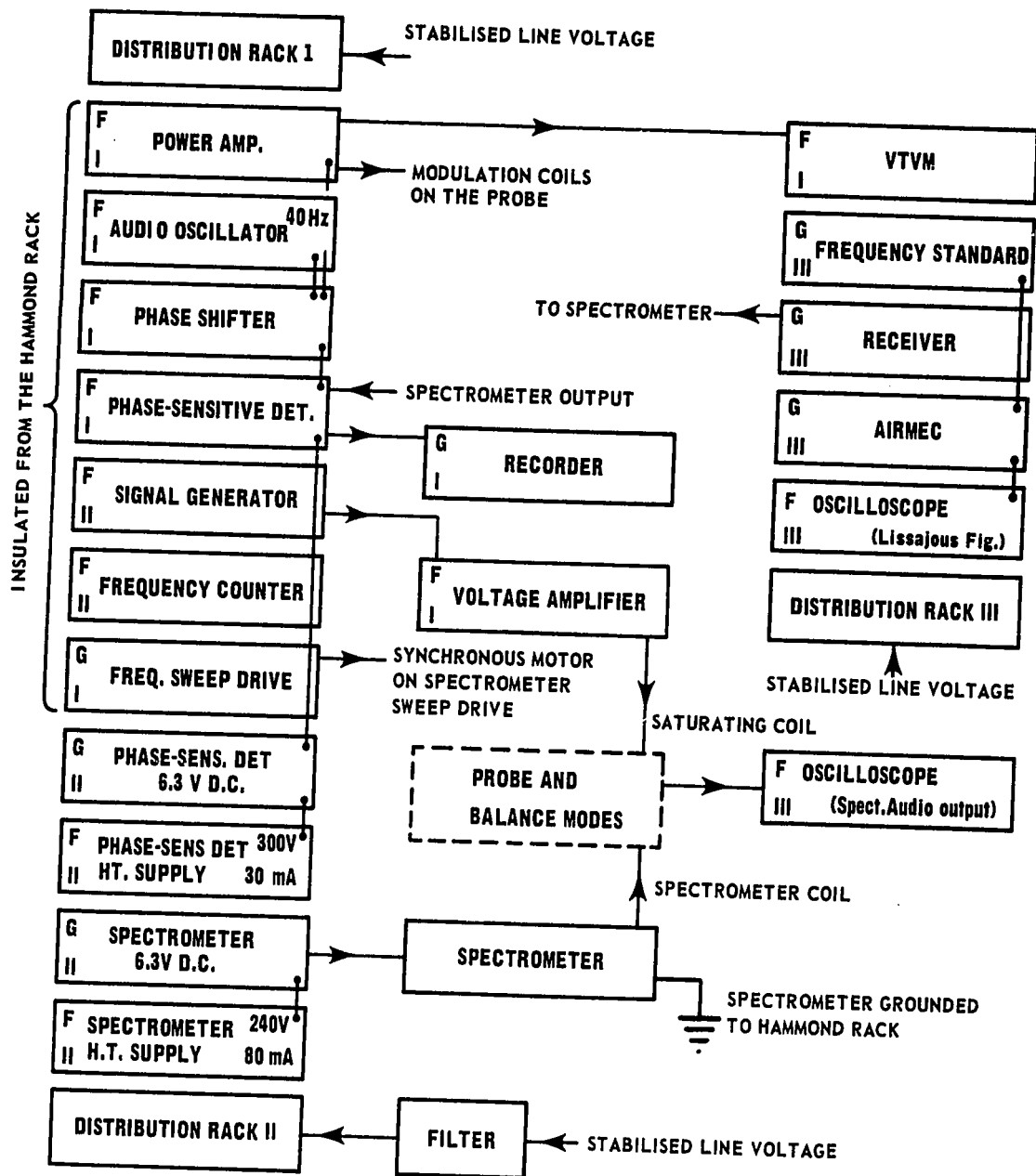
As is illustrated in Figure III d the orthogonal and in-phase modes are housed in compartments separated by a perspex insulating sheet. Both compartments were rigidly constructed from one quarter inch brass plate to form a completely closed unit. This provided shielding and reduced

the microphonic effects. The balance-mode system was located close to the spectrometer and probe to minimize the length of the connecting cables.

The correct grounding and shielding of the apparatus is of the greatest importance and this is particularly true as regards the case of the probe and the balance modes. The spectrometer and the saturating coils must have ground-return leads that are entirely separate so as to avoid interference between their respective signals. Furthermore, the housings should be grounded, yet in such a way that no ground-loop is created. The orthogonal-mode housing is grounded by the coaxial cable that brings in the signal from the saturation power amplifier. This casing also provides the ground for the delay line and in turn for the orthogonal coil that couples with the spectrometer coil. Thus the orthogonal-mode network is completely separate from the rest of the circuitry, except for the inductive coupling, yet it is always enclosed in a ground casing. It can be seen from Figure III d) that two connections are necessary between the probe and the in-phase mode housing. To avoid the ground loop problem, and yet maintain complete shielding, the ground of one coaxial cable is not connected to the housing even though it completes the return path of the coils. This was achieved by mounting the

Caption III e

Figure III e is a block diagram showing the interconnection of the units that make up our apparatus. Each unit is labelled to signify whether or not it is grounded. Also the distribution rack feeding the particular piece of equipment is shown.



F — ELECTRICALLY FLOATING EQUIPMENT

G — GROUNDED EQUIPMENT

I, II, III — REFERS TO PARTICULAR DISTRIBUTION RACK

coaxial connectors on insulating boards. This complicated situation becomes clear by consulting Figure III d . The two spectrometer-coil leads from the probe are especially sensitive to stray radiation and these were doubly-shielded using braid slipped over the cables and grounded only at the probe end of the cables. Thus, we have two completely independent ground-return paths for the two modes of the flux-balance system, and both are always contained in a shielded environment.

The performance of the balance mode system is discussed in detail in Section III i) 6.

h) Interconnection of units

We have already discussed in detail the most important parts of the equipment. During this discussion it was pointed out, particularly in connection with the balance-modes and the spectrometer, that grounding of the apparatus is of the utmost importance. As can be seen from Figure III e there are several units, which if grounded, would create ground-loops.

As is shown in the figure, the main power lines come to the apparatus by way of three distribution racks each with

six outlets. The line voltage feeding particularly sensitive pieces of equipment is stabilized by a line regulator. We have included in the figure an indication as to the distribution rack that feeds a particular unit, and whether or not the piece of apparatus is made floating with respect to the electrical ground.

i) Preliminary experimental procedures

This section is concerned with various measurements and calibrations that were necessary before the main experiment could be carried out.

1) The spectrometer

The performance of the spectrometer as a radio-frequency amplifier and detector was first checked at 7.5MHz using an audiomodulated radiofrequency carrier from the Marconi signal generator. This signal was traced through the various sections of the spectrometer, and components were altered until the performance of the system proved satisfactory. Further adjustments of the spectrometer components were carried out using the calibrator unit and the ^{23}Na NMR

signals from an aqueous solution of NaNO_3 and a single crystal of NaNO_3 . Suffice to say that this procedure took a good deal of time before satisfactory resonances were obtained.

2) Linearity and long-term stability of the spectrometer

The linearity and long-term stability of the spectrometer was investigated using the calibrator unit. A known calibrator voltage, sufficient to give a deflection on the chart comparable with that of the ^{23}Na signal in NaNO_3 , was fed into the spectrometer. The output from the phase-sensitive detector was then recorded for several hours. The long-term stability of the deflection caused by the calibrator signal was found to be satisfactory. The phase of the calibrator signal was then changed by 180° , resulting in a deflection in the opposite sense on the chart recorder. The total deflection corresponding to the magnitude of the calibrator signal was then measured. As pointed out in Section III a), the calibrator unit provides a pseudo resonance. The linearity of the spectrometer to NMR signals of different strength may therefore be checked by measuring the spectrometer sensitivity to different values of the calibrator voltage.

The procedure described above was therefore repeated for different calibrator voltages. The sensitivity in milli-

meters of recorder deflection per millivolt of calibrator signal is shown in Table III a. It is apparent that the system is linear in its sensitivity to within the limits imposed by the signal-to-noise ratio.

3) Phase-shift network

The phase-shift network provides the coherent 40Hz signals for the modulation coils, calibrator unit and the reference input to the phase-sensitive detector. Each output has an independent phase and amplitude control. Using an NMR sample containing an aqueous solution of NaNO_3 , the phase of the reference signal was adjusted until a maximum resonance signal was recorded. Then, using a calibrator signal, the phase of the calibrator was adjusted for maximum response on the chart. In this way, the correct phase relationships between the various signals was obtained.

4) Field modulation

The 40Hz modulation of the steady magnetic field is provided by means of the Helmholtz coil arrangement that is built into the probe. A small search-coil was used to investigate the magnitude and homogeneity of the modulation field produced in the region of the sample. The modulation

Table III a

Calibrator signal (millivolts)	Deflection (centimeters)	Deflection/Calibrator signal (centimeters/millivolts)
96.0	4.64	4.83×10^{-2}
134.3	6.41	4.77×10^{-2}
174.0	8.43	4.84×10^{-2}
214.0	10.28	4.81×10^{-2}

field was calibrated by measuring the voltage induced in the search coil by a known modulation signal. The amplitude V_0 in volts of the induced voltage is related to the modulation amplitude in gauss by the equation

$$B_0 = \frac{10^8 V}{NA \omega_m} \quad (\text{III } 3)$$

where ω_m is the modulation angular frequency, and NA is the area-turns of the search coil. Using an accurate flux-meter and a known magnetic field, the area-turns of our search-coil was found to be 103.8 cms^2 . The modulation field was found to be 1.6 ± 0.1 gauss peak-to-peak for a 1.0 volt peak-to-peak output from the power amplifier that fed the Helmholtz coils. This measurement was carried out for various positions in the probe sample region but no detectable variation in the field could be found over a region of several ccs.

5) Performance of the flux-balance system

We have discussed in Section III g) the problems involved with the crossed-coil probe and we outlined the arrangement that was developed to counteract the problems in our case. In this section we shall be concerned with the performance of the balance modes in a double resonance exper-

iment.

A gross indication of the saturating signal directly affecting the spectrometer can be seen by observing the spectrometer radio-frequency level meter as the saturating signal is increased. The pick-up by the spectrometer coil results in the spectrometer being forced to oscillate at the saturating signal frequency rather than at its own free-running value. The detector level indicates this by an initial decrease due to suppression of the free-running oscillation, followed by a rapid increase due to the complete breakdown of the spectrometer's operation.

A more sensitive indication of the effect of the saturating signal on the spectrometer can be obtained by observing the audio output from the spectrometer. This output contains a sinusoidal component whose frequency is the difference between the frequencies of the saturating and spectrometer signals. As the influence of the saturating signal on the spectrometer increases, so does the amplitude of this audio output.

The most sensitive criterion is the frequency of the spectrometer, particularly as illustrated by the Lissajous pattern on an oscilloscope. An extremely small unbalanced saturating signal will cause a change in the Lissajous display,

without it being perceptible to the unmusical ear.

The most important criterion is the effect that the saturating signal has on the spectrometer's sensitivity to an NMR signal. When the spectrometer is being to some degree driven, it is found that the NMR signal intensity is artificially increased.

This effect was investigated by measuring the intensity of the enhanced signal as a function of the deliberately-introduced coupling between the saturating and spectrometer coils. The crystal was orientated with respect to the field so that $\theta = 45^\circ$. This corresponded to a frequency separation between the saturating and spectrometer signals of approximately 42 kHz. A saturating voltage of 40 volts peak-to-peak was applied to the centre line component and observations of the high-frequency satellite intensity were made at an observing power of 25 millivolts and then repeated for an observing power of 60 millivolts. The misbalance was measured in terms of the amplitude of the audio signal from the spectrometer output. This amplitude was measured in centimeters on an oscilloscope with a 25 volts/cm sensitivity, and is to this extent an arbitrary measure. The data is given in Table III b and shown in Figure III f. For the case of a 25 millivolt observing level the intensity of the recorded enhanced

Table III b

i) 25 millivolt level

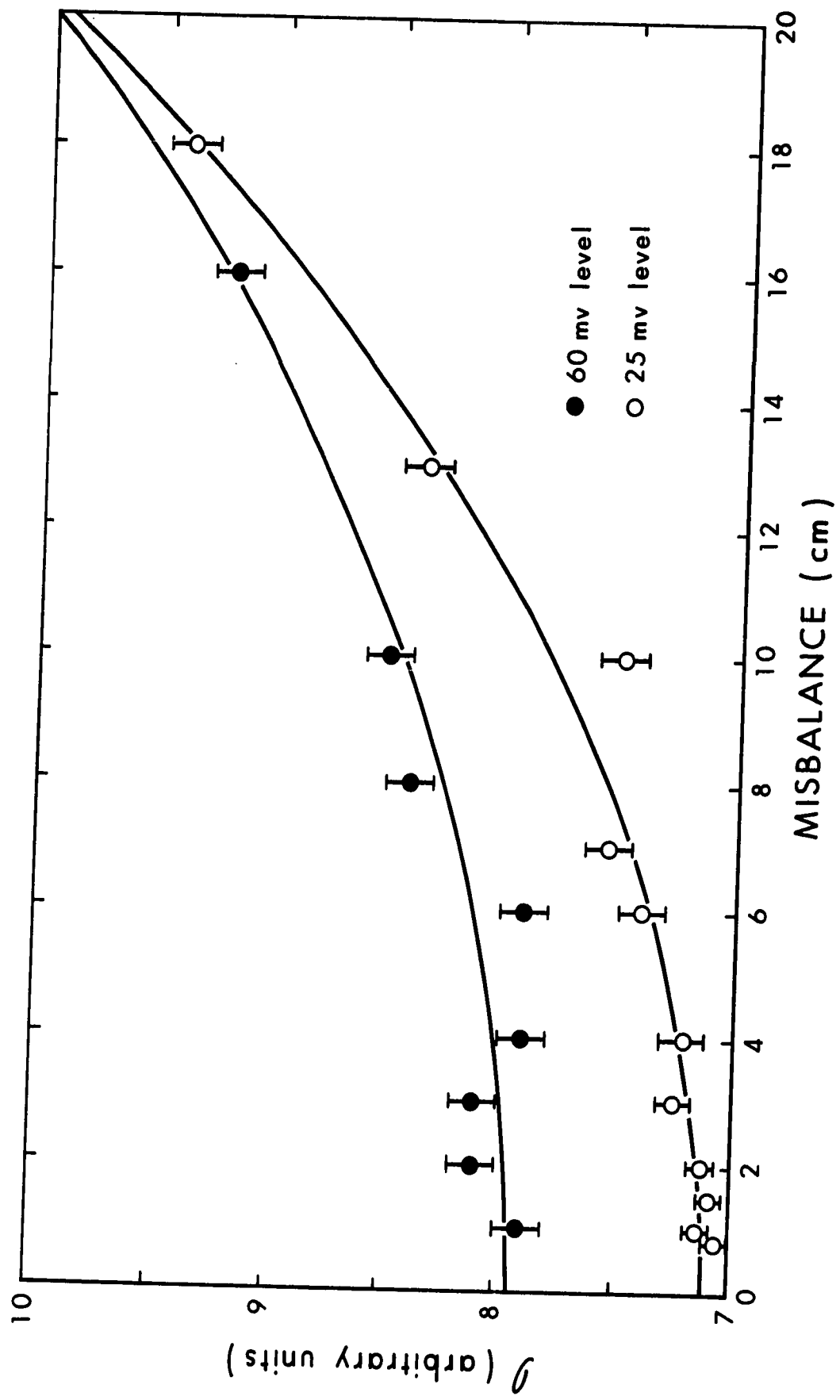
(arbitrary units)	Misbalance (centimeters)
7.05	0.80
7.125	1.00
7.07	1.50
7.117	2.00
7.25	3.00
7.20	4.00
7.40	6.00
7.55	7.00
7.50	10.00
8.35	13.00
9.40	18.00
9.80	20.00

ii) 60 millivolt level

(arbitrary units)	Misbalance (centimeters)
7.90	1.00
8.10	2.00
8.10	3.00
7.90	4.00
7.90	6.00
8.40	8.00
8.50	10.00
9.20	16.00

Caption III f

Figure III f shows the intensity of a satellite, recorded whilst the centre line component is severely saturated, as a function of the deliberate misbalance flux-balance system. The intensity of the satellite is given in arbitrary units and the deliberate misbalance is expressed as centimeters of audio signal from the spectrometer audio output as discussed in the text. The variation of intensity is given for two values of the spectrometer observing power corresponding to 25 millivolts and 60 millivolts peak-to-peak across the sample coil. For both sets of data, the saturating and spectrometer frequencies differed by 40 kHz.



signal does not begin to increase until the pick-up amplitude exceeds 2cm on the oscilloscope. A change in the note does not become audible until the pick-up exceeds about 3cm. After 4cm, the intensity rapidly increases, clearly illustrating that data taken above such a misbalance situation would lead to very erroneously values of the enhancement. It is noticed that the indication of the misbalance concerned with the suppression of the detector level and its subsequent increase is not observed until the degree of misbalance exceeds some 17cm.* Clearly, this criterion for balance is completely wrong and explains the large enhancement values reported in the author's M.Sc. thesis. For an observing power of 60 millivolts, the increase in the enhanced intensity occurs at a higher misbalance, as one would expect.

For all the enhancement data reported in this thesis, the pick-up was maintained below 2cm on the oscilloscope. If, during any run, the pick-up exceeded this value, the resonance was discarded and the run was repeated.

Let us now consider in absolute terms the ability of the balance modes to cancel out pick-up between the two coils. In order to measure the signal induced at the saturating frequency in the spectrometer coil, it was necessary to use a communications receiver in order to reject 2nd and higher

* We are grateful to M. Smith for pointing out that the intensity \propto (pickup)²

harmonics which otherwise would overwhelm the required signal. Because of the low input impedance of the receiver, a pre-amplifier unit was inserted between the coil and the receiver. This preamplifier had a low noise-figure, a gain of approximately 200 at 7.5 MHz, and an input impedance of 10^7 ohms shunted by a 2 μ pf. The preamplifier therefore did not significantly load the spectrometer coil.

A signal of 50 volts peak-to-peak was fed to the saturating coil with the flux-balance system disconnected, and the pick-up at the spectrometer coil was found to be 0.35 volts peak-to-peak. (This signal was so large that it could be measured directly on a calibrated oscilloscope. This voltage is the sum of the direct pick-up due to the non-orthogonality of the coils, and the orthogonal component caused by currents induced in the resistive body of the probe. The coupling between the saturating and spectrometer coils was then minimized using the in-phase flux-balance mode alone, and the pick-up was found to be 3.3 millivolts. Using both modes the minimum was 5 microvolts. The technique used to minimize the pick-up was to first use the in-phase mode and then make the final adjustment with the orthogonal mode. The in-phase mode was by far the most effective as one would expect since most of the coupling is due to the direct coupling.

The frequency of the saturating signal was now changed over a range of approximately 5kHz and the resultant pick-up was measured by means of the preamplifier-communications receiver combination. By readjusting to a position of minimum pick-up it was found that the in-phase mode was frequency-dependent while the orthogonal was apparently frequency-independent. We attribute this to the effect of stray capacitances in the probe and the in-phase mode housing. The results of the frequency dependence studies are given in Table III c and illustrated in Figure III g.

Let us now consider the temperature dependence of the flux-balance system. This was investigated by minimizing the pick-up and then changing the temperature of the laboratory by 5°C . Then the temperature of the laboratory was allowed to return to its original value, a process that took a few hours. Every ten to fifteen minutes, the degree of misbalance was measured using the centimeter criterion mentioned in Section III i) 5. At each temperature setting, the change in the saturation frequency needed to minimize the pick-up was found. Using the curve given in Figure III g, the frequency shifts were related to microvolt, levels and a temperature coefficient of $20\mu\text{V}/^{\circ}\text{C}$. was calculated. The data is given in Table III d.

Let us now propose a model to analyse the frequency

Table III c

ν (MH _z)	$ V ^2$ (μV) ²
7.5638	5516
7.5642	3873
7.5650	1821
7.5655	1382
7.5659	1466
7.5661	1647
7.5667	2798
7.5671	4127
7.5675	5609
7.5679	7683
7.5684	10835

Caption III g

Figure III g shows the square of the pick-up voltage as a function of the saturating frequency as the saturating frequency is mis-set. The setting of the flux-balance system was unaltered during these runs.

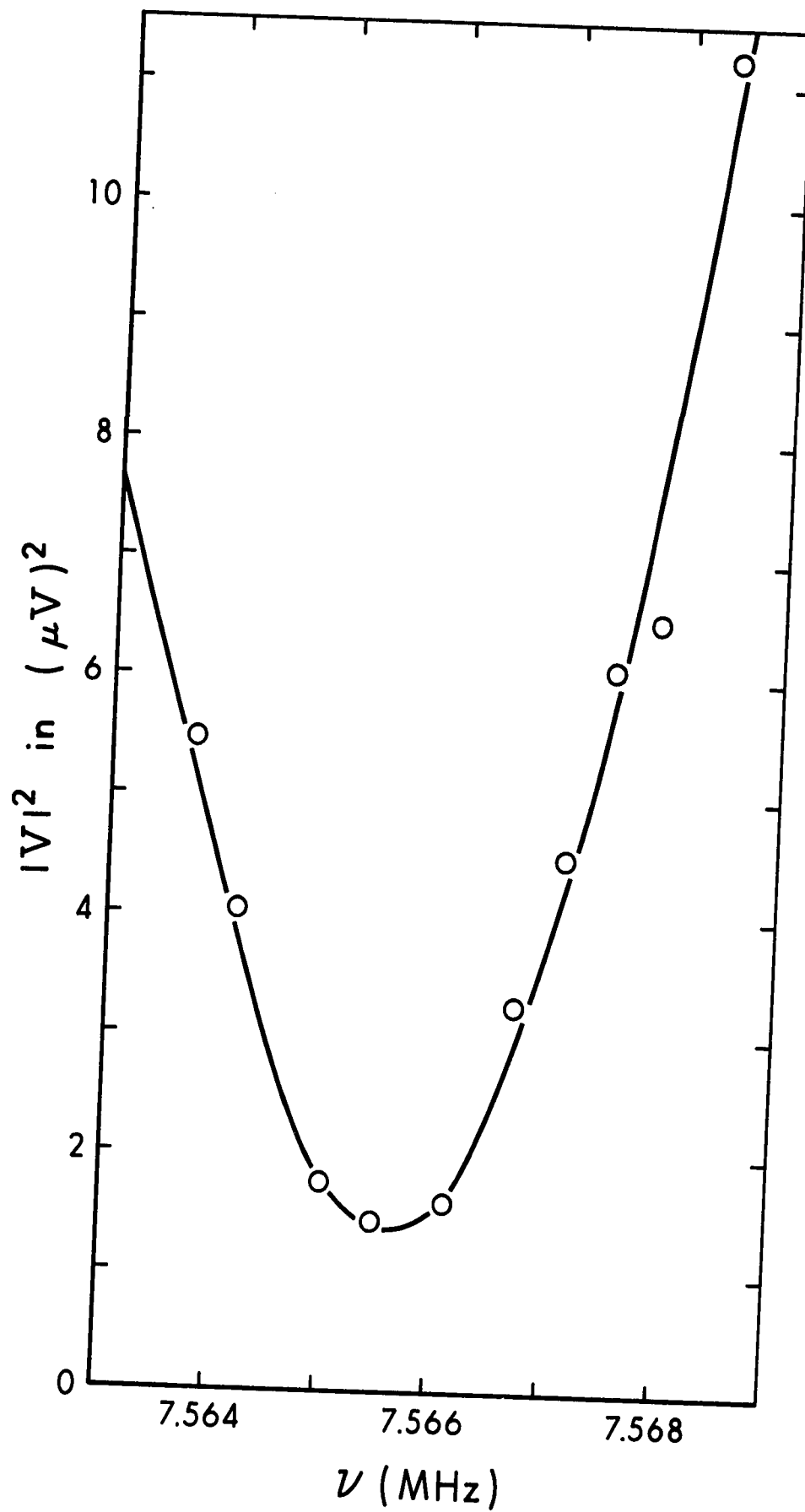


Table III d

Magnet temp. (°C)	Pick-up (μ V)
22.2	1.09
23.5	1.09
24.1	9.25
24.2	24.48
24.3	38.08
24.4	41.89

dependence of the pick-up of the system. Consider that there is a residual pick-up of magnitude V_1 that has a phase angle ϕ with respect to the in-phase component, and that this is frequency-independent. We also have an in-phase component of amplitude V_2 due to the direct coupling which the previous data shows is frequency dependent term. The resultant pick-up V is therefore related to these two terms by the expression

$$|V|^2 = (V_2 + V_1 \cos \phi)^2 + (V_1 \sin \phi)^2 \quad (\text{III } 4)$$

Now we can write V_2 in the approximate form

$$V_2 = K (\nu - \nu_0) \quad (\text{III } 5)$$

where K is some constant, ν is the saturating frequency and ν_0 is the frequency at which the in-phase component V_2 vanishes. Thus we can write (III 4) as

$$|V|^2 = K^2 \nu^2 + (2KV_1 \cos \phi - 2K\nu_0) \nu + (K^2 \nu_0^2 - 2K \cos \phi V_1 \nu_0 + V_1^2). \quad (\text{III } 6)$$

Such a model would predict that the frequency dependence of the pick-up would be in the form of a parabola, and this is indeed the case for the data shown in Figure III g).

Using a least squares analysis of the data, we find

$$|V^2| = (1221.38) \nu^2 + (-13690.82) \nu + (39726.23) \quad (\text{III } 7)$$

giving K the approximate value $35\mu\text{V}$ per kHz. The theoretical fit to the experimental data is shown in Figure III g.

The question remains as to the causes of the pick-up V_1 . By studying the operation of the spectrometer when recording enhanced signals it becomes apparent that the limitation of the flux-balance performance is due to microphonics. We therefore attribute V_1 to microphonic effects.

6) Effect of mis-setting of saturating frequency

To ensure the complete saturation of a component of the spectrum, the applied power must have sufficient magnitude and be applied at the correct frequency, corresponding to the maximum of the absorption curve. In the case of the recorded first derivative of the resonance this frequency will be the crossover value. An insufficient magnitude or incorrect frequency results in the recorded enhancement being less than the value for a completely saturated component. The effect of insufficient power will be discussed later. In this section we shall discuss the effect of deliberately mis-setting the frequency of the saturating signal.

According to the BPP theory, the saturation behaviour of a homogeneously-broadened resonance line is given by equation (II 65). However, it was pointed out by Redfield (1955) that the BPP theory was invalid for $S \gg 1$, where $S = \gamma_n^2 H_1^2 T_1 T_2$ and T_2 is the so-called spin-spin relaxation time, except for the particular case where the saturating power is applied to the centre of the resonance. This was confirmed experimentally by Goldberg (1961) by measuring M_z , the z-component of the nuclear magnetization, of the ^{23}Na spin system in NaCl as a function of the mis-setting of the satu-

rating frequency from the centre value. For $S = 1$, the measured M_z values were in agreement with the BPP theory. However, for $S = 10$, the BPP theory was obviously in error except when the saturation frequency corresponded to the centre of the resonance, but the measured values were in agreement with the Redfield theory. According to this theory it is not possible to obtain complete saturation of a resonance ($M_z=0$) using a steady-state technique if the saturating frequency is mis-set. It was therefore vitally important to investigate the effect, on the satellite enhancement, of deliberately mis-setting the frequency of the saturating signal applied to the centre line. Our data is shown in Figure III h for a field modulation amplitude of 0.65 G and 1.30 G. It is clear that mis-setting the saturating frequency seems to have a relatively small effect. Furthermore, the degree of mis-set necessary to produce a significant effect on the satellite enhancement is dependent on the modulation amplitude. This effect can be explained by realizing that the field modulation has the effect of modulating the saturating frequency across the centre line. It thus appears that so long as the saturating frequency is swept by the modulation across the centre of the resonance then essentially complete saturation can be produced even though the saturating signal is mis-set.

Table III e

i) Modulation amplitude 0.65G (0.73kHz)

$\delta\nu$ (Hz)	Unsaturated intensity (centimeters)	Saturated intensity (centimeters)	Enhancement
0	6.600	9.775	1.482
-100	6.575	9.525	1.450
-250	6.875	10.200	1.483
-500	6.575	9.625	1.465
-750	6.775	9.600	1.418
-1000	6.700	9.150	1.365
-1250	6.700	8.750	1.305
-1500	6.600	7.850	1.190
-1750	6.825	7.525	1.101
-2000	6.675	7.000	1.048
100	6.900	10.175	1.475
250	6.675	10.050	1.502
500	6.670	9.900	1.478
750	6.878	9.875	1.435
1000	6.800	9.250	1.360
1250	7.000	9.325	1.331
1500	6.725	8.275	1.225
1750	6.850	7.700	1.122
2000	6.500	7.150	1.090

Table III e

i) Modulation amplitude 0.65G (0.73kHz)

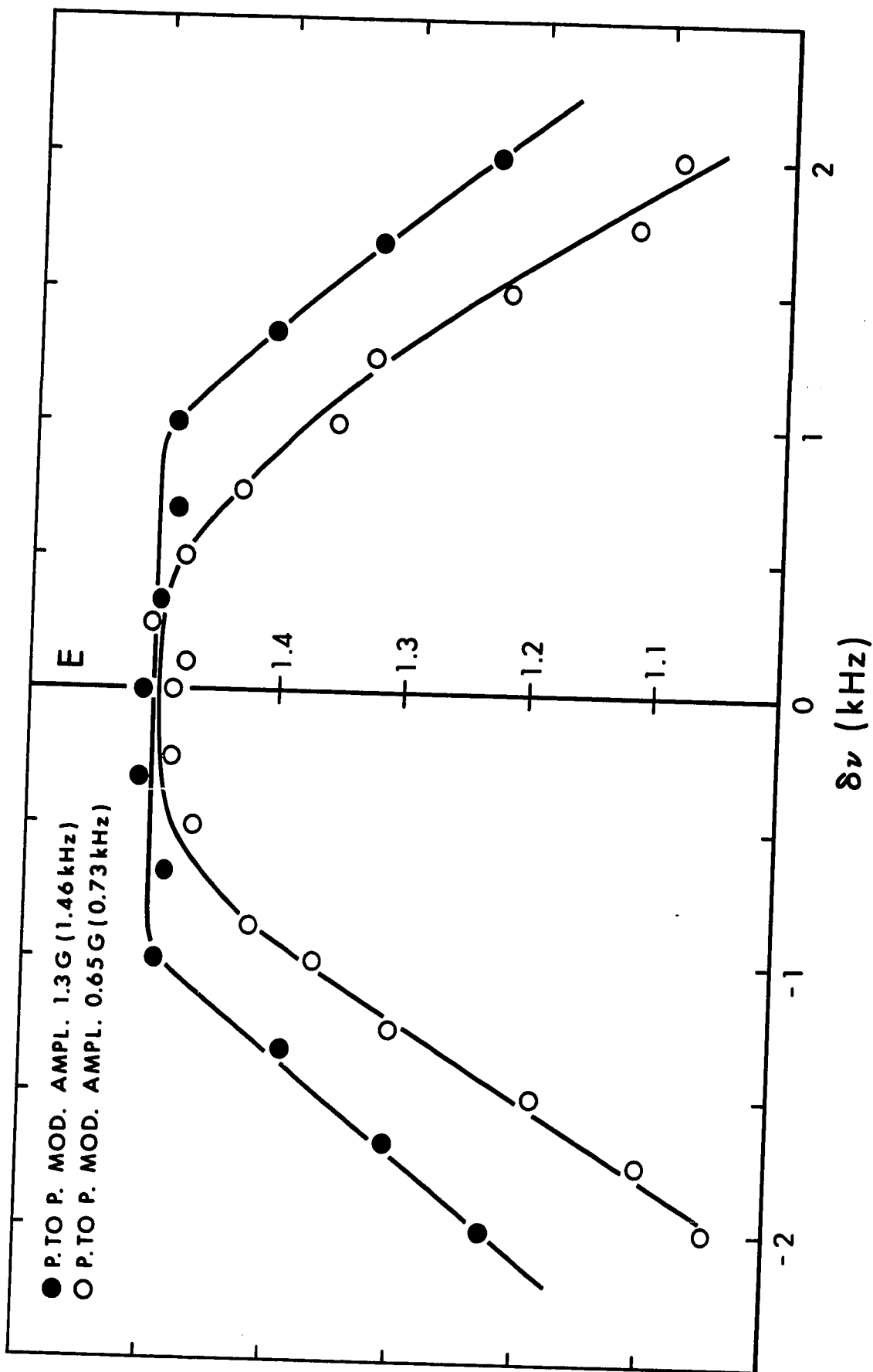
$\delta\nu$ (Hz)	Unsaturated intensity (centimeters)	Saturated intensity (centimeters)	Enhancement
0	6.600	9.775	1.482
-100	6.575	9.525	1.450
-250	6.875	10.200	1.483
-500	6.575	9.625	1.465
-750	6.775	9.600	1.418
-1000	6.700	9.150	1.365
-1250	6.700	8.750	1.305
-1500	6.600	7.850	1.190
-1750	6.825	7.525	1.101
-2000	6.675	7.000	1.048
100	6.900	10.175	1.475
250	6.675	10.050	1.502
500	6.670	9.900	1.478
750	6.878	9.875	1.435
1000	6.800	9.250	1.360
1250	7.000	9.325	1.331
1500	6.725	8.275	1.225
1750	6.850	7.700	1.122
2000	6.500	7.150	1.090

ii) Modulation amplitude 1.3G (1.46kHz)

$\delta\nu$ (Hz)	Unsaturated intensity (centimeters)	Saturated intensity (centimeters)	Enhancement
0	6.025	9.075	1.505
-330	5.800	8.775	1.510
-670	5.925	8.875	1.498
-1000	5.850	8.726	1.493
-1330	5.950	8.275	1.391
-1670	5.925	7.725	1.305
-2000	5.850	7.150	1.223
330	5.950	8.925	1.499
670	5.900	8.750	1.483
1000	6.050	9.000	1.487
1330	5.875	8.300	1.411
1670	5.950	7.875	1.324
2000	6.075	7.525	1.238

Caption III h

Figure III h shows the enhancement of the high frequency satellite due to severe saturation of the centre line as a function of the deliberate mis-set of the frequency of the saturating signal. The two curves correspond to field modulation amplitudes of 0.65 G and 1.30 G. The solid lines do not refer to any particular theory but are simply drawn through the points.



It should be possible to treat this effect by analyzing the frequency-modulated saturating signal in terms of its component sidebands. However, the important feature of the data is that it is not essential to maintain the saturating frequency at the centre frequency. In our determination of the enhancement, the saturating frequency was always maintained within $30H_z$ of the centre of the resonance. It might appear from Figure III h that the satellite enhancement is slightly dependent on the modulation amplitude at zero mis-set. However, later more careful measurements showed that this was not the case.

The experimental procedure for determining the saturating frequency was to measure the cross-over frequency of the resonance to be saturated, in the frequency-increasing and then frequency-decreasing sweep modes. These values were not exactly coincident because of the time constants of the apparatus. It is obvious that the correct cross-over frequency at which the saturating power should be applied is the mean of these two results.

In order to check that no large errors were made in the determining of the saturation frequency, the enhancement of a component was measured for the case of the saturating power being deliberately mis-set by $\pm 1\text{kHz}$. An incorrect

saturation frequency would show up by the enhancements being different in the two cases.

7) Calibration of the sample holder angular scale

It was necessary to calibrate the angular reading θ' on the rotation scale fixed to the sample holder in terms of the angle θ between the triad axis and the steady magnetic field. If the symmetry axis of the crystal is perpendicular to the axis of rotation, then $\theta = \theta' + \gamma$ where γ is a constant. The separation of the satellites is related to the angle θ by the equation

$$\Delta\nu = \frac{e^2 Qq}{2h} (3\cos^2 \theta - 1) \quad (\text{III } 8)$$

where $e^2 Qq/h$ is the quadrupole coupling constant. By measuring the satellite splitting as a function of θ' , we can fit the data to equation (III 8) to obtain the relation between θ and θ' . Furthermore, by comparing the measured quadrupole coupling constant with previous measured values (Pound, 1950, Andrew et al., 1962) we are able to check that the triad symmetry axis is essentially perpendicular to the axis of rotation of the crystal.

The satellite separation was measured at 30° intervals

Table III f

i) $\phi = 2.8 \pm 1.5^\circ$

θ' (degrees)	$\Delta\nu$ (kHz)
0	-128.23
30	94.24
60	307.05
90	295.30
120	77.78
150	-136.93

ii) $\phi = 32.8 \pm 1.5^\circ$

θ' (degrees)	$\Delta\nu$ (kHz)
0	330.20
30	252.85
60	-2.0
90	-164.23
120	-80.29
150	167.45

of θ' through a range of 180° . Such a procedure was carried out twice, once each for the two values of the azimuthal angle ϕ . The point of repeating the measurements for the second setting was to check that the symmetry axis was still perpendicular to the rotation axis after the re-orientation of the sample to change the ϕ value. The data for the two cases is given in Table III f. Using a least squares analysis technique (Whittaker and Robinson, 1925) a linearized equation giving the satellite separation $f(\theta')$ in kHzas.

$$f(\theta') = 84.87 + (-212.43) \cos 2\theta' + (132.92) \sin 2\theta' \quad (\text{III } 9)$$

can be obtained for the setting $\phi = 2.8 \pm 1.5^\circ$. For the case $\phi = 32.8 \pm 1.5^\circ$ the linearized form is

$$f(\theta') = 84.0 + (248.58) \cos 2\theta' + (47.25) \sin 2\theta' \quad (\text{III } 10)$$

The general form of this equation can be written as

$$f(\theta') = A + B \cos 2\theta' + C \sin 2\theta' \quad (\text{III } 11)$$

and the relationship between the angles θ and θ' can be written as

$$2\theta' + 2\gamma = 2\theta \quad \text{or} \quad \theta = \theta' + \gamma. \quad (\text{III } 12)$$

Therefore, we may write

$$R\cos(2\theta' + 2\gamma) = R\cos 2\theta' \cos 2\gamma - R\sin 2\theta' \sin 2\gamma = R\cos 2\theta \quad (\text{III } 13)$$

where $R = \sqrt{B^2 + C^2}$.

If we write

$$f(\theta') = A + R\cos(2\theta' + 2\gamma) \quad (\text{III } 14)$$

then by comparing equations (III 11) and (III 13) we obtain the relationships

$$R\cos 2\gamma = B, \quad R\sin 2\gamma = -C \quad \text{and therefore } \tan 2\gamma = -C/B \quad (\text{III } 15)$$

By re-arranging equation (III 13), we can write

$$f(\theta') = A + R\cos(2\theta' + 2\gamma) = A + R\cos 2\theta = (A - R) + 2R/3(3\cos^2 \theta). \quad (\text{III } 16)$$

Defining $X = A - R$ and $Y = 2R/3$ we have

$$f(\theta) = Y \left(3\cos^2 \theta - \frac{X}{Y} \right). \quad (\text{III } 17)$$

Knowing the values of A, B and C from the linearized equations we can calculate the angle 2γ and the coefficients X and Y.

For the case $\phi = 2.8 \pm 1.5^\circ$ we have $\gamma = 6^\circ 1'$ therefore giving the relationship

$$\theta = \theta' + 6^\circ 1' \quad (\text{III } 18)$$

Thus the satellite separation is given by

$$\Delta\nu = 167.1 (3\cos^2\theta - 165.6/167.1) \quad (\text{III } 19)$$

The experimental error in the quantities 165.6 and 167.1 is estimated at 1kHz. Equation (III 9) is thus of the form $\Delta\nu \propto (3\cos^2\theta - 1)$. The quadrupole coupling constant is therefore $334.0 \pm 2\text{kHz}$, and is in good agreement with the values given by Pound (1950) and Andrew et al. (1962).

For the case $\phi = 32.8 \pm 1.5^\circ$, by a similar technique we get

$$\theta = \theta' + 0^\circ 37' \quad (\text{III } 20)$$

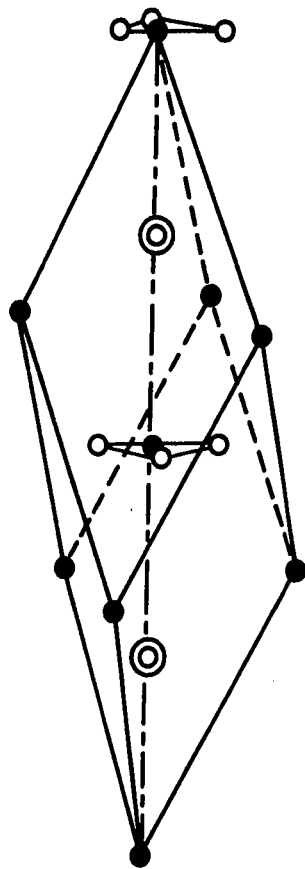
and a satellite separation given by

$$\Delta\nu = 168.0 (3\cos^2\theta - 169.0/168.0) \quad (\text{III } 21)$$

In this case the quadrupole coupling constant is $336.0 \pm 2\text{kHz}$, again in agreement with the accepted value. We therefore conclude that the symmetry axis of the crystal was in both cases essentially perpendicular to the axis of rotation of the sample.

Caption III i

Figure III i shows the rhombohedral unit cell of sodium nitrate. For clarity only two groups of oxygen atoms are shown.



- ⊙ Na
- N
- O

8) Crystallographic information on NaNO_3

Sodium nitrate crystallizes in the rhombohedral system (space group $R\bar{3}c$, D_{3d}^6) with two molecules in the unit cell. As shown in Figure III i, there are nitrogen atoms at each corner of the unit cell and also at the centre; the sodium atoms lie half-way between the nitrogen atoms on the triad axis of the cell at $\frac{1}{4} \frac{1}{4} \frac{1}{4}$ and $\frac{3}{4} \frac{3}{4} \frac{3}{4}$. The nitrate groups are planar, each nitrogen being situated at the centroid of an equilateral triangle of oxygen atoms whose plane is normal to the triad axis. The sides of the oxygen triangles lie parallel to the projection of the cell edges on a plane normal to the triad axis, the orientation of the triangles alternating by 180° as one proceeds along the triad axis. The oxygen positions are given by the parameters.

$$u, \bar{u}, 0; \bar{u}, 0, u; 0, u, \bar{u}; \frac{1-u}{2}, u+\frac{1}{2}, \frac{1}{2}; u+\frac{1}{2}, \frac{1}{2}, \frac{1-u}{2}; \frac{1}{2}, \frac{1-u}{2}, \frac{1+u}{2}.$$

The sodium atoms therefore have an environment of trigonal symmetry, and the axial field gradient tensor is axially symmetric.

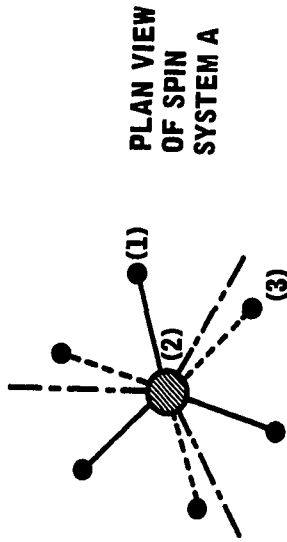
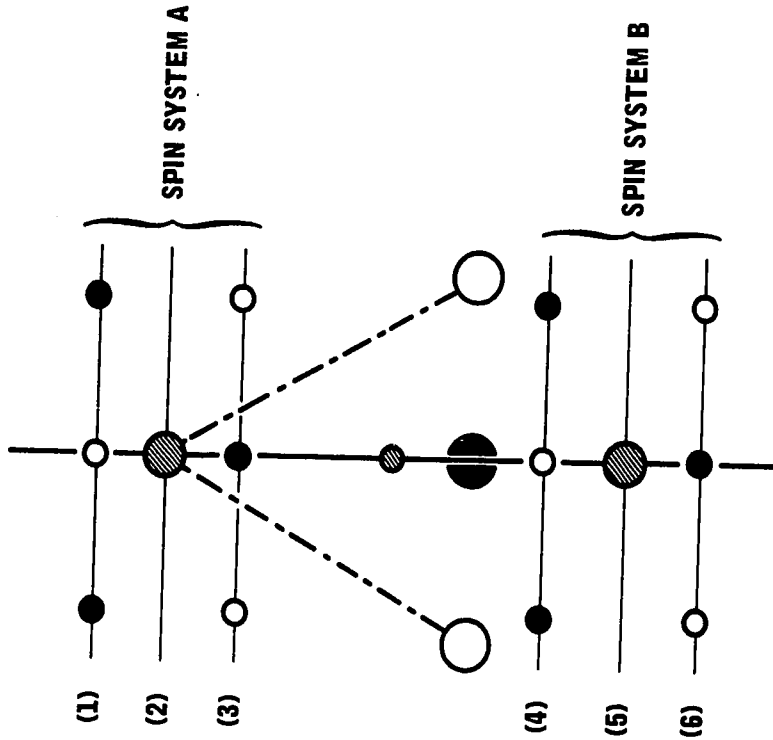
From close examination of the unit cell, it is clear that the environment of each sodium nucleus is similar. However, the environment of adjacent sodium sites situated on

the triad axis (as schematically shown in Figure III j) differ in one important respect. Since the orientation of the nitrate groups alternate by 180° as one moves along the triad axis the environments of the sodium sites are not identical. In fact each of the two sodium sites in the unit cell are inequivalent, in that they differ by a rotation as well as a translation. In other words, the principal axis defining the symmetry of the sodium environments have common z axis along the triad axis but the x and y axis are differently orientated. This difference stems from the orientation of the oxygens associated with the nitrate groups. If the nitrate groups possessed azimuthal symmetry, as would be the case if the groups rotated rapidly about their own triad axes, the sodium sites are no longer different. We note however, that since $\partial^2 V / \partial z^2$ is the same at each sodium site and $\partial^2 V / \partial x^2 = \partial^2 V / \partial y^2 = -\frac{1}{2} \partial^2 V / \partial z^2$ from Laplace's equation, the static quadrupole splitting is identical for each ^{23}Na site. This is why 3 resonances and not 5 (2 pairs of satellites and a centre line) are observed.

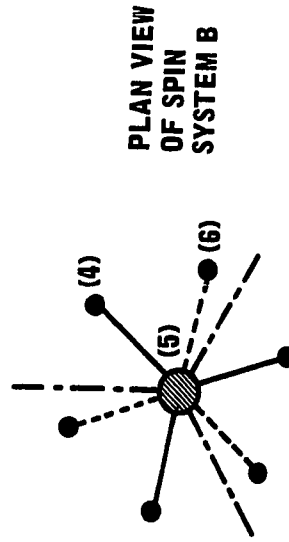
The question now arises as to whether there are two non-equivalent sodium sites in so far as quadrupole relaxation is concerned. The factor determining the quadrupole relaxation is the orientation of the externally applied magnetic field

Caption III j

Figure III j is a schematic representation of the two ^{23}Na sites believed to exist in sodium nitrate. The figure shows a side view illustrating the planes of nearest neighbour oxygen atoms that are associated with the two ^{23}Na nuclear sites. Also plan views are given for the two sites showing the orientation of the nearest neighbour oxygen atoms with respect to the projections of the rhombohedral unit cell edges on the planes perpendicular to the triad axis of the unit cell.



● nearest neighbour oxygen to Na nucleus



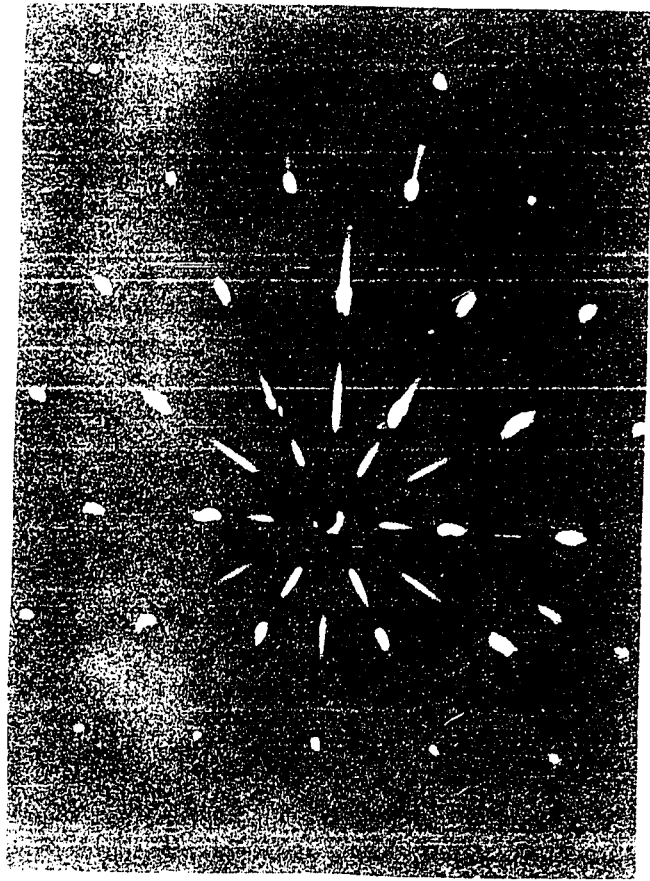
--- projection of rhombohedral unit cell edge onto a plane perpendicular to the triad axis.

relative to the environment of the relaxing nucleus. To consider this point we refer to the conventional xyz coordinate system for a rhombohedral system where the z axis coincides with the triad axis and the x axis is the projection of a rhombohedral unit cell edge on a plane perpendicular to the triad axis. These projections are shown in the plan-view diagrams in Figure III j. If the steady applied field H_0 lies in the x-z plane ($\phi = 0^\circ$) then the two sites are obviously equivalent. However, if ϕ is not equal to zero, then the two sodium sites are inequivalent from the point of view of quadrupole relaxation. This can also be shown theoretically by considering the expressions for W_1 and W_2 in terms of the M-component tensors. These M-components are determined by the local environments. Therefore, to have identical M-components, in particular M_{1113} and M_{1123} , for each ^{23}Na site, the orientation of the x axis in space for the two sites must be different. This would mean therefore that for an arbitrary magnetic field direction the angle would be different for the two sodium sites and hence the W_1 and W_2 for the ^{23}Na nuclei located at these two sites will in general be different.

The single crystal of NaNO_3 used in our work was in the form of a right circular cylinder, 0.9cm long and 1.0cm

Caption III k

Figure III k is an x-ray photograph taken of our single crystal of NaNO_3 using a precession X-ray camera. The incident X-ray beam was directed along the triad axis of the crystal. The crystal was mounted with the cylinder axis horizontal. The interpretation of the photograph enabling the determination of the orientation parameter ϕ is discussed in the text.



in diameter and was obtained from the Harshaw Chemical Company Cleveland, Ohio. The crystal was cut such that the triad axis was perpendicular to the cylinder axis. The sample was mounted in the magnet with the triad axis perpendicular to the vertical axis of rotation. Thus, by rotation the angle that the triad axis makes with the magnetic field could be varied from 0° to 180° .

As spectroscopic analysis showed the following impurities: Al-3ppm; Ca-8ppm; Mg-3ppm; Cu<1ppm and Si<1ppm. No trace of the paramagnetic ions Fe, Mn, and Ni was found. thereby indicating that magnetic relaxation should be negligibly small at room temperature.

The orientation of the x-axis (the projection of a rhombohedral unit cell edge on a plan perpendicular to the triad axis) relative to the crystal cylinder axis was found using X-rays. Figure III k shows a photograph taken with a precession camera with the X-ray beam directed along the triad axis.* For this photograph the crystal cylinder axis was horizontal (parallel to the short edge of the photograph). The diamond pattern of the spots is characteristic of the pattern obtained for a rhombohedral unit cell. The angle between the x axis and the cylinder axis of the crystal is found to be $32.8 \pm 1.5^{\circ}$. Since the crystal cylinder axis was vertical for most of the NMR measurements, the azimuthal angle ϕ was equal to $2.8 \pm 1.5^{\circ}$. For later measurements ϕ was equal to $32.8 \pm 1.5^{\circ}$.

* We are grateful to Dr. M. J. Bennett of the Department of Chemistry for taking the X-ray photographs.

j) Experimental procedure

We shall discuss in detail the experimental procedure for the particular crystal orientation $\phi = 2.8 \pm 1.5^\circ$ and $\theta = 0^\circ$ where the cylindrical axis of the crystal is vertical. Three cases were considered at this orientation: Case I, the enhancement of the high frequency satellite due to severe saturation of the centre line. Case II, the enhancement of the low frequency satellite due to severe saturation of the centre line and Case III, the enhancement of the centre line due to severe saturation of the high frequency satellite.

For Case I measurements, the centre line frequency was accurately determined in both the frequency increasing and decreasing sweep modes. As described earlier in this section, the mean of these two values gives the true centre of the centre line. This is the frequency of the saturating signal, the signal generator being kept within $\pm 30\text{Hz}$ of this value during saturation runs. By measuring the satellite frequencies at the same time, it was possible to check the correctness of the crystal orientation θ . Also, by monitoring the high frequency satellite frequency it was possible to detect slight frequency changes caused by the slow drift of the magnetic field. The saturating signal could therefore be adjusted to

compensate for this field drift without separately measuring the centre line frequency. The temperature coefficient of the quadrupole coupling constant (Andrew et al., 1962) is very small at room temperature so one can assume that it is essentially temperature independent in our laboratory.

In order to ensure that the centre line is completely saturated, we first measured the enhancement of the high frequency satellites a function of the saturating power P_{sat} applied to the centre line. The observing power applied to the high frequency satellite was kept as small as possible during these runs to minimize its effect. The experimental runs consisted of recording enhanced and unenhanced high frequency satellite resonances for different values of the saturating Power P_{sat} being applied. A measure of this power was provided by the voltage across the saturating coil monitored by an oscilloscope connected via a X50 by x50. To improve the accuracy, resonances were recorded several times, typically three enhanced and four unenhanced resonances recorded alternately. Throughout the enhanced runs, the balance mode criterion of 'two centimeters' was strictly observed.

The data is given in Table IV a and is shown in Figure IV a, The solid circles refer to measurements made with a modulation amplitude of 1.3G (1.46kHz) and the open

circles are for measurements made with a modulation amplitude of 0.65G (0.73kHz). This data was fitted to the BPP equation (II 65) using a least squares method. The fit is shown as a solid line in Figure IV a. The figure clearly shows the plateau region that results from the essentially complete saturation of the centre line component. From the theoretical curve it is found that the enhancement for $P_{\text{sat}} = 1600 \text{ volts}^2$ (corresponding to 40volts peak-to-peak across the saturating coil) differs by less than 0.1% from the 'ideal enhancement' with P_{sat} equal to infinity. The extrapolated enhancement corresponding to the infinite saturating power is shown on the figure by the dotted line. Accordingly, this value of P_{sat} was selected for all the measurements at this crystal orientation. Furthermore, since an error of 0.1% is significant, a correction for a non-infinite P_{sat} was always applied. In all cases this was done by measuring the enhancement as a function of P_{sat} and fitting to the BPP equation as described.

For the above results, the spectrometer power P_{obs} was set at a value corresponding to 20 millivolts peak-to-peak across the coils. The spectrometer level was indicated by the detector level meter. This was calibrated directly in terms of the millivolts peak-to-peak across the spectrometer

coil by measuring this voltage using an oscilloscope. However, the oscilloscope could not be left permanently attached to the spectrometer since it acted as an antenna leading to unwanted interference.

From the data in Figure IV a, we see that the enhancement is not dependent on the modulation amplitudes of 1.3G and 0.65G. As a result we chose to use a modulation amplitude of 0.975G for all the data taken at the crystal orientation $\phi = 2.8 \pm 1.5^\circ$.

The enhancement of the high frequency satellite was now measured (using an amplitude of modulation equal to 0.975G) as a function of the spectrometer observing power, P_{obs} , with $P_{\text{sat}} = 1600$ units. In the case of the lower observing powers we ran five saturated and seven unsaturated resonances. Fewer were required for the higher observing powers because of the improved signal-to-noise ratios. Once again the balance criterion was strictly adhered to, results violating the criterion being rejected. The data is shown in Figure IV b as Case I. The straight line represents a least squares fit of the data. A statistical test was used to determine whether data at large P_{obs} values should be rejected because they were outside of the linear region. The enhancement values shown in the figure have been corrected because

of the non-infinite saturating power as was discussed earlier. By substitution of the extrapolated enhancement at zero P_{obs} into equation (II 60) the ratio of the quadrupole transition probabilities W_2/W_1 may be calculated.

At this same orientation the above process was repeated for different resonance components. Case II, the enhancement of the low frequency satellite as a result of severe saturation of the centre line was measured and also Case III, the enhancement of the centre line due to saturation of the high satellite was investigated. These two cases are shown in Figure IV b. The data for Case II and Case III is given in Tables IV b to f. This data is discussed in Section IV.

Measurements similar to Case I were made at crystal orientations $\theta = 22.5^\circ, 42.0^\circ, 74.0^\circ, 90.0^\circ, 100.0^\circ, 112.5^\circ, 135.0^\circ, 150.0^\circ, 157.5^\circ,$ and 180.0° with $\phi = 2.8 \pm 1.5^\circ$. Finally, the crystal was remounted in the holder in such a way that ϕ was increased by 30° to $32.8 \pm 1.5^\circ$. This was done by rotating the crystal through 90° (this being equivalent to a 30° change) about an axis parallel to the symmetry axis. Measurements corresponding to Case I were then made at this value of ϕ for $\theta = 42.0^\circ, 69.0^\circ, 110.0^\circ$ and 138.0° .

SECTION IV Results and discussion

We first discuss the enhancement E of a component due to severe saturation of another component. The enhancement of the population difference is taken to be the ratio of the peak-to-peak intensity of the resonances with and without saturating power. This is the case only if the lineshape is the same in both cases. Such a situation is approximated by the use of small P_{obs} values. It is essential therefore to extrapolate to this limit for quantitative measurements.

The main purpose was to check the validity of applying equation (II 65) to our experiment. The measurements were carried out in detail at $\theta = 0^\circ$ and $\phi = 2.8 \pm 1.5^\circ$. The data is given in Table IV a and is shown in Figure IV a. The error bars are estimated errors determined by the signal-to-noise of the resonances. The solid line represents a least squares computer fit of the data to (II 65). The good agreement confirms the correctness of applying the BPP equation even though P_{obs} , although small, is non-zero. The finite P_{obs} will have the effect of changing

Table IV a

$$\theta = 0^\circ \text{ and } \phi = 2.8 \pm 1.5^\circ$$

The enhancement of the high frequency satellite as a function of the saturating power applied to the centre line. The spectrometer observing power corresponds to 20 millivolts peak-to-peak measured across the sample coil.

Modulation amplitude is 0.65 G peak-to-peak.

P_{sat} (arb. units)	Enhancement
0.16	0.993 ± 0.03
0.27	0.021 0.03
0.45	1.055 0.03
0.71	1.072 0.03
1.00	1.090 0.03
1.51	1.163 0.03
2.00	1.196 0.03
2.30	1.296 0.03
2.52	1.332 0.03
2.75	1.314 0.03
3.25	1.351 0.03
4.00	1.382 0.03
6.00	1.411 0.03
8.67	1.464 0.03

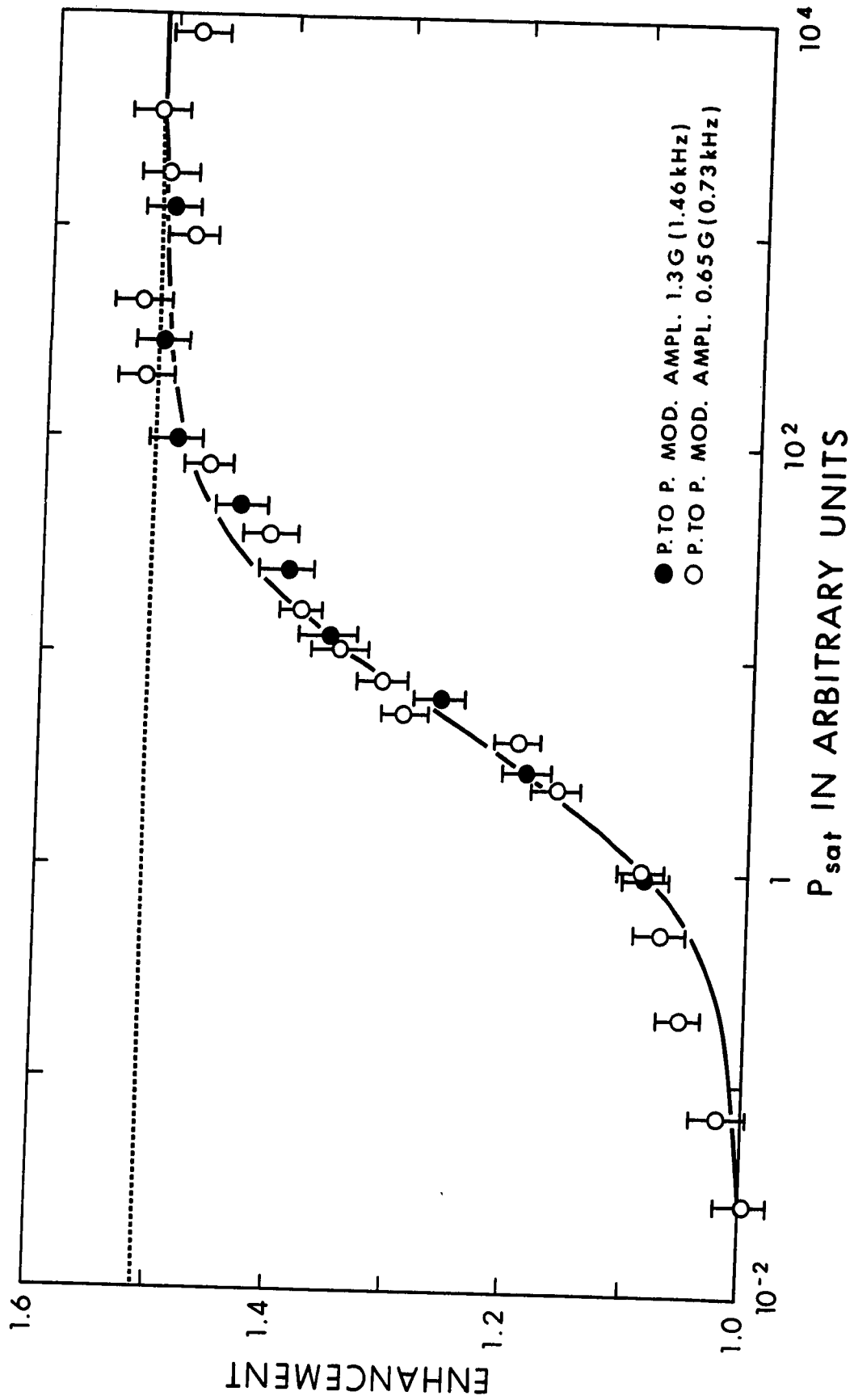
P_{sat} (arb. units)	Enhancement
14.00	1.520 ± 0.03
21.00	1.527 0.03
30.00	1.484 0.03
42.00	1.507 0.03
70.24	1.516 0.03
90.00	1.482 0.03

Modulation amplitude is 1.40 G peak-to-peak

P_{sat} (arb. units)	Enhancement
0.98	1.089 ± 0.03
1.70	1.189 0.03
2.50	1.262 0.03
3.50	1.359 0.03
5.00	1.395 0.03
7.00	1.435 0.03
10.00	1.492 0.03
17.00	1.509 0.03
35.00	1.500 0.03

Caption IV a

Figure IV a shows the enhancement of the high frequency satellite as a function of the saturating power applied to the centre line. The spectrometer observing power during these runs corresponded to 20 millivolts peak-to-peak measured across the sample coil. The solid line represents a least squares fit of equation (II 65) to the experimental points. The dotted line is the extrapolated enhancement of the satellite for infinite saturating power applied to the centre line.



the ordinate scale however this is of no consequence since we are only interested in checking the validity of the BPP equation and not in the determining of any absolute enhancement values. One can however use the data to obtain the correction factor for the non-infinite saturating power that will be applied in the measuring of the enhancement as a function of P_{obs} . The dotted line in Figure IV a represents the extrapolated enhancement at infinite saturating power.

Having confirmed the correctness of equation (II 65) it was necessary only to take some 7 points on the E/P_{sat} curves for the other crystal orientations in order to find the saturation correction factor. The E/P_{sat} data for the other crystal orientations is presented with the appropriate E/P_{obs} data. As a final point we note from Figure IV a that the enhancement values are independent of the amplitude modulation in contrast with data in Figure IIIe. All the data taken at other crystal orientations employed a modulation peak-to-peak amplitude of 0.97 G which was adjusted where necessary to maintain a fixed modulation amplitude/linewidth ratio.

The enhancement as a function of P_{obs} was measured at $\theta = 0^\circ$ and $\phi = 2.8 \pm 1.5^\circ$ for three specific cases: Case I, the enhancement of the high frequency satellite due to severe saturation of the centre line. Case II, the en-

hancement of the low frequency satellite due to the severe saturation of the centre line and Case III, the enhancement of the centre line due to the severe saturation of the high frequency satellite.

The data for these three cases is given in Tables IV b,d, and f and is shown in Figure IV b. The error bars represent estimated errors. It is clear that the enhancement exhibits a linear dependence on the small values of the spectrometer observing power P_{obs} , as predicted by Hughes (1966). The straight lines in Figure IV b represent a least squares computer fit of the data where the weighting factor for each point is taken as $1/(\text{estimated error})^2$. By examination of the deviation of each point from the least squares fit, some points at large P_{obs} were rejected as being outside of the linear region.

The extrapolated enhancement at $P_{\text{obs}} = 0$ is significantly different for the two cases I and II. The enhancement is indeed not expected to be the same in these two cases since the energy level spacings are unequal. It was for this reason that we developed the rate equations given in Section II taking into account this unequal splitting factor in the hope that our experimental data would be sufficiently accurate to illustrate the effect. Using equations (II 60) and (II 61) we find

Table IV b

$$\theta = 0^\circ \text{ and } \phi = 2.8^\circ \pm 1.5^\circ$$

Case I, the enhancement of the high frequency satellite due to severe saturation of the centre line as a function of the spectrometer observing power.

The correction for the non-infinite saturating power is 1.001

The correction $\delta = 0.022$

P_{obs} (arb. units)	Unenhanced intensity (arb. units)		Enhanced intensity (arb. units)		Enhancement (corrected)	
225.00	4.697	± 0.038	6.982	± 0.038	1.486	± 0.014
441.00	7.610	0.050	11.231	0.058	1.476	0.012
900.00	6.980	0.030	10.410	0.035	1.491	0.008
1225.00	6.642	0.039	10.045	0.039	1.512	0.011
1600.00	7.257	0.025	10.988	0.029	1.514	0.007
2500.00	7.369	0.026	11.226	0.032	1.523	0.007
3600.00	7.520	0.020	11.667	0.025	1.551	0.005
6400.00	6.247	0.017	10.045	0.021	1.608	0.006
10000.00	5.868	0.015	9.630	0.017	1.641	0.005

Table IV c

$$\theta = 0^\circ \text{ and } \phi = 2.8 \pm 1.5^\circ$$

The enhancement of the low frequency satellite as a function of the saturating power applied to the centre line. The spectrometer observing power corresponds to 20 millivolts peak-to-peak measured across the sample coil.

Modulation amplitude is 0.65 G peak-to-peak

P_{sat} (arb. units)	Enhancement
0.16	0.993 ± 0.03
0.27	1.021 0.03
0.45	1.055 0.03
0.71	1.072 0.03
1.00	1.090 0.03
1.51	1.163 0.03
2.00	1.196 0.03
2.30	1.296 0.03
2.52	1.332 0.03
2.75	1.314 0.03
3.25	1.351 0.03

P_{sat} (arb. units)	Enhancement
4.00	1.382 \pm 0.03
6.00	1.411 0.03
8.67	1.464 0.03
14.00	1.520 0.03
21.00	1.527 0.03
30.00	1.484 0.03
42.00	1.507 0.03
70.24	1.516 0.03
90.00	1.482 0.03

Table IV d

$$\theta = 0^\circ \text{ and } \phi = 2.8 \pm 1.5^\circ$$

Case II, the enhancement of the low frequency satellite due to severe saturation of the centre line as a function of the spectrometer observing power.

The correction for the non-infinite saturating power is 1.001

The correction $\delta = - 0.022$

P_{obs} (arb. units)	Unenhanced intensity (arb. units)		Enhanced intensity (arb. units)		Enhancement (corrected)	
225.00	3.888	± 0.040	5.770	± 0.046	1.484	± 0.019
400.00	4.696	0.040	7.057	0.049	1.503	0.017
900.00	5.535	0.029	8.511	0.035	1.538	0.010
1225.00	5.696	0.029	8.822	0.035	1.549	0.010
1681.00	5.765	0.029	8.859	0.035	1.537	0.010
2500.00	5.724	0.029	9.049	0.035	1.581	0.010
3600.00	5.850	0.028	9.284	0.028	1.587	0.009
4900.00	5.690	0.020	9.177	0.025	1.613	0.007
6400.00	5.367	0.017	8.914	0.022	1.661	0.007

Table IV e

$$\theta = 0^\circ \text{ and } \phi = 2.8 \pm 1.5^\circ$$

The enhancement of the centre line as a function of the saturating power applied to the high frequency satellite. The spectrometer observing power corresponds to 20 millivolts peak-to-peak across the sample coil.

Modulation amplitude is 0.65 G peak-to-peak

P_{sat} (arb. units)	Enhancement
2.00	1.240 \pm 0.03
3.00	1.391 0.03
5.00	1.575 0.03
7.00	1.638 0.03
10.00	1.638 0.03
20.00	1.695 0.03
40.00	1.681 0.03
50.00	1.674 0.03

Table IV f

$$\theta = 0^\circ \text{ and } \phi = 2.8 \pm 1.5^\circ$$

Case III, the enhancement of the centre line due to severe saturation of the high frequency satellite as a function of the spectrometer observing power.

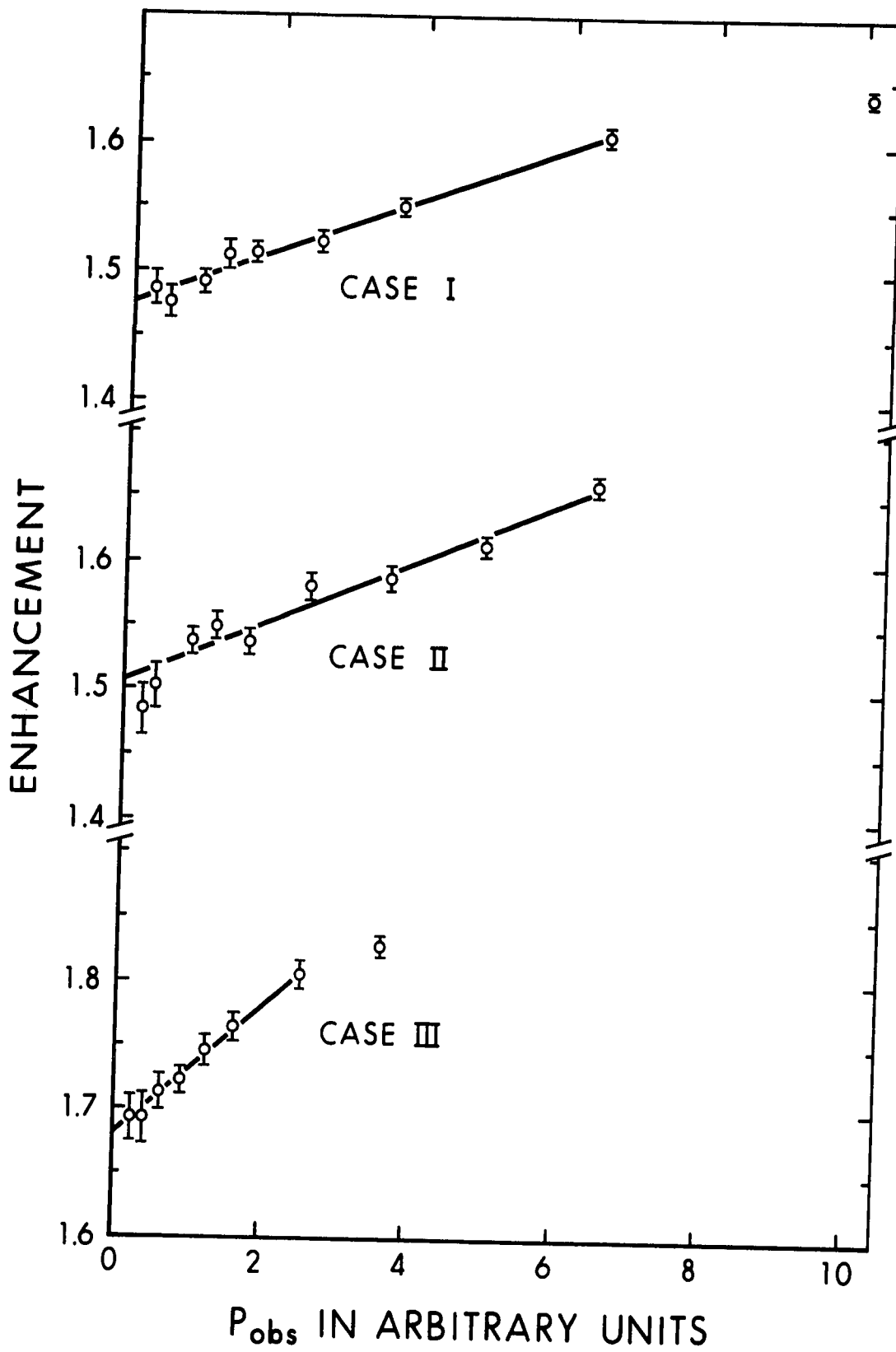
The correction for the non-infinite saturating power is 1.0017

The correction $\delta = 0.022$

P_{obs} (arb. units)	Unenhanced intensity (arb. units)		Enhanced intensity (arb. units)		Enhancement (corrected)	
225.00	4.250	± 0.038	7.195	± 0.038	1.693	± 0.018
400.00	5.375	0.050	9.098	0.058	1.693	0.018
625.00	5.700	0.039	9.767	0.039	1.713	0.014
900.00	6.075	0.030	10.468	0.035	1.723	0.010
1225.00	6.113	0.039	10.668	0.039	1.745	0.013
1600.00	6.087	0.025	10.735	0.029	1.764	0.009
2500.00	5.967	0.026	10.768	0.032	1.805	0.010
3600.00	5.757	0.020	10.518	0.025	1.827	0.008

Caption IV b

Figure IV b shows three cases of the enhancement of an ^{23}Na resonance component in a single crystal of NaNO_3 due to severe saturation of another component as a function of the spectrometer observing power P_{obs} . Case I is the enhancement of the high frequency satellite due to the severe saturation of the centre line, Case II is the enhancement of the low frequency satellite due to the severe saturation of the centre line and Case III is the enhancement of the centre line due to the severe saturation of the high frequency satellite. Each solid line represents a least squares fit of the data to the enhancement equation derived in the text.



that $W_2/W_1 = 0.952 \pm 0.015$ for Case I and $W_2/W_1 = 0.986 \pm 0.029$ for Case II. The error limits for W_2/W_1 are obtained from the scatter of the points from the straight line, and are sometimes referred to as external errors. The error limits on W_2/W_1 as obtained from the estimated errors are invariably larger than the external errors usually by a factor of 2 or 3. This is due to the difficulty of initially estimating the error limits in the measuring of the resonance intensities. For Case III, the value of W_2/W_1 derived by extrapolation is 0.988 ± 0.022 , in agreement with the values obtained for Case I and II.

Such agreement for W_2/W_1 would not be expected if magnetic relaxation due to paramagnetic ions were significant (BPP, 1948). We denote magnetic transition probability by (Andrew and Swanson, 1960)

$$W_{m \rightarrow m-1} = (I + m) (I - m + 1) W_3 \quad (\text{IV } 1)$$

and assume W_3 to be same throughout the crystal and the same for each transition. (This will be true for direct relaxation by a paramagnetic ion but not if the relaxation were determined by a spin diffusion). The rate equations for Case I, where $y = W_3/W_1$, are

$$\dot{N}_0/W_1 = N_1(1-x+3y) - N_0(2x+8y+8P_0) + N_{-1}(1-x+3y) + 2n_0(2x+y-1) \quad (\text{IV } 2)$$

$$\dot{N}_1 = -N_1(2+x+6y) + 4N_0(y+P_0) + N_{-1}(x) + 2n_0[1+y+\delta(1+3y+x)] \quad (\text{IV } 3)$$

$$\dot{N}_{-1} = N_1(x) + 4N_0(y+P_0) - N_{-1}(x+2+6y) + 2n_0[1+y-\delta(1+3y+x)]. \quad (\text{IV } 4)$$

Solving these equations in the usual way we find that the Case I enhancement, for zero observing power, is given to first order in y and δ by

$$E = \left[\frac{1+2x}{1+x} \right] \left[1 - \frac{3xy}{(1+x)(1+2x)} - \frac{x\delta}{1+2x} \right] \quad (\text{IV } 5)$$

The enhancement for Case II is from symmetry arguments given by

$$E = \left[\frac{1+2x}{1+x} \right] \left[1 - \frac{3xy}{(1+x)(1+2x)} + \frac{x\delta}{1+2x} \right] \quad (\text{IV } 6)$$

For Case III the rate equations are given by

$$\dot{N}_0 = N_1(1-x+3y+3P_1) - N_0(2x+8y) + N_{-1}(1-x+3y) + 2n_0(2x+y-1) \quad (\text{IV } 7)$$

$$\dot{N}_1 = -N_1(2+x+6y+6P_1) + 4N_0y + N_{-1}x + 2n_0[1+y+\delta(1+3y+x)] \quad (\text{IV } 8)$$

$$\dot{N}_{-1} = N_1x + 4N_0y - N_{-1}(x+2+6y) + 2n_0[1+y-\delta(1+3y+x)], \quad (\text{IV } 9)$$

and the enhancement of the centre line for zero observing power is given to first order in y and δ by

$$E = \left[\frac{2x+3}{x+2} \right] \left[1 + \frac{\delta(1+x)}{2x+3} - \frac{y(7x^2+8x+4)}{x(x+2)(2x+3)} \right]. \quad (\text{IV } 10)$$

Substituting the measured enhancement values for the Case I, II and III into equations (IV 5), (IV 6), and (IV 10), we find using a least squares analysis that

$$y = W_3/W_1 = -0.0040 \pm 0.0034 \quad (\text{IV } 11)$$

This shows that magnetic relaxation effects are completely negligible in our crystal. This is to be expected from the spectroscopic analysis given in Section III 8 where no trace of the paramagnetic impurities is indicated.

The enhancement data obtained for the various values of θ at $\phi = 2.8^\circ$ are given in Tables IV a + z. Further enhancement data obtained when the crystal was tipped through 90° as described in Section III are given for $\phi = 32.8^\circ$ in Tables $\alpha, \beta, \gamma, \delta, \epsilon, \eta, \xi,$ and ζ . From the enhancement data, the values of W_2/W_1 were obtained as described above, and are listed in Table IV T for $\phi = 2.8^\circ$ and in Table IV E for $\phi = 32.8^\circ$. The data for $\phi = 2.8^\circ$ is plotted in Figure IV c and for consistency the value at $\theta = 0^\circ$ is that obtained for Case I, since Case II and Case III were only carried out at $\theta = 0^\circ$. The error limits. The data for $\phi = 32.8^\circ$ is plotted in Figure IV d. The error limits shown in these figures are

Table IV g

$$\theta = 22.5^\circ \text{ and } \phi = 2.8 \pm 1.5^\circ$$

The enhancement of the high frequency satellite as a function of the saturating power applied to the centre line. The spectrometer observing power corresponds to 20 millivolts poka-to-peak measured across the sample coil.

P_{sat} (arb. units)	Enhancement
2.00	1.196 \pm 0.03
4.00	1.353 0.03
7.00	1.382 0.03
10.00	1.451 0.03
20.00	1.490 0.03
40.00	1.471 0.03

Table IV h

$$\theta = 22.5^\circ \text{ and } \phi = 2.8 \pm 1.5^\circ$$

Case I, the enhancement of the high frequency satellite due to severe saturation of the centre line as a function of the spectrometer observing power.

The correction for the non-infinite saturating power is 1.0013

The correction $\delta = 0.017$

P_{obs} (arb. units)	Unenhanced intensity (arb. units)		Enhanced intensity (arb. units)		Enhancement (corrected)	
400.00	2.467 \pm 0.038		3.680 \pm 0.038		1.492 \pm 0.028	
625.00	2.667	0.050	3.980	0.058	1.492	0.035
900.00	2.850	0.030	4.306	0.035	1.511	0.020
1225.00	2.930	0.039	4.456	0.039	1.521	0.024
1600.00	2.967	0.025	4.521	0.029	1.524	0.016
2025.00	3.350	0.026	5.182	0.032	1.547	0.015
3025.00	3.100	0.026	4.856	0.032	1.567	0.017
3600.00	2.730	0.020	4.306	0.025	1.577	0.015

Table IV i

$$\theta = 42^\circ \text{ and } \phi = 2.8 \pm 1.5^\circ$$

The enhancement of the high frequency satellite as a function of the saturating power applied to the centre line. The spectrometer observing power corresponds to 20 millivolts peak-to-peak measured across the sample coil.

P_{sat} (arb. units)	Enhancement
2.00	1.193 \pm 0.03
5.00	1.298 0.03
7.00	1.340 0.03
10.00	1.451 0.03
20.00	1.523 0.03
40.00	1.515 0.03

Table IV j

$$\theta = 42^\circ \text{ and } \phi = 2.8 \pm 1.5^\circ$$

Case I, the enhancement of the high frequency satellite due to severe saturation of the centre line as a function of the spectrometer observing power.

The correction for the non-infinite saturating power is 1.001

The correction $\delta = 0.007$

P_{obs} (arb. units)	Unenhanced intensity (arb. units)		Enhanced intensity (arb. units)		Enhancement (corrected)	
400.00	2.175 \pm 0.038		3.278 \pm 0.032		1.507 \pm 0.032	
625.00	2.467	0.050	3.754	0.058	1.522	0.039
900.00	2.600	0.030	3.979	0.035	1.530	0.022
1225.00	2.600	0.040	4.004	0.039	1.540	0.028
1600.00	2.650	0.025	4.079	0.029	1.539	0.018
2025.00	2.630	0.026	4.104	0.032	1.560	0.020
3600.00	2.365	0.020	3.779	0.025	1.598	0.017

Table IV k

$$\theta = 74^\circ \text{ and } \phi = 2.8 \pm 1.5^\circ$$

The enhancement of the high frequency satellite as a function of the saturating power applied to the centre line. The spectrometer observing power corresponds to 20 millivolts peak-to-peak measured across the sample coil.

P_{sat} (arb. units)	Enhancement
2.00	1.215 \pm 0.03
5.00	1.397 0.03
7.00	1.454 0.03
10.00	1.464 0.03
20.00	1.473 0.03
40.00	1.473 0.03

Table IV 1

$$\theta = 74^\circ \text{ and } \phi = 2.8 \pm 1.5^\circ$$

Case I, the enhancement of the high frequency satellite due to severe saturation of the centre line as a function of the spectrometer observing power.

The correction for the non-infinite saturating power is 1.001

The correction $\delta = 0.008$

P_{Obs} (arb. units)	Unenhanced intensity (arb. units)		Enhanced intensity (arb. units)		Enhancement (corrected)	
400.00	2.600 \pm 0.038		3.837 \pm 0.038		1.476 \pm 0.026	
625.00	2.783	0.050	4.179	0.058	1.502	0.034
900.00	2.850	0.030	4.279	0.035	1.501	0.020
1225.00	2.800	0.040	4.221	0.039	1.508	0.026
1600.00	3.075	0.025	4.672	0.029	1.519	0.016
4096.00	2.117	0.020	3.303	0.025	1.560	0.019

Table IV m

$$\theta = 90^{\circ} \text{ and } \phi = 2.8 \pm 1.5^{\circ}$$

The enhancement of the high frequency satellite as a function of the saturating power applied to the centre line. The spectrometer observing power corresponds to 20 millivolts peak-to-peak measured across the sample coil

P_{sat} (arb. units)	Enhancement	
1.00	1.073 \pm 0.03	
1.50	1.158	0.03
2.00	1.221	0.03
2.50	1.276	0.03
3.50	1.353	0.03
6.00	1.427	0.03
10.00	1.417	0.03
20.00	1.414	0.03
40.00	1.426	0.03

Table IV n

$$\theta = 90^{\circ} \text{ and } \phi = 2.8 \pm 1.5^{\circ}$$

Case I, the enhancement of the high frequency satellite due to severe saturation of the centre line as a function of the spectrometer observing power.

The correction for the non-infinite saturating power is 1.0007

The correction $\delta = 0.011$

P_{obs} (arb. units)	Unenhanced intensity (arb. units)		Enhanced intensity (arb. units)		Enhancement (corrected)	
100.00	3.233	± 0.049	4.688	± 0.055	1.450	± 0.028
225.00	4.411	0.042	6.564	0.049	1.488	0.018
400.00	5.147	0.046	7.715	0.056	1.499	0.017
625.00	5.812	0.037	8.773	0.043	1.509	0.012
900.00	6.165	0.037	9.347	0.043	1.516	0.011
1225.00	6.195	0.034	9.532	0.042	1.539	0.011
1600.00	6.332	0.029	9.962	0.035	1.573	0.009
2500.00	6.345	0.026	10.122	0.032	1.595	0.008
3600.00	6.585	0.029	10.332	0.035	1.569	0.009
5184.00	6.362	0.020	10.075	0.025	1.584	0.006

Table IV 0

$$\theta = 100^\circ \text{ and } \phi = 2.8 \pm 1.5^\circ$$

The enhancement of the high frequency satellite as a function of the saturating power applied to the centre line. The spectrometer observing power corresponds to 20 millivolts peak-to-peak across the sample coil.

P_{sat} (arb. units)	Enhancement
2.00	1.128 \pm 0.03
3.00	1.319 0.03
5.00	1.441 0.03
7.00	1.467 0.03
10.00	1.493 0.03
20.00	1.484 0.03
40.00	1.493 0.03

Table IV p

$$\theta = 100^\circ \text{ and } \phi = 2.8 \pm 1.5^\circ$$

Case I, the enhancement of the high frequency satellite due to severe saturation of the centre line as a function of the spectrometer observing power.

The correction for the non-infinite saturating power is 1.0015

The correction $\delta = 0.010$

P_{obs} (arb. units)	Unenhanced intensity (arb. units)	Enhanced intensity (arb. units)	Enhancement (corrected)
361.00	2.760 ± 0.038	4.156 ± 0.038	1.506 ± 0.025
625.00	3.280 0.050	4.957 0.058	1.511 0.029
900.00	3.483 0.030	5.238 0.035	1.517 0.016
1225.00	3.450 0.030	5.258 0.035	1.524 0.017
1600.00	3.467 0.025	5.358 0.029	1.545 0.014
2500.00	3.300 0.026	5.158 0.032	1.563 0.016
3600.00	3.230 0.020	5.033 0.025	1.558 0.012

Table IV q

$$\theta = 112.5^\circ \text{ and } \phi = 2.8 \pm 1.5^\circ$$

The enhancement of the high frequency satellite as a function of the saturating power applied to the centre line. The spectrometer observing power corresponds to 20 millivolts peak-to-peak measured across the sample coil.

P_{sat} (arb. units)	Enhancement
3.00	1.325 \pm 0.03
5.00	1.432 0.03
8.00	1.500 0.03
10.00	1.488 0.03
20.00	1.490 0.03
40.00	1.474 0.03

Table IV r

$$\theta = 112.5^\circ \text{ and } \phi = 2.8 \pm 1.5^\circ$$

Case I, the enhancement of the high frequency satellite due to severe saturation of the centre line as a function of the spectrometer observing power.

The correction for the non-infinite saturating power is 1.0009

The correction $\delta = 0.006$

P_{obs} (arb. units)	Unenhanced intensity (arb. units)		Enhanced intensity (arb. units)		Enhancement (corrected)	
400.00	4.400	± 0.035	6.756	± 0.035	1.535	± 0.015
625.00	4.400	0.021	6.806	0.026	1.547	0.009
900.00	5.070	0.035	7.957	0.035	1.569	0.013
1225.00	4.900	0.044	7.707	0.044	1.573	0.017
1600.00	4.880	0.035	7.682	0.035	1.574	0.013
2500.00	4.730	0.023	7.657	0.028	1.619	0.010
3600.00	4.330	0.035	7.056	0.042	1.630	0.016

Table IV s

$$\theta = 135^\circ \text{ and } \phi = 2.8 \pm 1.5^\circ$$

The enhancement of the high frequency satellite as a function of the saturating power applied to the centre line. The spectrometer observing power corresponds to 20 millivolts peak-to-peak measured across the sample coil.

P_{sat} (arb. units)	Enhancement
2.00	1.250 ± 0.03
5.00	1.467 0.03
7.50	1.524 0.03
10.00	1.579 0.03
20.00	1.571 0.03
40.00	1.582 0.03

Table IV t

$$\theta = 135^\circ \text{ and } \phi = 2.8 \pm 1.5^\circ$$

Case I, the enhancement of the high frequency satellite due to severe saturation of the centre line as a function of the spectrometer observing power.

The correction for the non-infinite saturating power is 1.0013

The correction $\delta = 0.006$

P_{Obs} (arb. units)	Unenhanced intensity (arb. units)		Enhanced intensity (arb. units)		Enhancement (corrected)	
625.00	3.860	± 0.014	5.988	± 0.017	1.551	± 0.007
900.00	4.100	0.023	6.388	0.023	1.558	0.010
1296.00	4.030	0.029	6.408	0.029	1.590	0.013
1600.00	4.170	0.035	6.629	0.035	1.590	0.016
1936.00	4.130	0.029	6.609	0.035	1.600	0.014
2500.00	4.070	0.023	6.559	0.028	1.611	0.011
3600.00	4.217	0.035	6.934	0.042	1.644	0.017
4900.00	4.010	0.023	6.759	0.028	1.685	0.012

Table IV u

$$\theta = 150^\circ \text{ and } \phi = 2.8 \pm 1.5^\circ$$

The enhancement of the high frequency satellite as a function of the saturating power applied to the centre line. The spectrometer observing power corresponds to 20 millivolts peak-to-peak measured across the sample coil.

P_{sat} (arb. units)	Enhancement
2.00	1.263 ± 0.03
5.00	1.433 0.03
7.00	1.468 0.03
10.00	1.527 0.03
20.00	1.536 0.03
40.00	1.517 0.03

Table IV v

$$\theta = 150^\circ \text{ and } \phi = 2.8 \pm 1.5^\circ$$

Case I, the enhancement of the high frequency satellite due to severe saturation of the centre line as a function of the spectrometer observing power.

The correction for the non-infinite saturating power is 1.0009

The correction $\delta = 0.014$

P_{obs} (arb. units)	Unenhanced intensity (arb. units)		Enhanced intensity (arb. units)		Enhancement (corrected)	
400.00	3.250	± 0.038	4.954	± 0.038	1.524	± 0.021
625.00	2.840	0.050	4.384	0.058	1.544	0.034
900.00	3.250	0.030	5.055	0.035	1.555	0.018
1225.00	3.500	0.040	5.455	0.039	1.559	0.021
1600.00	3.417	0.025	5.380	0.029	1.574	0.014
2500.00	3.280	0.026	5.305	0.032	1.617	0.016
3600.00	3.050	0.020	4.954	0.025	1.624	0.013

Table IV w

$$\theta = 157.5^\circ \text{ and } \phi = 2.8 \pm 1.5^\circ$$

The enhancement of the high frequency satellite as a function of the saturating power applied to the centre line. The spectrometer observing power corresponds to 20 millivolts peak-to-peak across the sample coil.

P_{sat} (arb. units)	Enhancement
3.00	1.313 \pm 0.03
5.00	1.408 0.03
7.00	1.432 0.03
10.00	1.492 0.03
20.00	1.519 0.03
40.00	1.551 0.03
60.00	1.508 0.03

Table IV x

$$\theta = 157.5^\circ \text{ and } \phi = 2.8 \pm 1.5^\circ$$

Case I, the enhancement of the high frequency satellite due to severe saturation of the centre line as a function of the spectrometer observing power.

The correction for the non-infinite saturating power is 1.0016

The correction $\delta = 0.017$

P_{obs} (arb. units)	Unenhanced intensity (arb. units)		Enhanced intensity (arb. units)		Enhancement (corrected)	
225.00	2.575	± 0.035	3.839	± 0.035	1.491	± 0.024
400.00	3.275	0.035	4.883	0.035	1.491	0.019
625.00	3.700	0.030	5.559	0.035	1.502	0.015
900.00	3.900	0.030	5.909	0.035	1.515	0.015
1225.00	3.600	0.039	5.509	0.039	1.530	0.020
1600.00	3.867	0.025	5.859	0.029	1.515	0.012
2500.00	3.783	0.026	5.884	0.032	1.555	0.014
3600.00	3.583	0.020	5.709	0.025	1.593	0.011

Table IV y

$$\theta = 180^\circ \text{ and } \phi = 2.8 \pm 1.5^\circ$$

The enhancement of the high frequency satellite as a function of the saturating power applied to the centre line. The spectrometer observing power corresponds to 20 millivolts peak-to-peak measured across the sample coil.

P_{sat} (arb. units)	Enhancement
2.00	1.286 \pm 0.03
4.00	1.440 0.03
7.00	1.496 0.03
10.00	1.508 0.03
20.00	1.508 0.03
40.00	1.515 0.03

Table IV z

$$\theta = 180^\circ \text{ and } \phi = 2.8 \pm 1.5^\circ$$

Case I, the enhancement of the high frequency satellite due to severe saturation of the centre line as a function of the spectrometer observing power.

The correction for the non-infinite saturating power is 1.0007

The correction $\delta = 0.022$

P_{obs} (arb. units)	Unenhanced intensity (arb. units)		Enhanced intensity (arb. units)		Enhancement (corrected)	
225.00	3.350	± 0.038	4.983	± 0.038	1.488	± 0.020
400.00	4.130	0.050	6.164	0.058	1.493	0.023
625.00	4.525	0.040	6.805	0.048	1.504	0.017
900.00	4.880	0.030	7.325	0.035	1.501	0.012
1225.00	4.825	0.039	7.305	0.039	1.514	0.015
1600.00	4.780	0.025	7.305	0.029	1.528	0.010
2500.00	4.610	0.026	7.230	0.032	1.568	0.011
3600.00	4.030	0.020	6.404	0.025	1.589	0.010

Table IV α

$$\theta = 42^\circ \text{ and } \phi = 32.8 \pm 1.5^\circ$$

The enhancement of the high frequency satellite as a function of the saturating power applied to the centre line. The Spectrometer observing power corresponds to 20 millivolts peak-to-peak measured across the sample coil.

P_{sat} (arb. units)	Enhancement
1.00	1.134 \pm 0.03
3.00	1.333 0.03
5.00	1.452 0.03
7.00	1.484 0.03
10.00	1.516 0.03
20.00	1.517 0.03
40.00	1.548 0.03
60.00	1.533 0.03

Table IV β

$$\theta = 42^\circ \text{ and } \phi = 32.8 \pm 1.5^\circ$$

Case I, the enhancement of the high frequency satellite due to the severe saturation of the centre line as a function of the spectrometer observing power.

The correction for the non-infinite saturating power is 1.0010

The correction $\delta = 0.008$

P_{obs} (arb. units)	Unenhanced intensity (arb. units)		Enhanced intensity (arb. units)		Enhancement (corrected)	
400.00	3.100 \pm 0.038		4.835 \pm 0.038		1.560 \pm 0.023	
625.00	3.425	0.050	5.380	0.058	1.571	0.029
900.00	3.600	0.030	5.706	0.035	1.585	0.016
1225.00	3.700	0.030	5.881	0.035	1.589	0.016
1600.00	3.750	0.025	5.986	0.029	1.596	0.013
2500.00	2.900	0.026	4.730	0.032	1.631	0.018

Table IV γ

$$\theta = 69^\circ \text{ and } \phi = 32.8 \pm 1.5$$

The enhancement of the high frequency satellite as a function of the saturating power applied to the centre line. The spectrometer observing power corresponds to 20 millivolts peak-to-peak across the sample coil.

P_{sat} (arb. units)	Enhancement
2.00	1.048 ± 0.03
3.00	1.346 0.03
5.00	1.375 0.03
7.00	1.433 0.03
10.00	1.500 0.03
20.00	1.548 0.03
40.00	1.548 0.03

Table IV δ

$$\theta = 69^\circ \text{ and } \phi = 32.8 \pm 1.5^\circ$$

Case I, the enhancement of the high frequency satellite due to the severe saturation of the centre line as a function of the spectrometer observing power.

The correction for the non-infinite saturating power is 1.0016

The correction $\delta = 0.007$

P_{obs} (arb. units)	Unenhanced intensity (arb. units)		Enhanced intensity (arb. units)		Enhancement (corrected)	
400.00	3.100	± 0.038	4.808	± 0.038	1.551	± 0.023
625.00	3.530	0.050	5.459	0.058	1.546	0.027
900.00	3.750	0.030	5.909	0.035	1.576	0.016
1225.00	4.050	0.030	6.360	0.035	1.570	0.014
1600.00	3.530	0.025	5.659	0.029	1.603	0.014
2500.00	3.130	0.026	5.108	0.032	1.632	0.017
4225.00	2.625	0.02	4.457	0.025	1.698	0.016

Table IV. ϵ

$$\theta = 110^\circ \text{ and } \phi = 32.8 \pm 1.5^\circ$$

The enhancement of the high frequency satellite as a function of the saturating power applied to the centre line. The spectrometer observing power corresponds to 20 millivolts peak-to-peak measured across the sample coil.

P_{sat} (arb. units)	Enhancement
2.00	1.276 ± 0.03
5.00	1.414 0.03
7.00	1.448 0.03
10.00	1.483 0.03
20.00	1.509 0.03
40.00	1.472 0.03

Table IV η

$$\theta = 110^\circ \text{ and } \phi = 32.8 \pm 1.5^\circ$$

Case I, the enhancement of the high frequency satellite due to the severe saturation of the centre line as a function of the spectrometer observing power.

The correction for the non-infinite saturating power is 1.0007

The correction $\delta = 0.007$

P_{obs} (arb. units)	Unenhanced intensity (arb. units)		Enhanced intensity (arb. units)		Enhancement (corrected)	
400.00	2.867 \pm 0.038		4.213 \pm 0.038		1.469 \pm 0.024	
625.00	3.250	0.050	4.778	0.058	1.470	0.029
900.00	3.500	0.030	5.179	0.035	1.480	0.016
1225.00	3.675	0.030	5.454	0.035	1.484	0.015
1600.00	3.630	0.025	5.404	0.029	1.489	0.013
2500.00	3.475	0.026	5.229	0.032	1.505	0.015
3600.00	3.150	0.020	4.803	0.025	1.525	0.013

Table IV ξ

$$\theta = 138^\circ \text{ and } \phi = 32.8 \pm 1.5^\circ$$

The enhancement of the high frequency satellite as a function of the saturating power applied to the centre line. The spectrometer observing power corresponds to 20 millivolts peak-to-peak measured across the sample coil.

P_{sat} (arb. units)	Enhancement
3.00	1.300 \pm 0.03
5.00	1.388 0.03
7.00	1.463 0.03
10.00	1.463 0.03
20.00	1.463 0.03
40.00	1.476 0.03

Table IV ζ

$$\theta = 138^\circ \text{ and } \phi = 32.8 \pm 1.5^\circ$$

Case I, the enhancement of the high frequency satellite due to the severe saturation of the centre line as a function of the spectrometer observing power.

The correction for the non-infinite saturating power is 1.0011

The correction $\delta = 0.007$

P_{obs} (arb. units)	Unenhanced intensity (arb. units)	Enhanced intensity (arb. units)	Enhancement (corrected)
400.00	2.150 ± 0.038	3.204 ± 0.038	1.490 ± 0.032
900.00	2.510 0.030	3.779 0.035	1.506 0.023
1225.00	2.750 0.030	4.155 0.035	1.511 0.021
1600.00	2.750 0.025	4.180 0.029	1.520 0.017
2500.00	2.700 0.026	4.155 0.032	1.539 0.019
3600.00	2.380 0.020	3.729 0.025	1.567 0.017

Table IV T

$$\phi = 2.8 \pm 1.5^\circ$$

The data being measured under the conditions of Case I, the enhancement behaviour of the high frequency satellite due to severe saturation of the centre line

θ (degrees)	W_2/W_1	
0.0	0.952 \pm 0.015	
22.5	0.976	0.017
42.0	1.026	0.016
74.0	0.898	0.015
90.0	0.885	0.021
100.0	0.994	0.017
112.5	1.119	0.023
135.0	1.163	0.017
150.0	1.077	0.018
157.5	0.956	0.022
180.0	0.936	0.016

$\theta = 0^\circ$ for Case II measurements gives $W_2/W_1 = 0.986 \pm 0.029$

$\theta = 0^\circ$ for Case III measurements gives $W_2/W_1 = 0.988 \pm 0.22$

Caption IV c

Figure IV c shows the orientation dependence of our values of W_2/W_1 at $\phi = 2.8 \pm 1.5^\circ$. The solid line is a least squares fit of the Pietila theoretical equations.

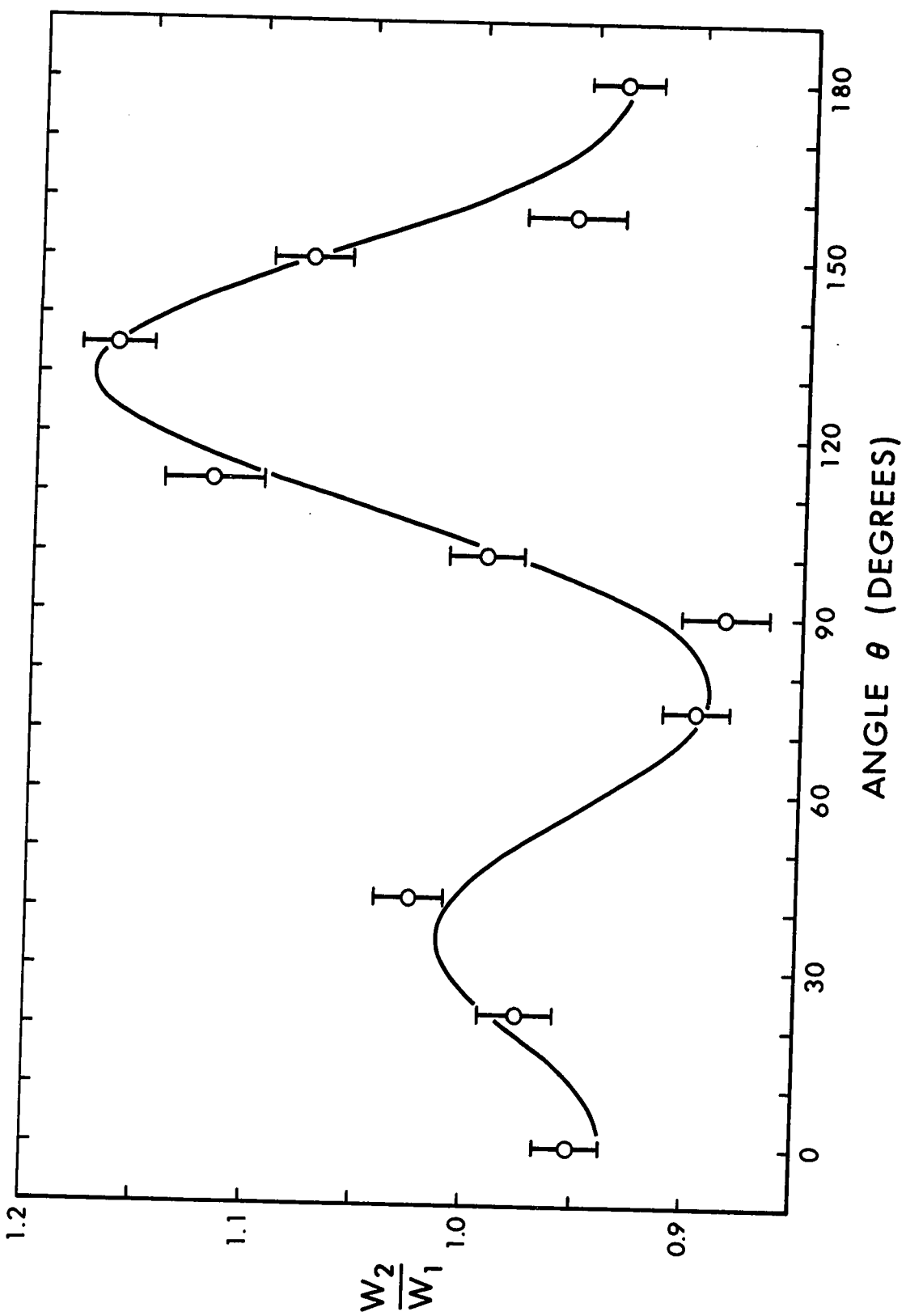


Table IV E

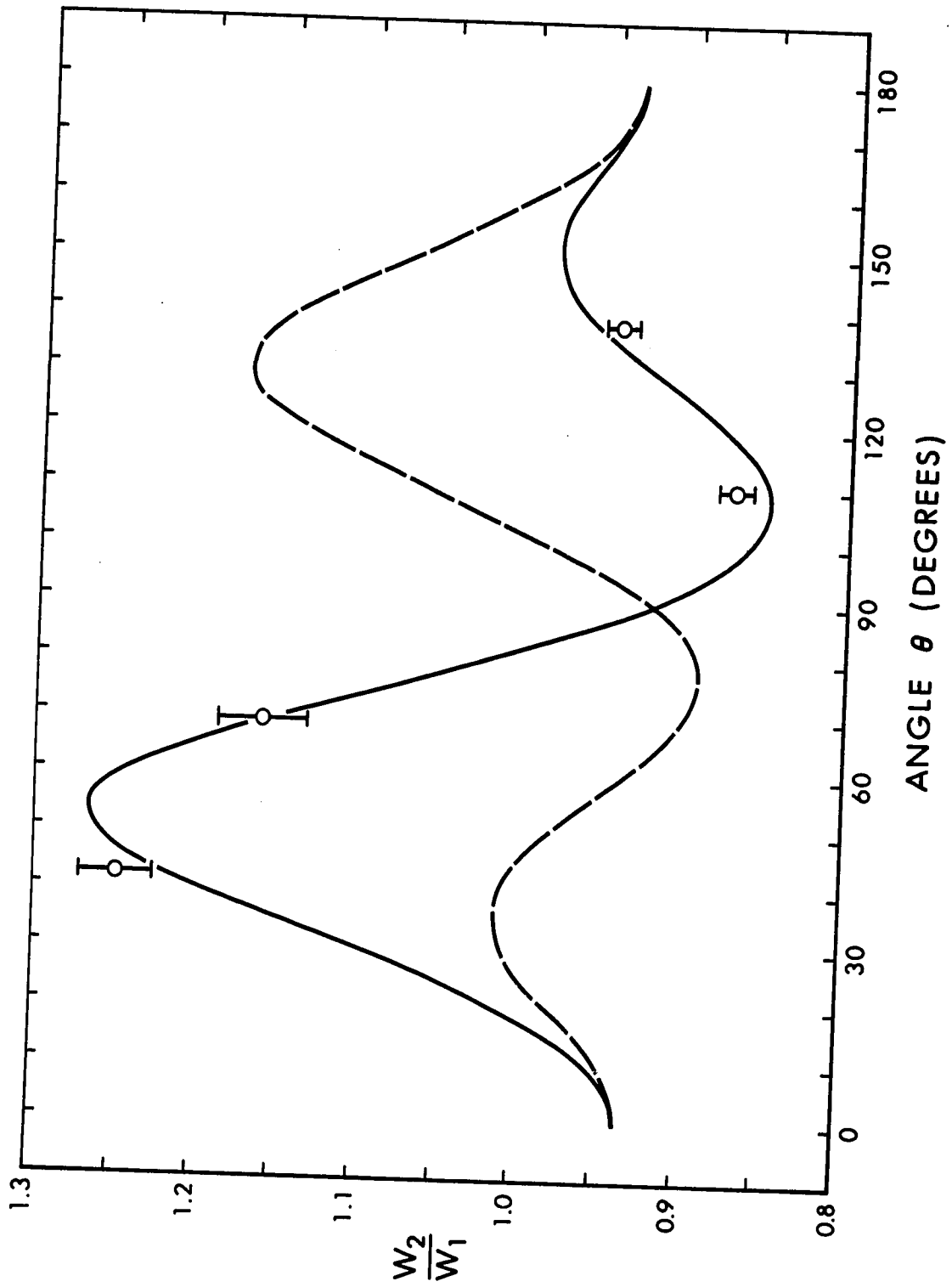
$$\phi = 32.8 \pm 1.5^\circ$$

The data being measured under the conditions of Case I, the enhancement of the high frequency satellite as a result of the severe saturation of the centre line

θ (degrees)	W_2/W_1
42.0	1.249 \pm 0.023
69.0	1.160 0.027
110.0	0.871 0.010
138.0	0.945 0.010

Caption IV d

Figure IV d shows the orientation dependence of our values of W_2/W_1 at $\phi = 32.8 \pm 1.5^\circ$. The solid line is a least squares fit of the Pietila theoretical equations. The dashed line shows the least squares fit for $\phi = 2.8 \pm 1.5^\circ$.



the external errors obtained from the linear fit of the enhancement data. This means that our estimated errors are not directly involved in the limits except in so far as they determine the weighting factor applied to each point. Since various checks mentioned in Section III showed no evidence of non-linearity and since the enhancement values are the simple ratio of successive resonances we are confident that systematic errors are negligible in our measurements of W_2/W_1 . We therefore place a high degree of reliance on the error limits on the values of W_2/W_1 shown in Figure IV c and Figure IV d. The work at $\theta = 0^\circ$ has been published by Hughes, Reed and Snyder (1970).

We now consider the comparison of this data with the theoretical orientation dependence as developed in Section II. Since we have not measured W_1 and W_2 independently, we are unable to determine all the parameters M_{1111} , M_{1313} , M_{3333} , M_{1113} , and M_{1123} . We therefore normalize with respect to M_{1111} and define the following quantities

$$M'_{1313} = M_{1313}/M_{1111}$$

$$M'_{3333} = M_{3333}/M_{1111}$$

$$M'_{1113} = M_{1113}/M_{1111}$$

$$M'_{1123} = M_{1123}/M_{1111}. \quad (\text{IV } 12)$$

Assuming that the values of the M components are the same for W_1 and W_2 , the orientation dependence is therefore, from equation (II 86)

$$\begin{aligned} & (1+4M'_{1313} + 2M'_{3333}) + (6-6M'_{3333})\cos^2\theta \\ \frac{W_1}{W_2} = & \frac{+(1-4M'_{1313}+2M'_{3333})\cos^4\theta + 4(M'_{1113}\cos 3\phi + M'_{1123}\sin 3\phi)\sin^3\theta\cos\theta}{(4+4M'_{1313}-M'_{3333}) - (12M'_{1313}-9M'_{3333})\cos^2\theta} \\ & - (4-16M'_{1313}+8M'_{3333}) - 16(M'_{1113}\cos 3\phi + M'_{1123}\sin 3\phi)\sin^3\theta\cos\theta \end{aligned} \quad (\text{IV } 13)$$

The solid line in Figure IV c represents a least square fit of the crystal data to equation (IV 13) giving the following M' values

$$M'_{1313} = 0.850 \pm 0.015 \quad (\text{IV } 14)$$

$$M'_{3333} = 0.822 \pm 0.016 \quad (\text{IV } 15)$$

$$M'_{1113}\cos 3\phi + M'_{1123}\sin 3\phi = -0.092 \pm 0.014 \quad (\text{IV } 16)$$

where $\phi = 2.8^\circ$.

The agreement between the experimental values and the theory is very good, thus confirming the correctness of equation (IV 13) and the assumption that the M-components are the same for W_1 and W_2 . As was discussed in Section II this implies that the quadrupole relaxation is via an indirect mechanism. This is not unexpected, since the direct process should not contribute significantly compared to the indirect process. Moreover we would not expect rapid reorientation of the NO_3 groups at a temperature so far below the melting point of the crystal.

Figure IV d shows the W_2/W_1 data for $\phi = 32.8 \pm 1.5^\circ$. The purpose of these measurements was to determine $M'_{1113}\cos\phi + M'_{1123}\sin\phi$ from a value of different from that in the first case so that by combining with the data at $\phi = 2.8^\circ$, one can find M'_{1123} and M'_{1113} . Using the values of M'_{1313} , M'_{3333} given earlier, we found at $\phi = 32.8 \pm 1.5^\circ$,

$$M'_{1113}\cos 3\phi + M'_{1123}\sin 3\phi = 0.162 \pm 0.014 \quad (\text{IV } 17)$$

From (IV 16), (IV 17) we find

$$M'_{1113} = -0.115 \pm 0.018$$

and

$$M'_{1123} = 0.147 \pm 0.017$$

(IV 18)

These runs were made at $\theta = 42^\circ, 69^\circ, 110^\circ$ and 138° where the term $\sin^3\theta\cos\theta$ is relatively large. This enables $M'_{1113}\cos\phi +$

Table IV A

$$\text{i) } \phi = 2.8 \pm 1.5^\circ$$

$$M'_{1313} = 0.85 \pm 0.015$$

$$M'_{3333} = 0.822 \pm 0.016$$

$$M'_{1113} \cos 3\phi + M'_{1123} \sin 3\phi = -0.092 \pm 0.014$$

$$\text{ii) } \phi = 32.8 \pm 1.5$$

$$M'_{1113} \cos 3\phi + M'_{1123} \sin 3\phi = 0.162 \pm 0.014$$

Solving the last two expressions gives

$$M'_{1113} = -0.115 \pm 0.018$$

$$M'_{1123} = 0.147 \pm 0.017$$

$M'_{1123} \sin \phi$ to be determined with the most precision. Values between 42° and 69° and between 110° and 138° were avoided due to the proximity of the satellites and centre line.

We now discuss results of the orientation dependence of W_2 and W_1 published by Niemela (1967) during the course of this work. Niemela measured W_2 and W_1 for ^{23}Na in a single crystal of NaNO_3 at 77°K for several values of θ in the range 0° to 90° . The data is shown in Figure IV.e. In these measurements the time dependent behaviour of the spin system following the saturation of a different transition was studied using a pulse method. This method was first suggested by Goldberg (1959) but is different from the one actually used by Goldberg. Niemela measured the resonance intensities as a function of the time after applying the saturating signal. In contrast, Goldberg only measured the resonance intensity immediately following the application of the saturating signal.

As was mentioned in Section I, we did not use a pulse method because of the danger of exciting other components with the 90° pulse. Strictly speaking, the duration of the 90° pulse should be much longer than T_2 , the spin-spin relaxation time. Moreover, τ^{-1} should be much less than the separation between the adjacent ^{23}Na resonances. The pulse duration used by Niemela was 40 microseconds. Since T_2 is $\sim 10^{-4}$ seconds

and the minimum resonance separation (at $\theta = 40^\circ$ and 73.5°) was approximately 60 kHz away from the central value (8MHz), it is clear therefore that Niemela was in fact observing an induction decay signal which included a significant contribution from a component other than that being studied. Since the recovery behaviour of all the resonances is not the same, this admixture of resonances will give rise to errors in the measured values of W_1 and W_2 , especially at $\theta = 40^\circ$ and 73.5° . It should be pointed out that the magnetic relaxation contribution in Niemelas crystal at 77°K was by no means negligible, the value of W_3/W_1 being approximately 0.10, at least 30 times larger than in our crystal. While it is possible to correct for the effect of magnetic relaxation it is necessary to assume that the W_3 is uniform throughout the sample. For large magnetic effects, this may not be valid.

In fitting the data to the orientation dependence given by Pietila (1968), Niemela used an incorrect symmetry argument in showing that $M_{1113}\cos 3\phi + M_{1123}\sin 3\phi$ is zero. According to Niemela the symmetry of the NaNO_3 crystal is such that the crystal is invariant under the rotation $\theta \rightarrow \theta + \pi$ and therefore $M_{1113}\cos 3\phi + M_{1123}\sin 3\phi$ as given in equation (II 86) must vanish. This is incorrect for two reasons. Firstly, the NaNO_3 crystal is not invariant under the rotation $\theta \rightarrow \theta + \pi$.

Secondly, even if it were, it does not follow from equation (II 86) that the term $M_{1113}\cos 3\phi + M_{1123}\sin 3\phi$ is zero. The dashed line in Figure IV e represent a least squares fit of Niemela's data to equation (II 86) with $M_{1113}\sin 3\phi + M_{1123}\cos 3\phi$ set to zero. This fit differs slightly from Niemela's because of a partial error in his theoretical expressions (Pietila, 1968). The corresponding M-values are given by

$$e^2 Q^2 M_{1111} = 2.35 \pm 0.10 \times 10^{-2} \text{ seconds}^{-1} \quad (\text{IV } 19)$$

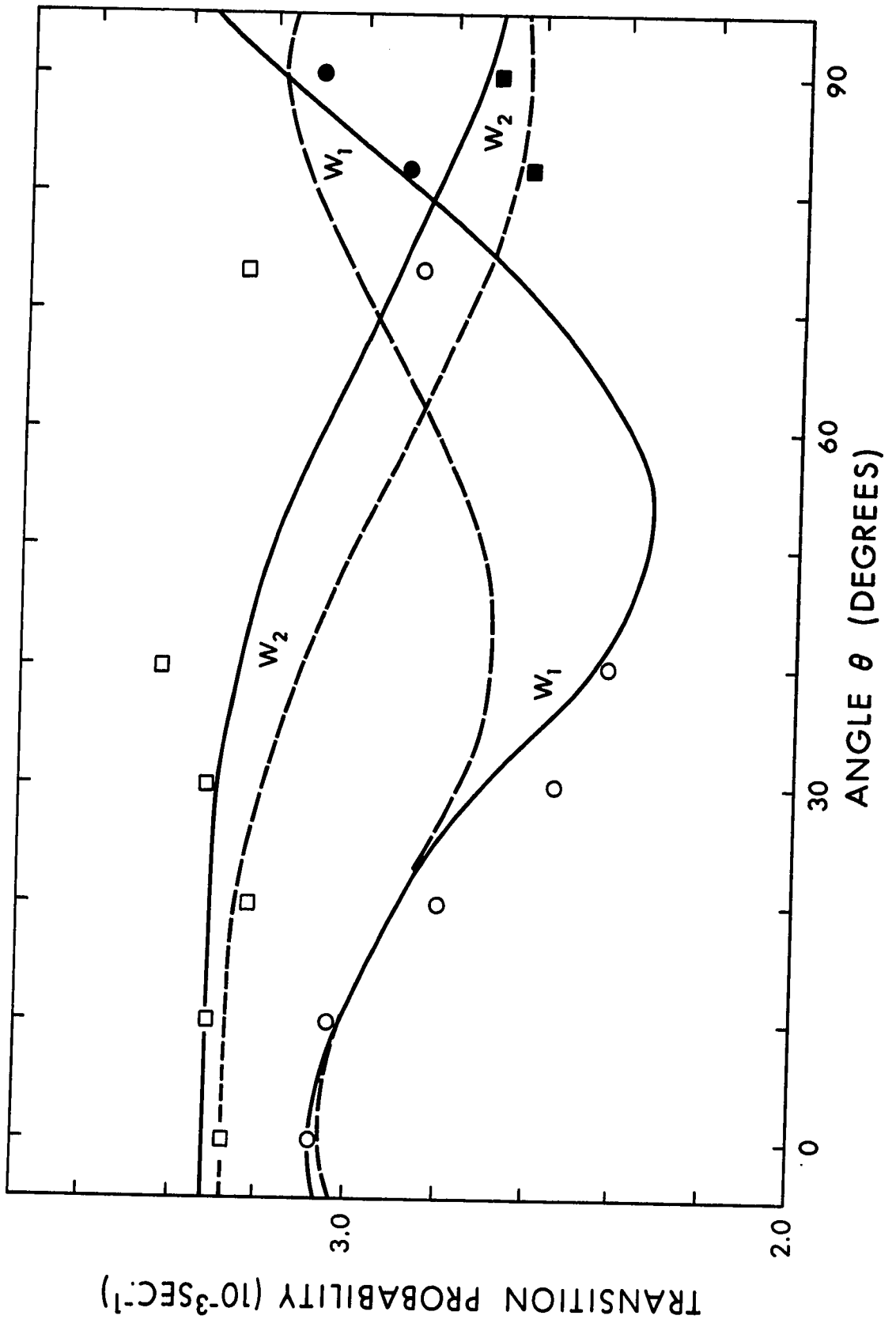
$$e^2 Q^2 M_{1313} = 1.83 \pm 0.09 \times 10^{-2} \text{ seconds}^{-1} \quad (\text{IV } 20)$$

$$e^2 Q^2 M_{3333} = 1.51 \pm 0.29 \times 10^{-2} \text{ seconds}^{-1} \quad (\text{IV } 21)$$

where the error limits are external errors determined by the scatter of the data points about the theoretical curves. While the fit between experiment and theory agree within the error limits given by Niemela, the fit is unsatisfactory because most of the W_1 points lie below the theoretical curve and most of the W_2 points lie above the theoretical curve. We have therefore re-analyzed the data with $M_{1113}\cos 3\phi + M_{1123}\sin 3\phi \neq 0$. A least squares fit of the data is shown as a solid line in Figure IV e. For the crystal orientation used by Niemela, the angle ϕ is 0° when measured with

Caption IV e

Figure IV e shows the orientation dependence of W_2 and W_1 obtained by Niemela at 77°K . The dashed line represents a least squares fit of the data to the theoretical form given by Pietila with $M_{1113} = 0$. The solid line represents a least squares fit of the data with $M_{1113} \neq 0$.



respect to the projection of a rhombohedral unit cell edge in a plane perpendicular to the symmetry axis. In such a coordinate system, the M-values are given by

$$e^2 Q^2 M_{1111} = 2.42 \pm 0.05 \times 10^{-2} \text{ seconds}^{-1} \quad (\text{IV } 22)$$

$$e^2 Q^2 M_{1313} = 1.84 \pm 0.05 \times 10^{-2} \text{ seconds}^{-1} \quad (\text{IV } 23)$$

$$e^2 Q^2 M_{3333} = 1.68 \pm 0.05 \times 10^{-2} \text{ seconds}^{-1} \quad (\text{IV } 24)$$

$$e^2 Q^2 M_{1113} = 0.51 \pm 0.10 \times 10^{-2} \text{ seconds}^{-1}. \quad (\text{IV } 25)$$

The importance of the M_{1113} term is more clearly illustrated in Figure IV f where the ratio W_2/W_1 is shown as a function of θ . The best fit with $M_{1113} = 0$ is shown as a dashed line and the corresponding ratios of the M-values are

$$M_{1313}/M_{1111} = 0.77 \pm 0.09 \quad (\text{IV } 26)$$

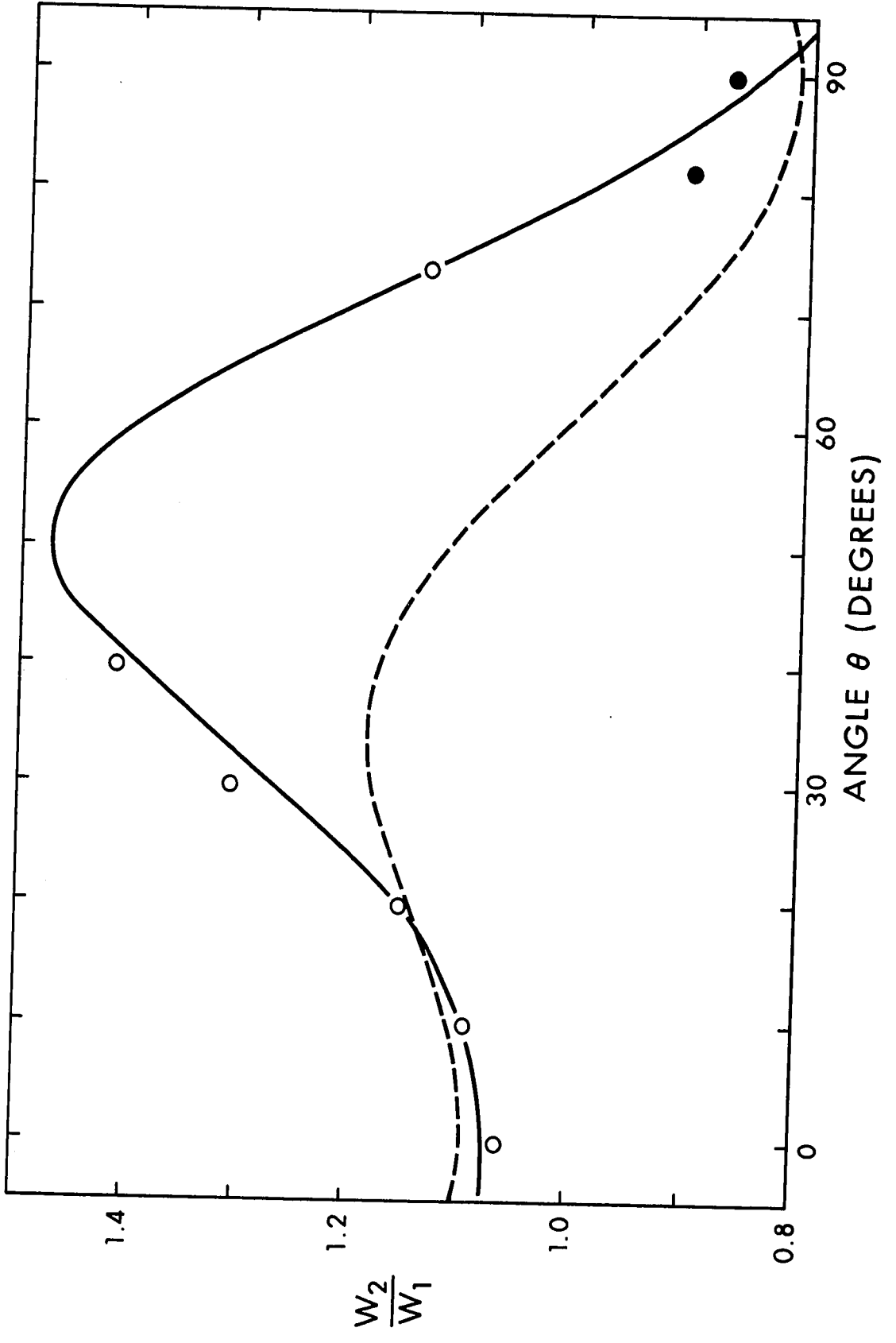
$$M_{3333}/M_{1111} = 0.59 \pm 0.17. \quad (\text{IV } 27)$$

With $M_{1113} \neq 0$, the best fit is the solid line and the corresponding ratios of the M-values are

$$M_{1313}/M_{1111} = 0.78 \pm 0.02 \quad (\text{IV } 28)$$

Caption IV f

Figure IV f shows the orientation dependence of the ratio W_2/W_1 obtained by Niemela at 77°K . The dashed line is a least squares fit of the theoretical form with $M_{1113} = 0$. The solid line is a least squares fit with $M_{1113} \neq 0$.



$$M_{3333}/M_{1111} = 0.66 \pm 0.04 \quad (\text{IV } 29)$$

$$M_{1113}/M_{1111} = 0.26 \pm 0.02 \quad (\text{IV } 30)$$

We conclude that the experimental data are much more precise than was first believed (Niemela, 1967), the agreement being highly satisfactory so long as $M_{1113}\cos 3\phi + M_{1123}\sin 3\phi$ is not set to zero.

We now compare the experimental values of the M-components obtained at 77°K by Niemela (as re-analyzed by us, Hughes, Reed and Snyder, 1970) and by ourselves at room temperature with the theoretical predictions given in Section II. At 77°K, M_{1111} , M_{1313} and M_{3333} are all positive as expected for components of the form $M_{\alpha\beta\alpha\beta}$. Our values are in agreement with this since M_{1313}/M_{1111} and M_{3333}/M_{1111} are also positive. Also, M_{1113}^2 at 77°K is less than $M_{1111}M_{1313}$. Similarly at room temperature we find that $M_{1113}^2 < M_{1111}M_{1313}$ and $M_{1123}^2 < M_{1111}M_{2323}$ (since it was shown by Snyder and Hughes (1970) that $M_{2323} = M_{1313}$).

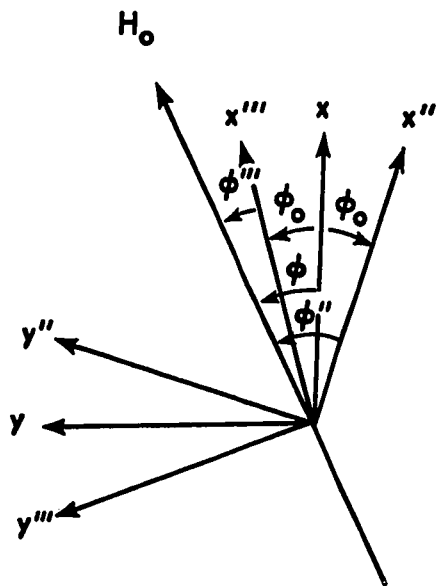
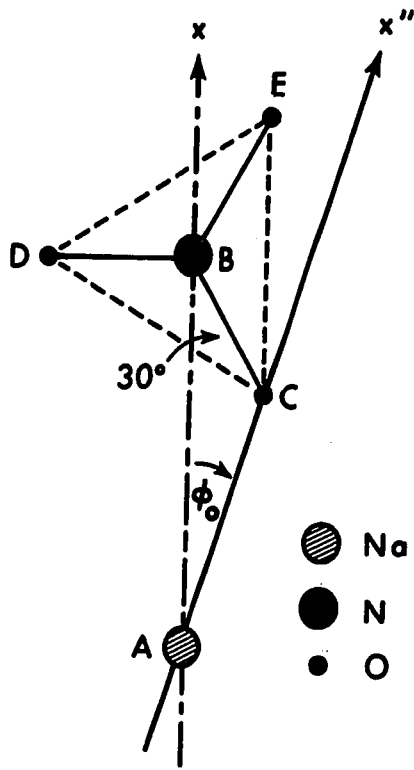
We now consider the relationship between W_1^A and W_1^B , the transition probabilities for the spin systems A and B and also the relationship between W_2^A and W_2^B . For simplicity we first suppose that the nearest neighbour oxygens alone are

responsible for the time-dependent electric field gradient at the particular ^{23}Na site. This assumption is not unreasonable since as will be seen the quadrupole spin-lattice interaction falls off very rapidly as r^{-8} or r^{-10} . The relationship of these six nearest-neighbour oxygen atoms to the ^{23}Na site is shown in Figure III j for cases A and B. As was pointed out in Section III 8, the two lattice sites are equivalent apart from a translational and rotational operation. It is convenient to define a coordinate system (x'' , y'' , z'') for the spin systems A lattice site where z'' axis coincides with the triad axis and the x'' axis is orientated so that two oxygen atoms lie in the $x''z''$ plane. It is clear from Figure IIIj that this $x''z''$ plane (there are of course 3 of them orientated at 120° to each other) is a mirror plane for these nearest neighbours (however this is not so if one considers further neighbours). We denote the angle between the x'' axis and the x axis (defined previously as the projection of the rhombohedral unit cell edge on a plane perpendicular to the crystal triad axis) by ϕ_0 .

A plan view of the situation is shown in Figure IV g. From the crystallographic information the angle ϕ_0 is calculated to equal 18° . For the B lattice sites one can define a similar system of axis (x''' , y''' , z''') such that x'''

Caption IV g

Figure IV g shows schematically the two spin sites with their appropriate principal axis and the angles ϕ_0 .



z''' plane is again a mirror plane containing two nearest neighbour oxygen atoms. Again the angle between the x''' and the x axis is 18° , the sense of rotation from x to x''' being opposite to that from x to x'' .

The two lattice sites A and B are completely equivalent if A and B are viewed from their respective coordinate systems. The values of the M-components will therefore be the same for the two systems if they are defined in the appropriate coordinate system. We denote the M-components at A sites that are non-zero for the symmetry by M'_{1111} , M'_{1313} , M'_{3333} , M'_{1113} and M'_{1123} . We can therefore write quite generally

$$W_1^A = \frac{e^2 Q^2}{48} \left[4M'_{1111} + 4M'_{1313} - M'_{3333} - (12M'_{1313} - 9M'_{3333}) \cos^2 \theta - (4M'_{1111} - 16M'_{1313} + 8M'_{3333}) \cos^4 \theta - 16(M'_{1113} \cos 3\phi'' + M'_{1123} \sin 3\phi'') \sin^3 \theta \cos \theta \right] \quad (\text{IV } 31)$$

where ϕ'' is the azimuthal angle of \vec{H}_0 relative to the (x'', y'', z'') system. For our choice of x'' axis the $x''-z''$ plane is a mirror plane if we consider only the nearest neighbour oxygens. The transition probability W_1^A will therefore be invariant with respect to mirror reflections in the $x''-z''$ plane. Such a mirror reflection corresponds to the

change $\phi'' \rightarrow -\phi''$ in equation (IV 3). This invariance property requires that M''_{1123} be equal to zero. This can also be shown from the invariance of W_2^A .

We denote the M-components for the type B system relative to the $(x'' y'' z'')$ coordinate system by M''_{1111} , M''_{1313} , M''_{3333} , M''_{1113} and M''_{1123} . Using argument similar to that applied to type A it follows that M''_{1123} is zero. Moreover, since the sites A and B are equivalent when viewed from their appropriate (principal) coordinates systems, the values of the corresponding M-components are equal. Putting $M''_{1111} = M''_{1111}$ etc., the transition probabilities can be written

$$W_1^A = \frac{e^2 Q^2}{48} \left[(4M''_{1111} + 4M''_{1313} - M''_{3333}) - (12M''_{1313} - 9M''_{3333}) \cos^2 \theta \right. \\ \left. - (4M''_{1111} - 16M''_{1313} + 8M''_{3333}) \cos^4 \theta - 16M''_{1113} \cos 3\phi'' \sin^3 \theta \cos \theta \right] \quad (\text{IV } 32)$$

$$W_2^A = \frac{e^2 Q^2}{48} \left[(M''_{1111} + 4M''_{1313} + 2M''_{3333}) + (6M''_{1111} - 6M''_{3333}) \cos^2 \theta \right. \\ \left. + (M''_{1111} - 4M''_{1313} + 2M''_{3333}) \cos^4 \theta + 4M''_{1113} \cos 3\phi'' \sin^3 \theta \cos \theta \right] \quad (\text{IV } 33)$$

$$W_1^B = \frac{e^2 Q^2}{48} \left[(4M_{1111}' + 4M_{1313}' - M_{3333}') - (12M_{1313}' - 9M_{3333}') \cos^2 \theta \right. \\ \left. - (4M_{1111}' - 16M_{1313}' + 8M_{3333}') \cos^4 \theta - 16M_{1113}' \cos 3\phi'' \sin^3 \theta \cos \theta \right]. \quad (\text{IV } 34)$$

$$W_2^B = \frac{e^2 Q^2}{48} \left[(M_{1111}' + 4M_{1313}' + 2M_{3333}') + (6M_{1111}' - 6M_{3333}') \cos^2 \theta \right. \\ \left. + (M_{1111}' - 4M_{1313}' + 2M_{3333}') \cos^4 \theta + 4M_{1113}' \cos 3\phi'' \sin^3 \theta \cos \theta \right] \quad (\text{IV } 35)$$

The quantities W_1 and W_2 , whose ratio is measured in our double resonance experiment, are equal to $(W_1^A + W_1^B)/2$ and $(W_2^A + W_2^B)/2$. Therefore from equations (IV 32), (IV 33), (IV 34) and (IV 35) it follows that

$$W_1 = \frac{e^2 Q^2}{48} \left| (4M_{1111}' + 4M_{1313}' - M_{3333}') - (12M_{1313}' - 9M_{3333}') \cos^2 \theta \right. \\ \left. - (4M_{1111}' - 16M_{1313}' + 8M_{3333}') - 8M_{1113}' (\cos 3\phi'' + \cos 3\phi''') \sin^3 \theta \cos \theta \right| \quad (\text{IV } 36)$$

$$W_2 = \frac{e^2 Q^2}{48} \left| (M_{1111}' + 4M_{1313}' + 2M_{3333}') + (6M_{1111}' - 6M_{3333}') \cos^2 \theta \right. \\ \left. + (4M_{1111}' - 4M_{1313}' + 2M_{3333}') \cos^4 \theta + 2M_{1113}' (\cos 3\phi'' + \cos 3\phi''') \right. \\ \left. \sin^3 \theta \cos \theta \right| \quad (\text{IV } 37)$$

But from Figure IV g it is clear that

$$\phi'' = \phi + \phi_0 \quad (\text{IV } 38)$$

and

$$\phi''' = \phi - \phi_0 \quad (\text{IV } 39)$$

Substituting in equations (IV 36) and (IV 37) we get

$$W_1 = \frac{e^2 Q^2}{48} \left[(4M''_{1111} + 4M''_{1313} - M''_{3333}) - (12M''_{1313} - 9M''_{3333}) \cos^2 \theta \right. \\ \left. - (4M''_{1111} - 16M''_{1313} + 8M''_{3333}) - 16M''_{1113} (\cos 3\phi_0 \cos 3\phi) \sin^3 \theta \cos \theta \right] \quad (\text{IV } 40)$$

$$W_2 = \frac{e^2 Q^2}{48} \left[(M''_{1111} + 4M''_{1313} + 2M''_{3333}) + (6M''_{1111} - 6M''_{3333}) \cos^2 \theta \right. \\ \left. + (M''_{1111} - 4M''_{1313} + 2M''_{3333}) \cos^4 \theta + 4M''_{1113} (\cos 3\phi_0 \cos 3\phi) \sin^3 \theta \cos \theta \right] \quad (\text{IV } 41)$$

The expressions for W_1 and W_2 are comprised of independent M-components only one of which, M''_{1113} , involves the angle ϕ'' . Since a redefining of the x'' axis is equivalent to a change in the angle ϕ'' it follows that the M-components M''_{1111} , M''_{1313} and M''_{3333} will be independent of the choice of

the x'' axis. A change in ϕ'' will however affect the M''_{1113} term. The M''_{1113} term will change in such a manner as to keep the value of W_1 and W_2 invariant for the change in ϕ'' . We can therefore write

$$M''_{1111} = M_{1111}$$

$$M''_{1313} = M_{1313}$$

(IV 42)

$$M''_{3333} = M_{3333}$$

where the unprimed M-components refer to the unprimed coordinate system where the x axis is along the projection of the rhombohedral cell edge in a plane perpendicular to the triad axis. Finally it is convenient to replace $M''_{1113} \cos 3\phi_0$ by M_{1113} . Equations (IV 40) and (IV 41) can now be written

$$W_1 = \frac{e^2 Q^2}{48} \left[(4M_{1111} + 4M_{1313} - M_{3333}) - (12M_{1313} - 9M_{3333}) \cos^2 \theta \right. \\ \left. - (4M_{1111} - 16M_{1313} + 8M_{3333}) - 16M_{1113} \cos 3\phi \sin^3 \theta \cos \theta \right] \quad (\text{IV } 43)$$

$$W_2 = \frac{e^2 Q^2}{48} \left[(M_{1111} + 4M_{1313} + 2M_{3333}) + (6M_{1111} - 6M_{3333}) \cos^2 \theta \right. \\ \left. + (M_{1111} - 4M_{1313} + 2M_{3333}) \cos^4 \theta + 4M_{1113} \cos 3\phi \sin^3 \theta \cos \theta \right] \quad (\text{IV } 44)$$

showing that the spin system comprising type A and type B are equivalent to a single spin species with $M_{1113} = M'_{1113} \cos 3\phi_0$. In the above calculation it was assumed that the relaxation was caused by nearest neighbour oxygen atoms. However, the result is independent of this assumption as can be seen from the following argument. Suppose that the nearest neighbour oxygens do not contribute at all to the quadrupole relaxation. Then the A and B spin species are no longer different, the xz plane is now a mirror plane and $\phi = \phi'' = \phi'''$. We would then get the same results as above except that ϕ_0 is 0° instead of 18° . In reality, the quadrupole relaxation field will be partly due to the oxygen and nitrogen atoms and partly due to the rest of the lattice neighbours. In considering we note that the principal coordinate systems $(x''y''z'')$ and $(x'''y'''z''')$ can always be selected such that M'_{1123} and M''_{1123} are zero. Furthermore, from the symmetry of the NaNO_3 crystal structure, the x'' and x''' will be symmetrically disposed with respect to the x axis. While it is not obvious what the angle between the x and x'' or x and x''' axes will be, it seems likely that ϕ_0 should lie between 0° and 18° , the values obtained from the extreme cases where the oxygen does not contribute to relaxation and where the oxygen is wholly responsible for the relaxation. Due to the short range of the

quadrupole interactions, one would expect that ϕ_0 would lie closer to 18° than to 0° . We therefore conclude that (IV 43) and (IV 44) will be valid whatever the source of the quadrupole relaxation.

It is quite generally implied by equations (IV 43) and (IV 44) that M_{1123} must be zero for the ^{23}Na spin system in NaNO_3 . This is in marked contrast to our experimental results which shows that M_{1123} is numerically larger than M_{1113} . Since there is no evidence that our crystal is in any way defective, we interpret this surprising result as implying that the crystal structure of NaNO_3 at room temperature is not that previously accepted. While our data indicate that the ^{23}Na spins are located at sites possessing triad symmetry, the orientation of the principal coordinate systems describing the quadrupole relaxation is not in agreement with that deduced from the crystal structure. Confirmation of the correctness of the ϕ values is obtained from consideration of the ^{23}Na linewidth as a function of θ . For the first setting of measurements (at $\phi = 2.8^\circ$), the linewidth was found to be approximately symmetrical about $\theta = 90^\circ$. In contrast the second set of measurements ($\phi = 32.8^\circ$), the linewidth was found to be quite assymmetric about $\theta = 90^\circ$. Comparison with the linewidth measurements by Andrew et al. (1962) indicates that ϕ is

approximately zero in the first set of measurements and 30° in the second set of measurements.

It is convenient to interpret the M'_{1113} and M'_{1123} values in a slightly different way. We assume that the ^{23}Na sites possess triad symmetry but that the orientation of the principal (x) axis is rotated at an angle ϕ^* from that predicted by the accepted structure. We can therefore write $M'_{1113}\cos 3\phi + M'_{1123}\sin 3\phi$ in the form $A\cos 3(\phi - \phi^*)$. Using the measured values for $M'_{1113} = -0.115 \pm 0.018$ and $M'_{1123} = 0.147 \pm 0.017$ we find $A = 0.187 \pm 0.011$ and $\phi^* = 17.3 \pm 1.8^\circ$. The quantity A may be regarded as a magnitude of the ϕ -dependent term and ϕ^* is the rotation necessary to be able to account for our data. We note that the angle ϕ^* is remarkably close to the value of the angle ϕ_0 considered earlier. Our data could at first sight be interpreted by supposing that the Na spins are all either type A or type B. However, it is not possible to arrange the nitrate groups in the NaNO_3 such that this can occur. A tentative qualitative explanation of our data is that the nitrate groups are rotated from their accepted equilibrium positions in such a way that the angle between x and x'' is greater than ϕ_0 (18°) while the angle between x and x''' is correspondingly less than 18° . However, measurements at the other angles of ϕ are now required in order to confirm

that the ϕ -dependent term really is of the form $A\cos 3(\phi - \phi^*)$ as assumed above. In this connection, measurements at 77°K for $\phi \neq 0$ to complement Niemela's data would be useful.

Finally we compare the predictions of a very simple model with the experimental values of the ratios of the M-components. Guided by the accepted configuration of the nearest neighbour oxygens, we consider a simple model in which the ^{23}Na nucleus, located at the origin of the coordinate system, is surrounded by six point charges q situated at

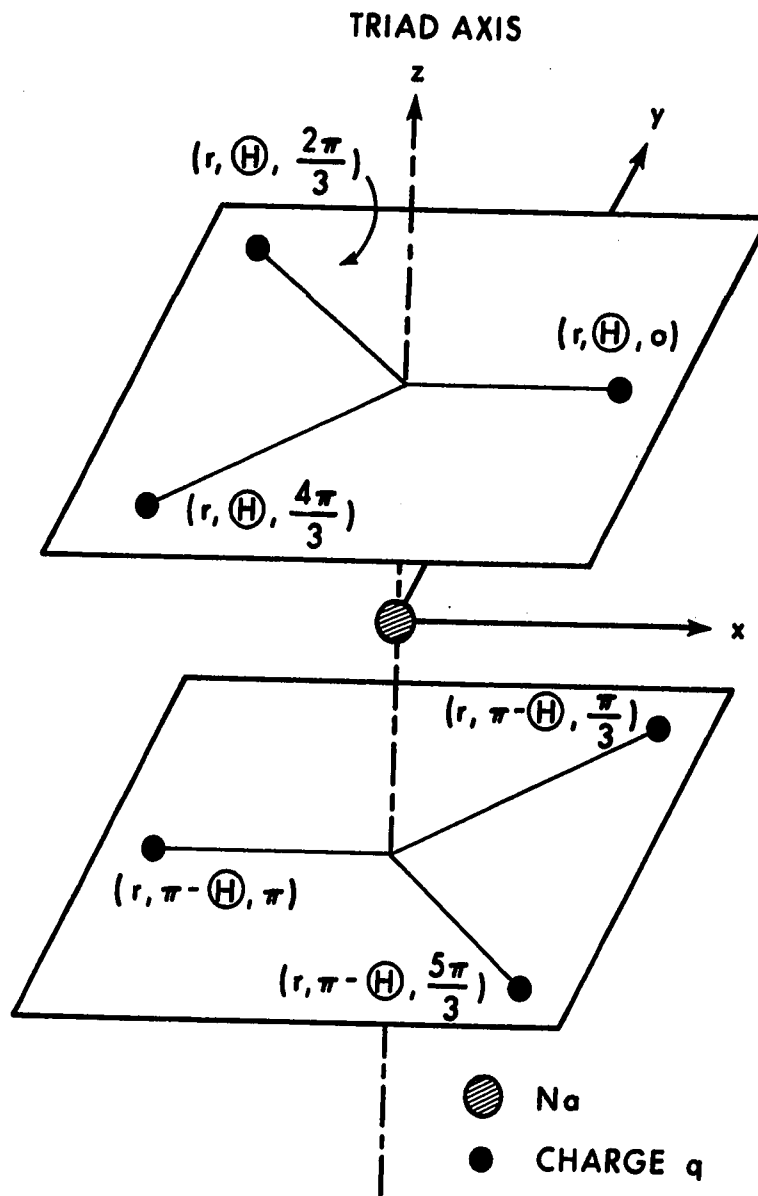
$$(r, \theta, 0), (r, \theta, 2\pi/3), (r, \theta, 4\pi/3), (r, \pi - \theta, \pi/3)$$

$$(r, \pi - \theta, \pi) \text{ and } (r, \pi - \theta, 5\pi/3).$$

The environment of the ^{23}Na nucleus has therefore triad symmetry and inversion symmetry as is the case in NaNO_3 . In the real crystals the relative motions are very complicated and little is known about the relative motion of the ^{23}Na nuclei and their nearest neighbours. We therefore make the simplifying assumption that the motion of each of the six charges relative to the ^{23}Na nucleus is isotropic. In other words, there is no preferential direction in space of the relative motions. We now calculate for this simple model the fluctuations in the electric field gradient at the origin which are caused by this isotropic motion of the point charges. We

Caption IV h

Figure IV h is a schematic representation of the charge configuration used in the point charge calculation of the various M-components.



shall consider two cases. In the first case we shall calculate the changes in the electric field gradient which are linear in displacement. In the second case, we shall calculate the fluctuation in the electric field gradient which are quadratic in displacement. The first case would correspond to the anharmonic Raman phonon process and the second case to the indirect harmonic Raman phonon process.

Considering first a simple charge located at (x, y, z) , we have

$$V_{zz} = q(2z^2 - x^2 - y^2) (x^2 + y^2 + z^2)^{-5/2} \quad (\text{IV } 45)$$

The change $\delta(V_{zz})$ arising from a displacement u of the charge q from its equilibrium site is in the linear case given by

$$\delta(V_{zz}) = \frac{\partial}{\partial x}(V_{zz})dx + \frac{\partial}{\partial y}(V_{zz})dy + \frac{\partial}{\partial z}(V_{zz})dz \quad (\text{IV } 46)$$

where

$$dx = u \sin \theta \cos \phi, \quad dy = u \sin \theta \sin \phi \quad \text{and} \quad dz = u \cos \theta \quad (\text{IV } 47)$$

and θ and ϕ are the polar angles of the displacement \vec{u} relative to the (xyz) coordinate system. It can be seen from the definition of the $M_{\alpha\beta\alpha'\beta'}$ equation II 81) that M_{3333} for example is proportional to the square of the fluctuations V_{zz}

integrated over all relative vibrations. Taking into account all six charges and ignoring constants such as $e^2 Q^2$ in equation (II 81) one can write

$$M_{3333} = \Sigma_q (1/4\pi) \int_0^\pi \left[\delta(V_{zz}) \right]^2 \sin\theta \, d\theta \int_0^{2\pi} d\phi \quad (\text{IV } 48)$$

where Σ_q signifies that the expression is summed over the configuration of six charges as shown in Figure IV h. After some manipulation we find that

$$M_{3333} = 18q^2 u^2 r^{-8} (1 - 2\cos^2\theta + 5\cos^4\theta). \quad (\text{IV } 49)$$

We have generalized this expression to the extent of allowing the vibration in the z direction to be different from that in the x and y direction. This is allowed for by introducing a factor λ for the vibration along the z direction. The value $\lambda = 1$ therefore corresponds to the isotropic case considered above. The value $\lambda \rightarrow 0$ corresponds to relative motion predominantly in the x-y plane as was suggested by Andrew et al. (1962). The value $\lambda \rightarrow \infty$ represents the situation where the relative motion is predominantly in the z direction along the triad axis. Equation (IV 49) becomes

$$M_{3333} = 18q^2 u^2 r^{-8} \left[(5\cos^2\theta - 1)^2 (1 - \cos^2\theta) + \lambda^2 (3 - 5\cos^2\theta)^2 \cos^2\theta \right] \quad (\text{IV } 50)$$

Similarly it can be shown for the linear process

$$M_{1111} = 6q^2 u^2 r^{-8} [\sin^2 \theta [(3-5\sin^2 \theta)^2 + (1/2)(3-5\sin^2 \theta/4)^2 + (3/2)(-1+5\sin^2 \theta/4)] + \lambda^2 \cos^2 \theta [(5\sin^2 \theta - 1)^2 + 2(-1+5\sin^2 \theta/4)^2]] \quad (\text{IV } 51)$$

$$M_{1313} = 6q^2 u^2 r^{-8} [\cos^2 \theta [(1-5\sin^2 \theta)^2 + (75/8)\sin^4 \theta] + (3/2) + \lambda^2 \sin^2 \theta (1-5\cos^2 \theta)^2] \quad (\text{IV } 52)$$

$$M_{1113} = 6q^2 u^2 \sin \theta \cos \theta r^{-8} [(3-5\sin^2 \theta)(1-5\sin^2 \theta) + (15/4)\sin^2 \theta \times (1-5\sin^2 \theta/4) - (3-5\sin^2 \theta/4)(1-5\sin^2 \theta/4) - (15\lambda^2/4)(1-5\cos^2 \theta)\sin^2 \theta]. \quad (\text{IV } 53)$$

From symmetry the M_{1123} is zero in this case. We recall that the M_{1113} as measured experimentally is $M'_{1113} \cos 3\phi_0$. The quantity given in equation (IV 53) is M'_{1113} . Accordingly, to compare with experiment, this should be multiplied by $\cos 3\phi_0$. Hence we can write

$$M_{1113} = 6q^2 u^2 r^{-8} \sin \theta \cos \theta \cos 3\phi_0 [(3-5\sin^2 \theta)(1-5\sin^2 \theta) + (15/4)\sin^2 \theta \times (1-5\sin^2 \theta/4) - (3-5\sin^2 \theta/4)(1-5\sin^2 \theta/4) - (15\lambda^2/4)(1-5\cos^2 \theta)\sin^2 \theta] \quad (\text{IV } 54)$$

Figures IV i, IV j, IV k illustrate the dependence of M_{1111} , M_{1313} , M_{3333} and M_{1113} on the angle θ for three values of $\lambda = 0.80, 1.00, \text{ and } 1.25$. The large dependence on θ indicates that the local lattice environment has a large effect on the M-components. Some indication of the effect of anisotropy of the lattice vibrations is given by comparing the curves for different values of λ .

For the quadratic case, the change in V_{zz} caused by a displacement \vec{u} can be written as

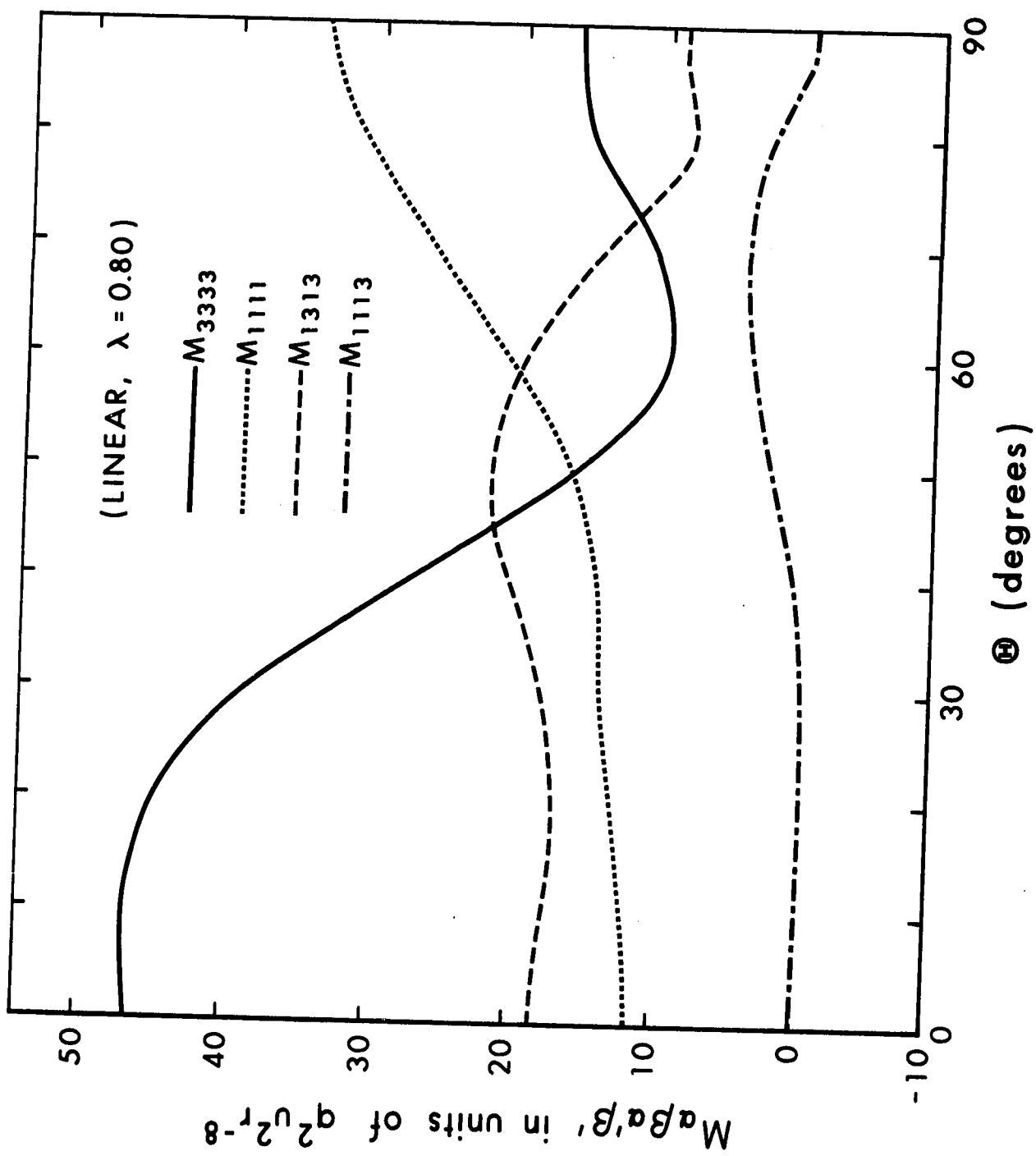
$$\delta V_{zz} = (1/2) \left[\frac{\partial^2 V_{zz}}{\partial x^2} dx^2 + \frac{\partial^2 V_{zz}}{\partial y^2} dy^2 + \frac{\partial^2 V_{zz}}{\partial z^2} dz^2 + \frac{2\partial^2 V_{zz}}{\partial x \partial y} dx dy + \frac{2\partial^2 V_{zz}}{\partial x \partial z} dx dz + 2 \frac{\partial^2 V_{zz}}{\partial y \partial z} dy dz \right] \quad (\text{IV } 55)$$

Using equation (IV 55) and substituting for the derivatives in equation (IV 55) to determine $\overline{[V_{zz}]^2}$, it can be shown that M_{3333} for the charge configuration shown in Figure IV h is given by

$$M_{3333} = (9q^2 u^4 r^{-10} / 10) \left[[8(1-5\cos^2\theta)^2 + 40(1-5\cos^2\theta)(7\cos^2\theta - 1)\sin^2\theta + 75(7\cos^2\theta - 1)^2 \sin^4\theta] + \lambda^2 [(2)(3-30\cos^2\theta + 35\cos^4\theta) \times \right.$$

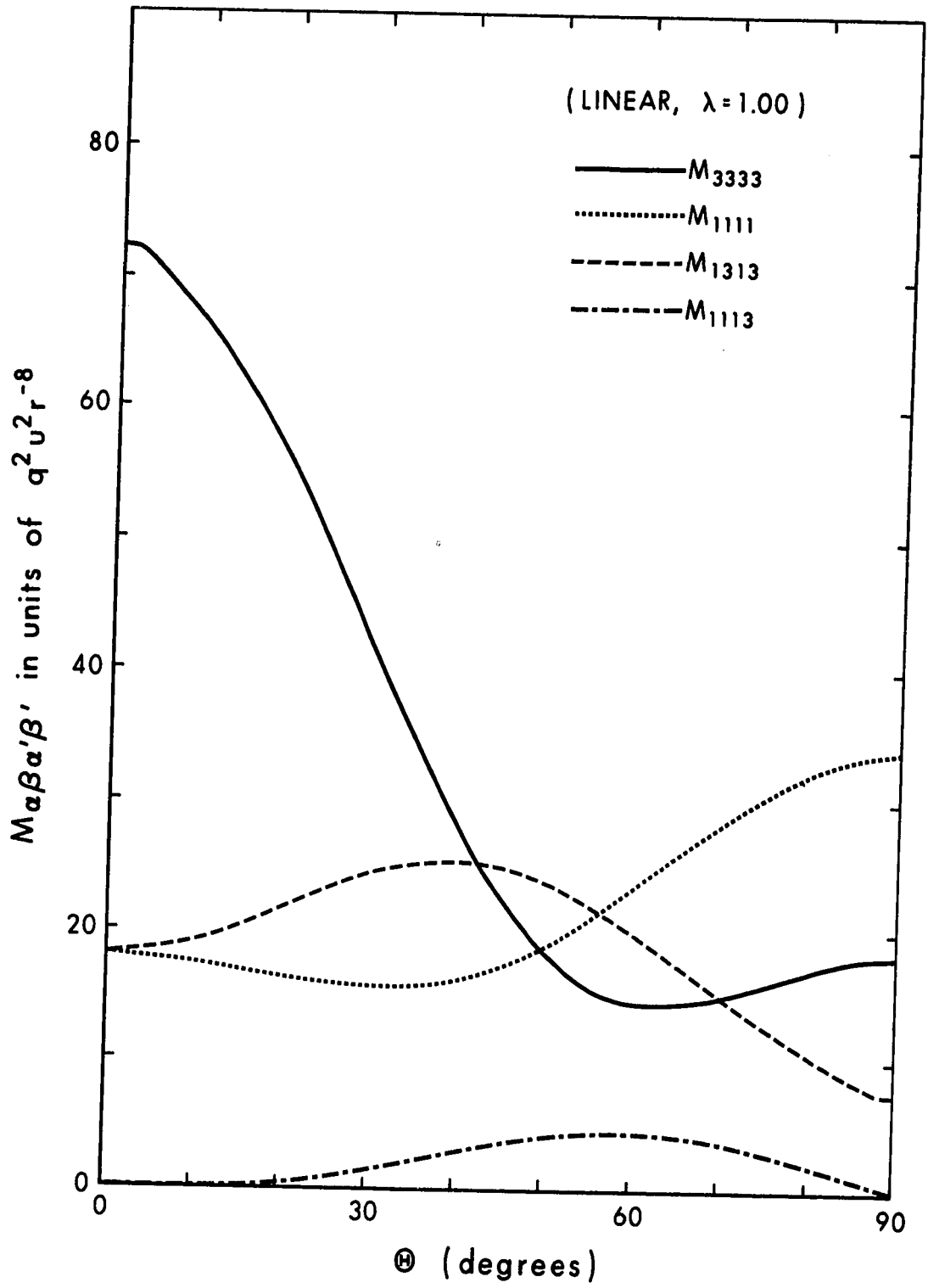
Caption IV i

Figure IV i shows the M-components M_{1111} , M_{1313} , M_{3333} and M_{1113} as a function of θ for the linear process and $\lambda = 0.80$.



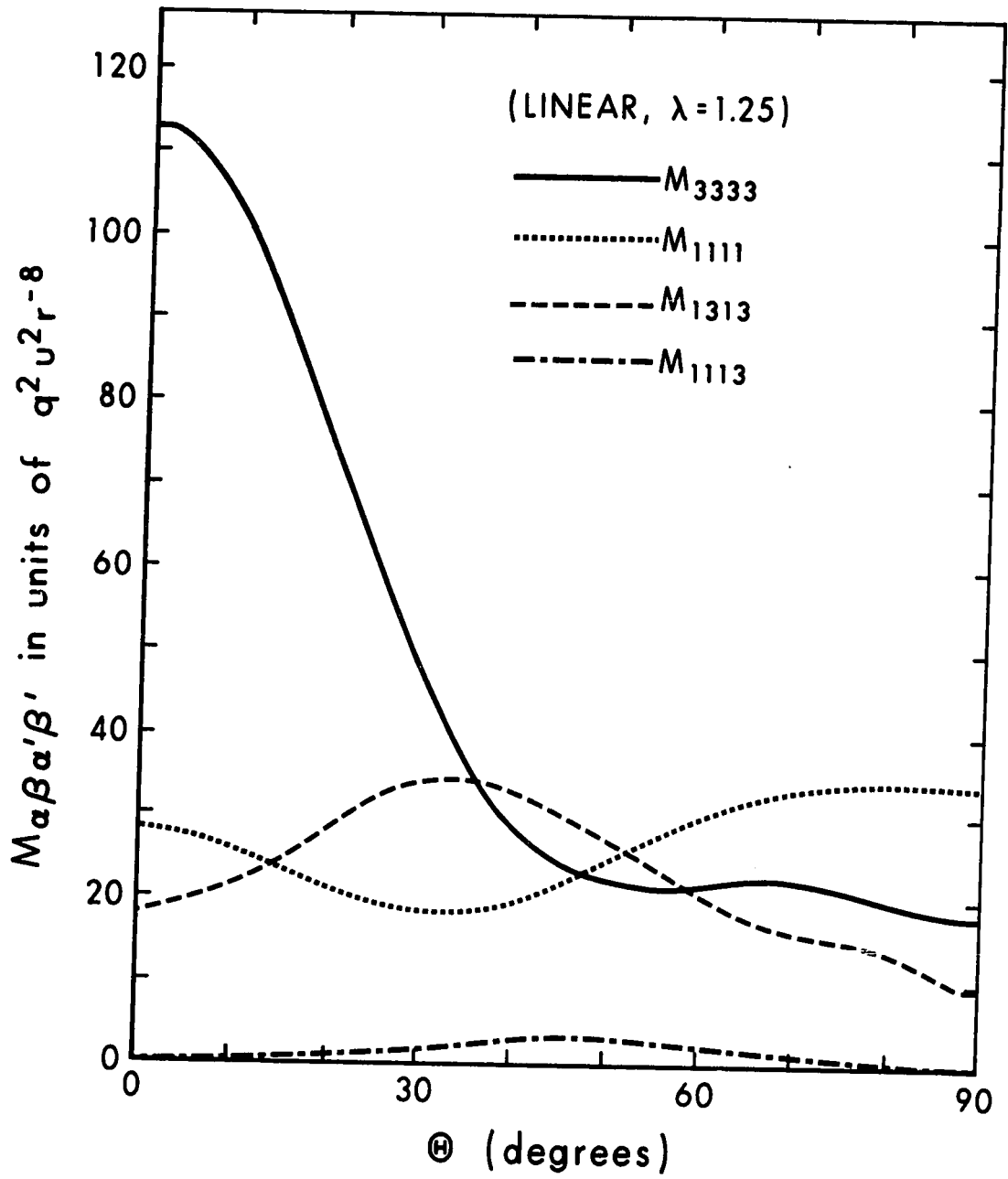
Caption IV j

Figure IV j shows the M-components M_{1111} , M_{1313} , M_{3333} and M_{1113} as a function of θ for the linear process and $\lambda = 1.00$.



Caption IV k

Figure IV k shows the M-components M_{1111} , M_{1313} , M_{3333} and M_{1113} as a function of θ for the linear process and $\lambda = 1.25$.



$$\begin{aligned}
& \times [2(1-5\cos^2\theta) + 5\sin^2\theta(7\cos^2\theta - 1)] + 100\cos^2\theta\sin^2\theta(7\cos^2\theta - 3)^2] \\
& + 3\lambda^4 [3 - 30\cos^2\theta + 35\cos^4\theta]^2].
\end{aligned} \tag{IV 56}$$

Similarly it can be shown that

$$\begin{aligned}
M_{1111} = & (3q^2u^4r^{-10}/10) \left[3(3 - 30\sin^2\theta + 35\sin^4\theta)^2 + 3(1 - 5\sin^2\theta)^2 \right. \\
& + 2(3 - 30\sin^2\theta + 35\sin^4\theta)(1 - 5\sin^2\theta) + 6[3 - (30/4)\sin^2\theta + (35/16)\sin^4\theta]^2 \\
& + 6[1 - 5\sin^2\theta + (105/15)\sin^4\theta]^2 + (300/8)\sin^4\theta(3 - 7\sin^2\theta/4)^2 \\
& + 4[3 - (30/4)\sin^2\theta + (35/16)\sin^4\theta][1 - 5\sin^2\theta + (105/16)\sin^4\theta] \\
& + \lambda^2 [100\cos^2\theta\sin^2\theta(7\sin^2\theta - 3)^2 - 2(4 - 35\sin^2\theta\cos^2\theta)^2 \\
& + 50\sin^2\theta\cos^2\theta [(3 - 7\sin^2\theta/4)^2 + 3(1 - 7\sin^2\theta/4)^2] \\
& \left. + 3\lambda^4 [(4 - 35\sin^2\theta\cos^2\theta)^2 + 2[(15/4)\sin^2\theta - 4 + (35/4)\sin^2\theta\cos^2\theta]^2] \right],
\end{aligned} \tag{IV 57}$$

$$\begin{aligned}
M_{1313} = & (3q^2u^4r^{-10}/10) \left[\sin^2\theta\cos^2\theta [75(7\sin^2\theta - 3)^2 - 50(7\sin^2\theta - 3) + 75 \right. \\
& + (75/2)(3 - 7\sin^2\theta/4) + (75/2)(1 - 21\sin^2\theta/4) + 150(1 - 7\sin^2\theta/4)^2 \\
& \left. + (50/2)(3 - 7\sin^2\theta/4)(1 - 21\sin^2\theta/4) \right]
\end{aligned}$$

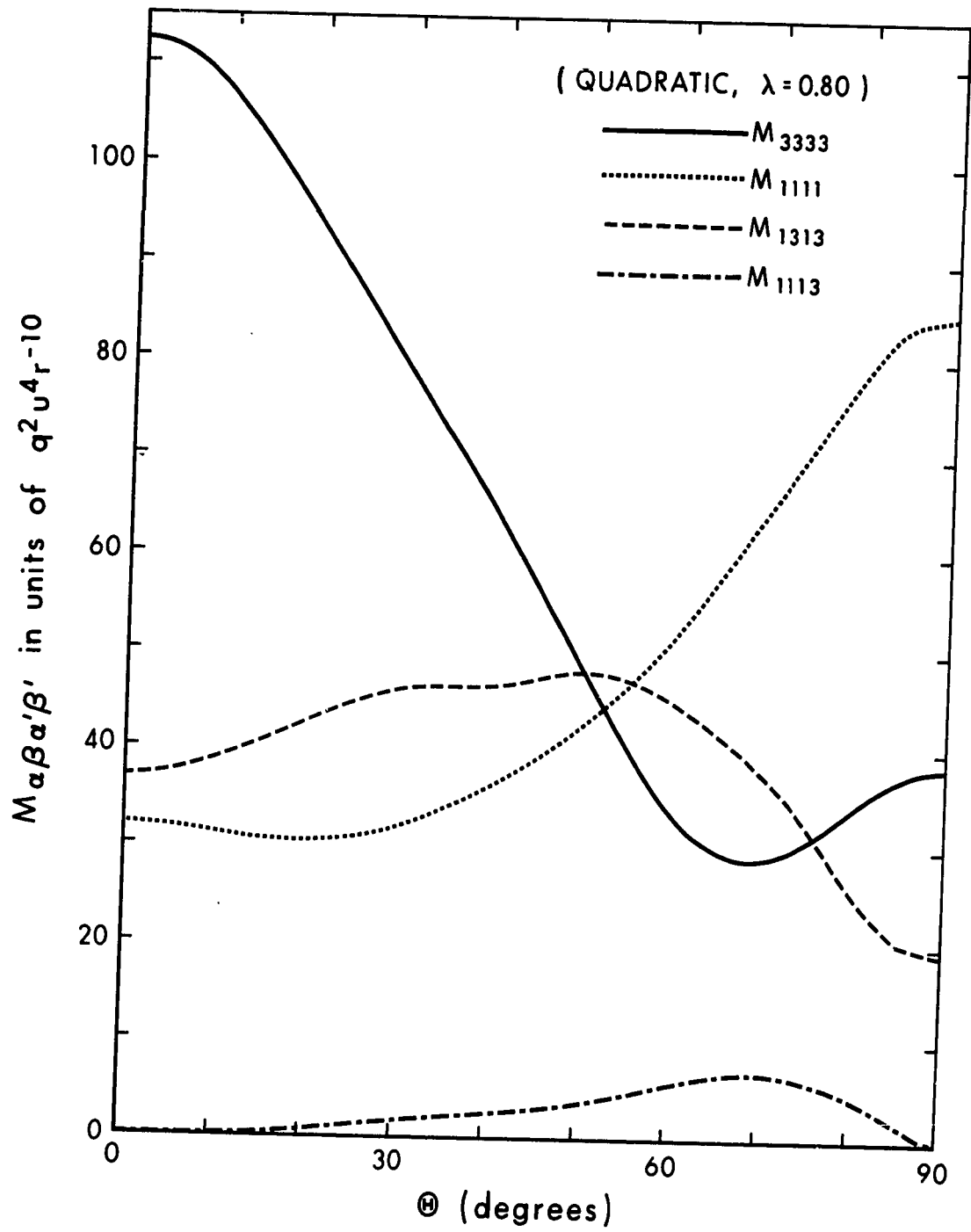
$$\begin{aligned}
& + \lambda^2 [4(35\sin^2\theta\cos^2\theta-4)^2 - 50\sin^2\theta\cos^2\theta (3-7\cos^2\theta)^2 \\
& + 2(35\sin^2\theta\cos^2\theta + 15\sin^2\theta-16)^2 + (75/2)\sin^4\theta(7\cos^2\theta-1)^2 \\
& - (50/2)\sin^2\theta\cos^2\theta (3-7\cos^2\theta)^2] \\
& + \lambda^4 (225/2)\sin^2\theta\cos^2\theta (7\cos^2\theta - 3)^2] \quad \text{(IV 58)}
\end{aligned}$$

$$\begin{aligned}
M_{1113} = & (3q^2u^4\sin\theta\cos\theta\cos 3\phi_0 r^{-10}/2) \left[3(7\sin^2\theta-3)(3-30\sin^2\theta+35\sin^4\theta) \right. \\
& - 3(5\cos^2\theta-4) - (3-30\sin^2\theta + 35\sin^4\theta) + (7\sin^2\theta-3)(5\cos^2\theta-4) \\
& - 3(3-7\sin^2\theta/4) [3-(30/4)\sin^2\theta + (35/16)\sin^4\theta] \\
& - 3(-1+21\sin^2\theta/4) [5\cos^2\theta-4 + (105/16)\sin^4\theta] \\
& + \lambda^2 [(35\sin^2\theta\cos^2\theta - 4)(42\sin^2\theta-20) - 16(7\sin^2\theta-12) \times \\
& \times (15\sin^2\theta-16 + 35\sin^2\theta\cos^2\theta) - 60\sin^2\theta(7\cos^2\theta-1)(7\sin^2\theta-4) \\
& - 8(3-7\cos^2\theta)(15\sin^2\theta - 16 + 35\sin^2\theta\cos^2\theta)] \\
& \left. + \lambda^4 [12(7\cos^2\theta-3)(105\sin^2\theta\cos^2\theta-15\sin^2\theta) \right] \quad \text{(IV 59)}
\end{aligned}$$

Figure IV 1, IV m and IV n illustrate the dependence of M_{1111} , M_{1313} , M_{3333} and M_{1113} on the angle θ for $\lambda = 0.80, 1.00$ and 1.25 for the quadratic case.

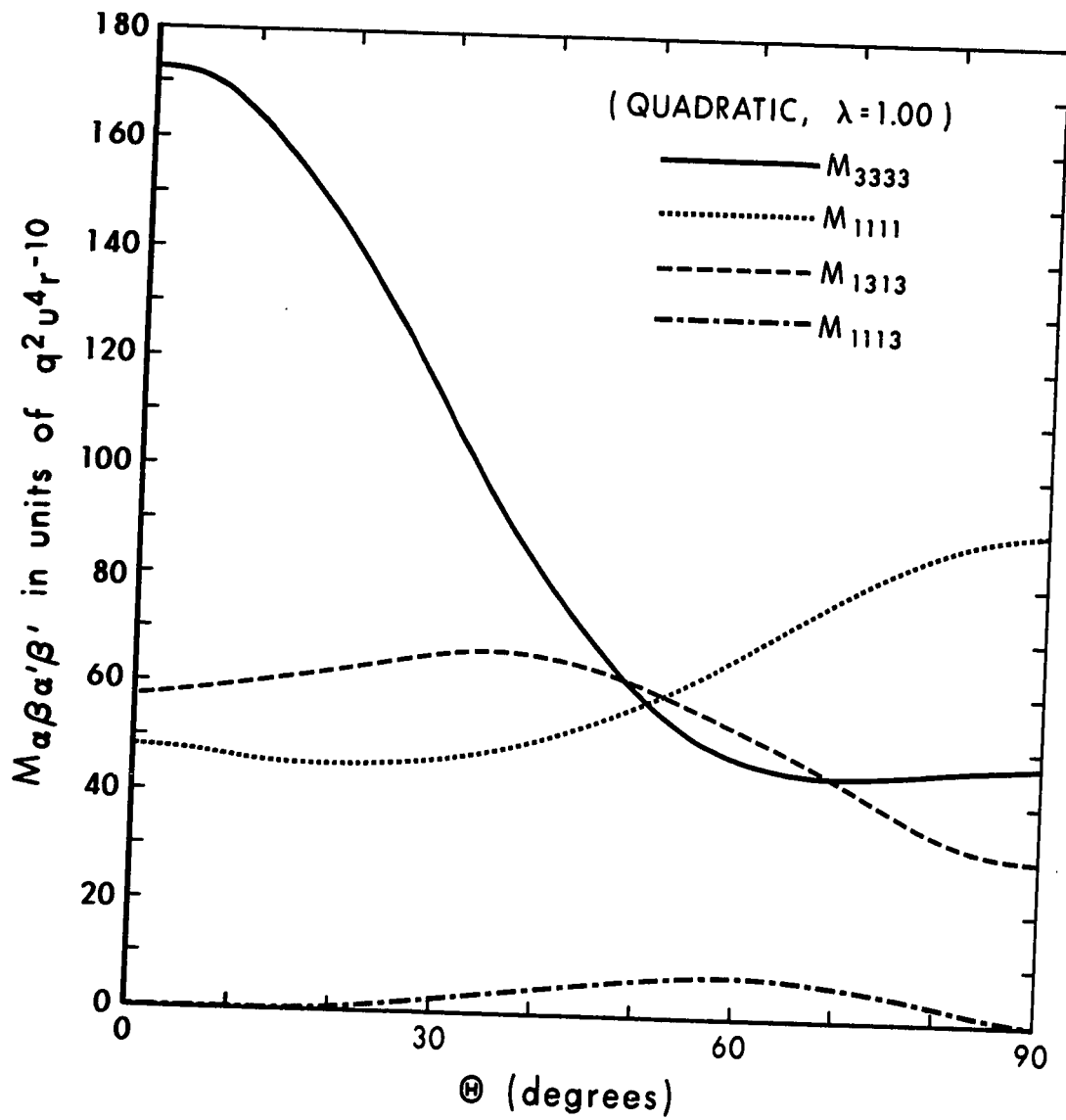
Caption IV 1

Figure IV 1 shows the M-components M_{1111} , M_{1313} , M_{3333} and M_{1113} as a function of θ for the quadratic process and $\lambda = 0.80$.



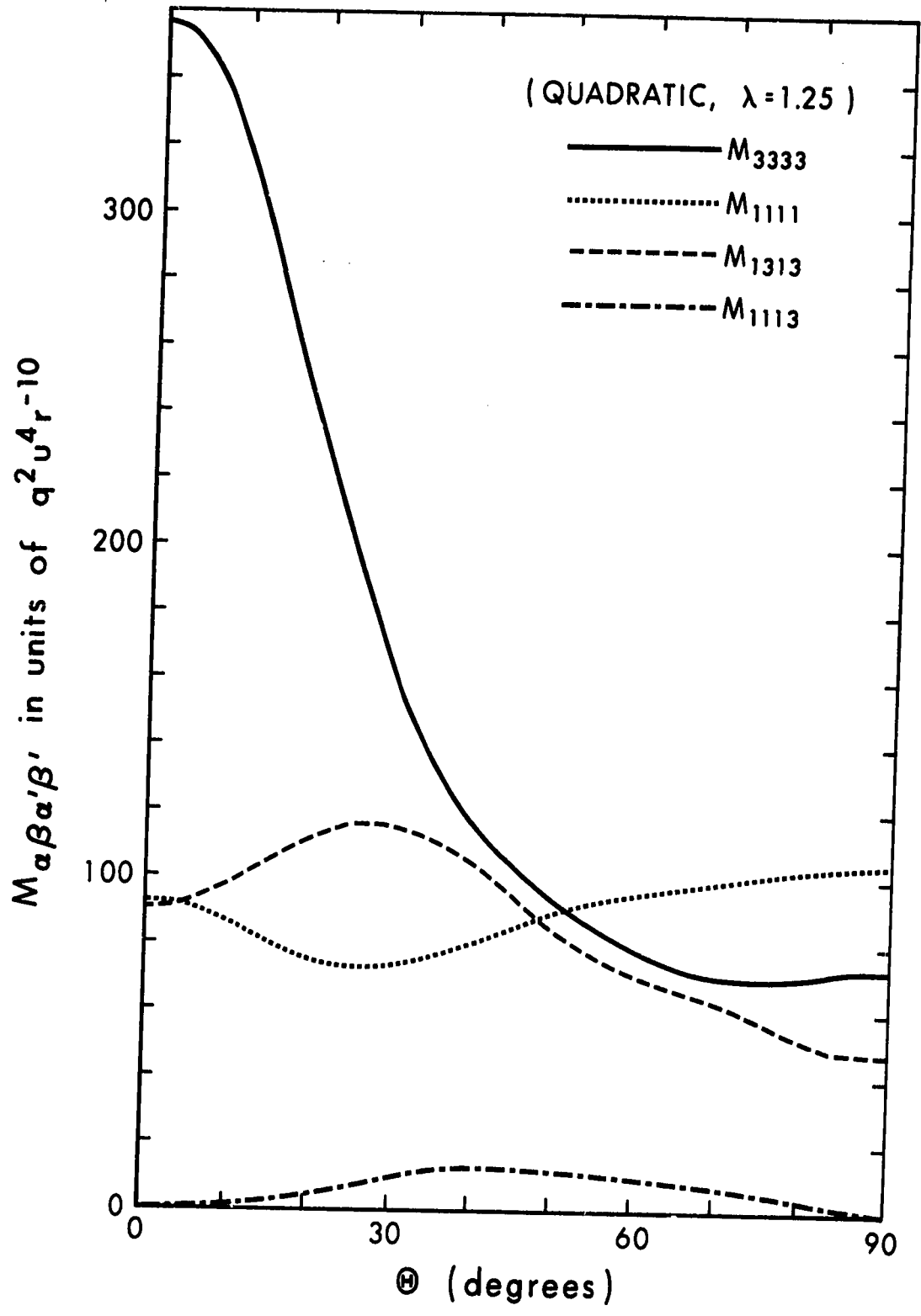
Caption IV m

Figure IV m shows the M-components M_{1111} , M_{1313} , M_{3333} and M_{1113} as a function of θ for the quadratic case and $\lambda = 1.00$.



Caption IV n

Figure IV n shows the M-components M_{1111} , M_{1313} , M_{3333} and M_{1113} as a function of θ for the quadratic case and $\lambda = 1.25$.

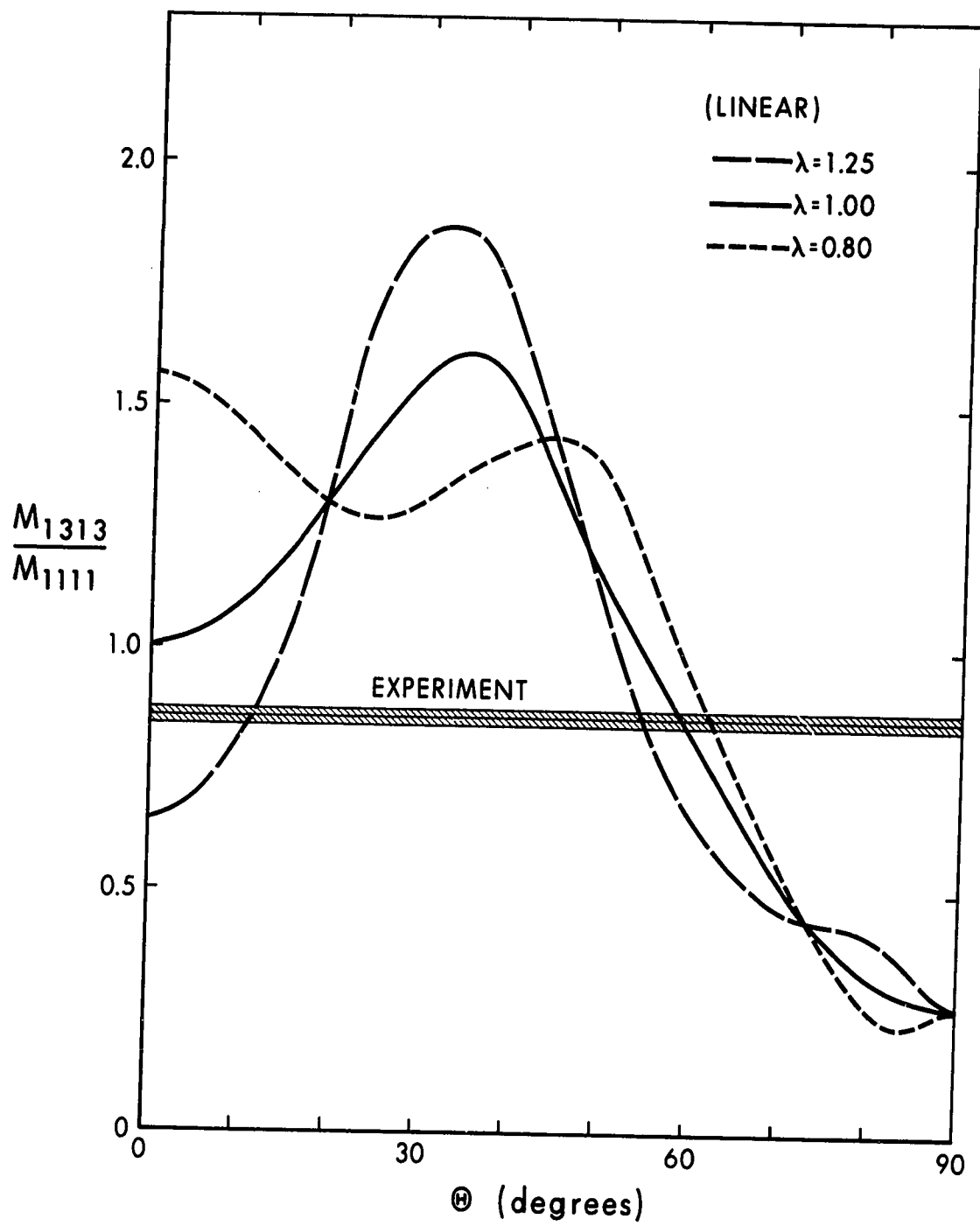


Since our experiment was concerned with the ratios of the M-components and not absolute values of these components, we have plotted M_{1313}/M_{1111} , M_{3333}/M_{1111} and M_{1113}/M_{1111} for the linear case in Figures IV o, IV p and IV q respectively for $\lambda = 0.80, 1.00$ and 1.25 . Similarly, these quantities are shown in Figures IV r, IV s and IV t for the quadratic case, again for $\lambda = 0.80, 1.00$ and 1.25 . Our experimental values are shown on each of graphs IV o + t along with the uncertainties. In Figure IV q and IV t, we have shown not the experimental value of M_{1113}/M_{1111} but the total magnitude of the ϕ -dependent term defined by $\sqrt{M_{1113}^2 + M_{1123}^2} / M_{1111}$. This is justifiable since M_{1123} is zero for the theoretical model we considered.

We first note that the θ dependence is similar in the linear and quadratic cases for the ratios M_{1313}/M_{1111} and M_{3333}/M_{1111} . However, the ratio M_{1113}/M_{1111} is significantly smaller in the quadratic case than in the linear case. We see that in all cases except for the M_{1113}/M_{1111} quadratic case, the value of θ which corresponds with the experimentally measured ratios is approximately 54° and this happens to be the polar angle θ of the nearest neighbour oxygen atom in the NaNO_3 crystal. The appreciable difference between the theoretical linear and quadratic terms for M_{1113}/M_{1111} leads one to wonder

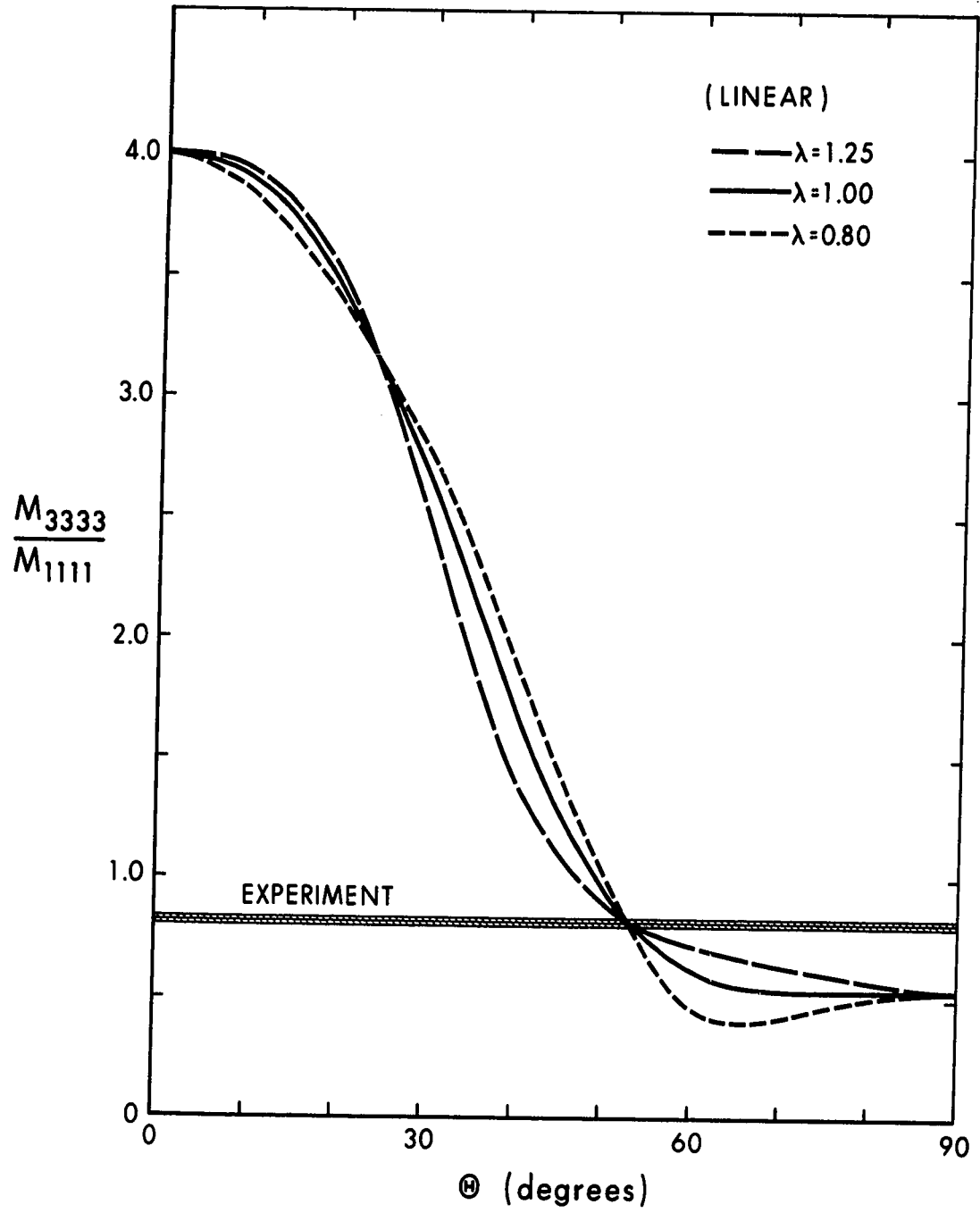
Caption IV o

Figure IV o shows the ratio M_{1313}/M_{1111} as a function of θ for the linear process and $\lambda = 0.80, 1.00$ and 1.25 . Also shown is our experimental value of M_{1313}/M_{1111} for ^{23}Na in NaNO_3 . The shaded region indicates the limits of experimental errors.



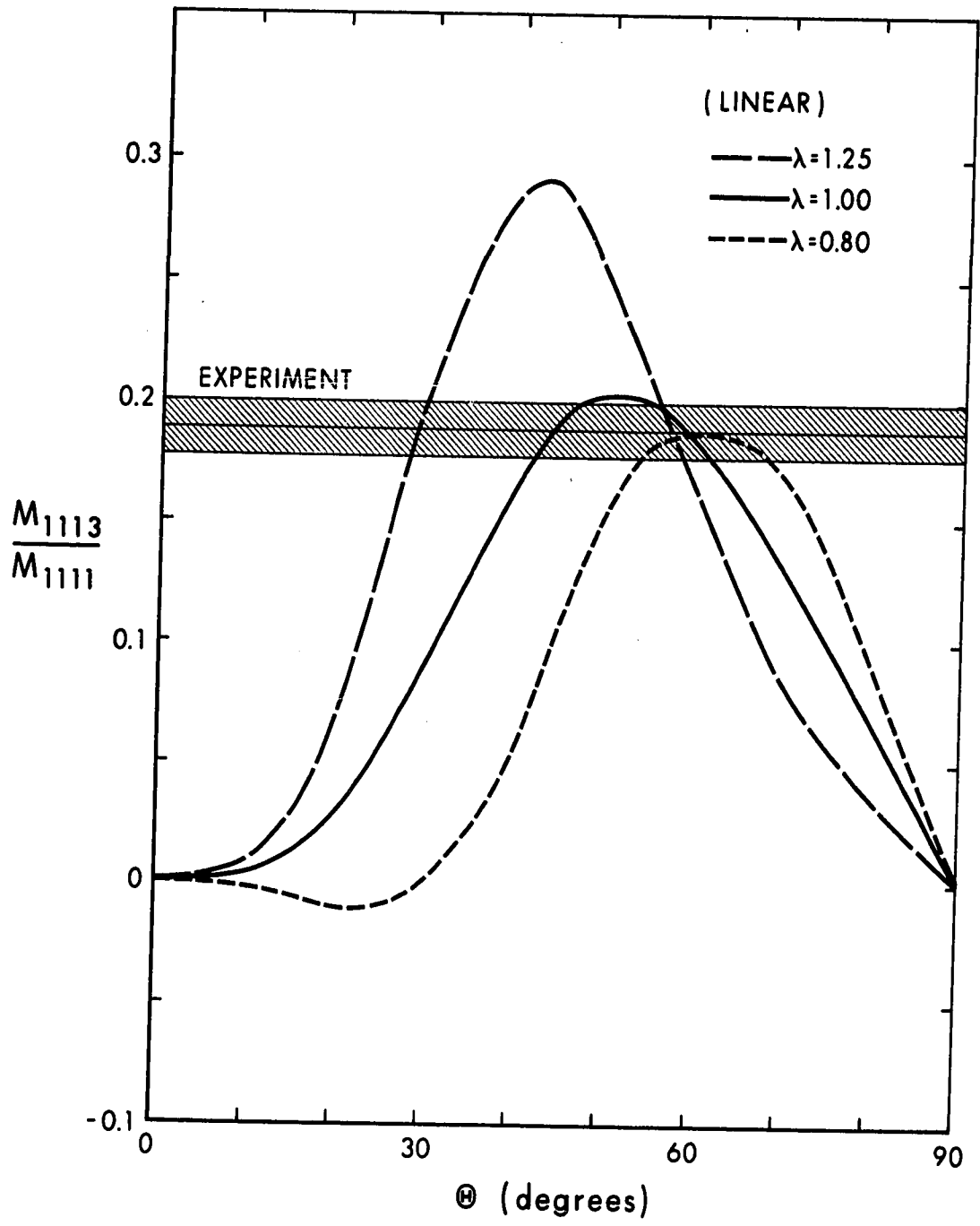
Caption IV p

Figure IV p shows the ratio M_{3333}/M_{1111} as a function of θ for the linear process and $\lambda = 0.80, 1.00$ and 1.25 . Also shown is our experimental value of M_{3333}/M_{1111} for ^{23}Na in NaNO_3 . The shaded region indicates the limits of the experimental error.



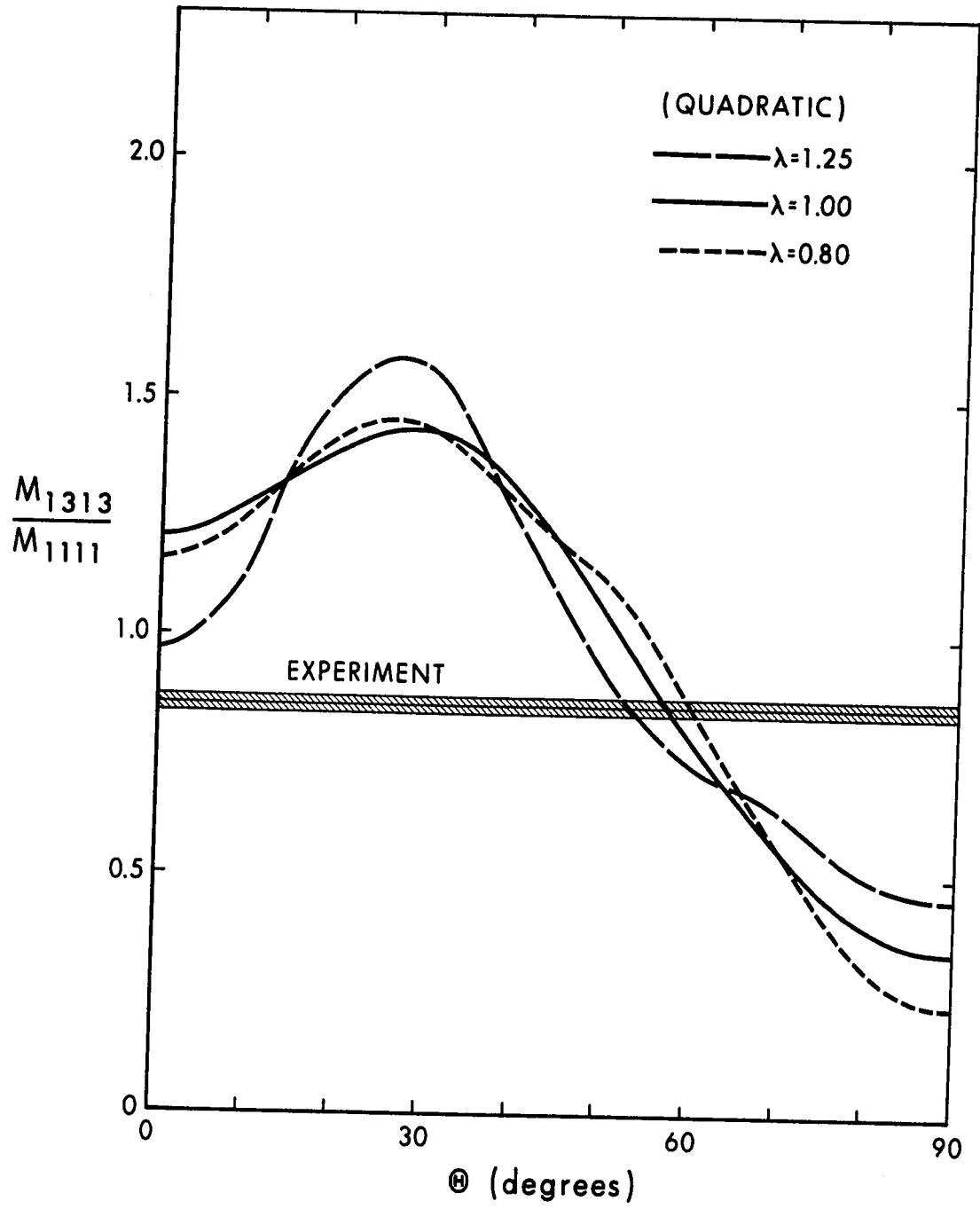
Caption IV q

Figure IV q shows the ratio M_{1113}/M_{1111} as a function of θ for the linear process and $\lambda = 0.80, 1.00$ and 1.25 . Also shown is our experimental value of $\frac{\sqrt{M_{1113}^2 + M_{1123}^2}}{M_{1111}}$ for the ^{23}Na in NaNO_3 . The shaded region indicates the limits of experimental error.



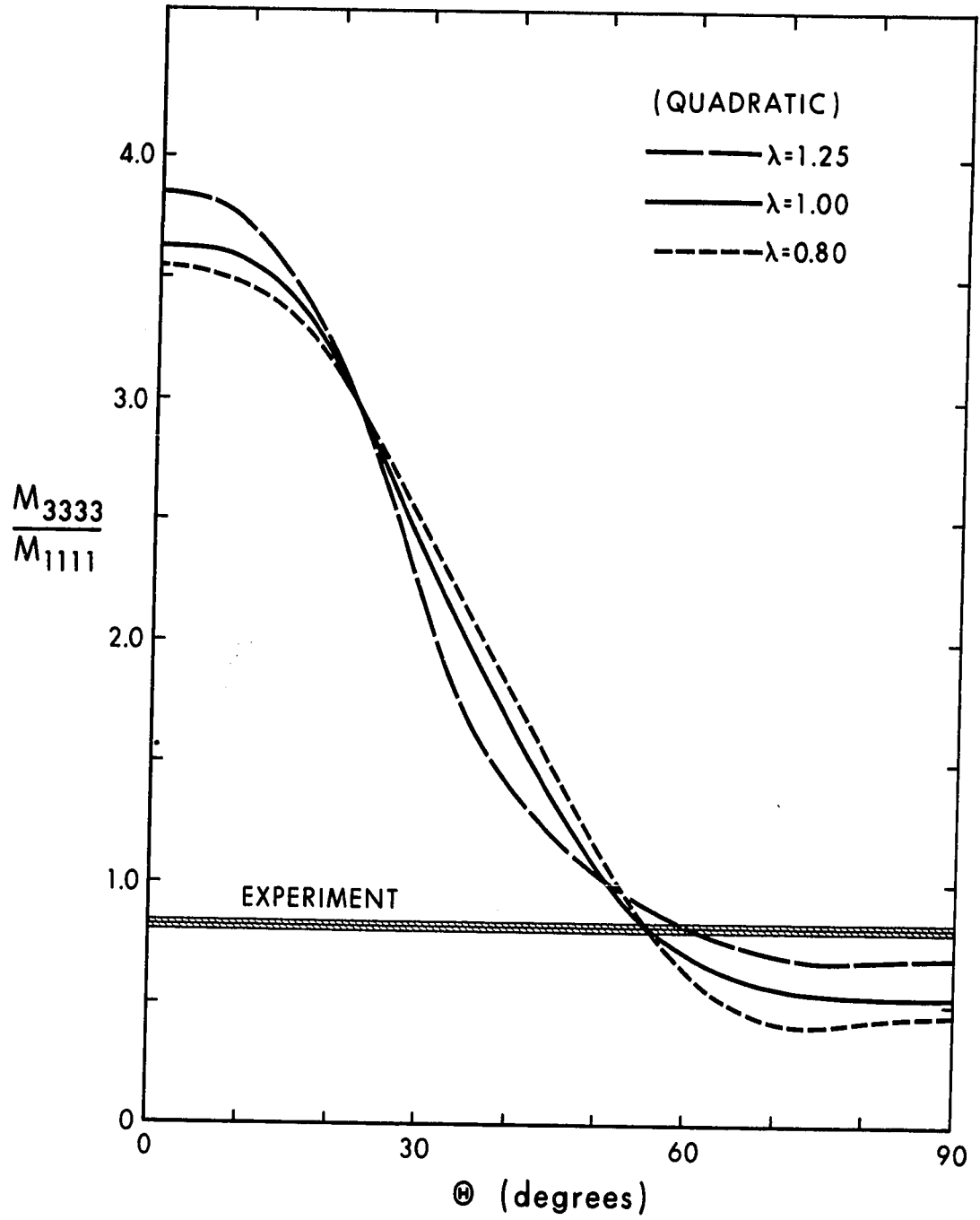
Caption IV r

Figure IV r shows the ratio M_{1313}/M_{1111} as a function of θ for the quadratic process and $\lambda = 0.80, 1.00$ and 1.25 . Also shown is our experimental value of M_{1313}/M_{1111} for ^{23}Na in NaNO_3 . The shaded region indicates the limits of experimental error.



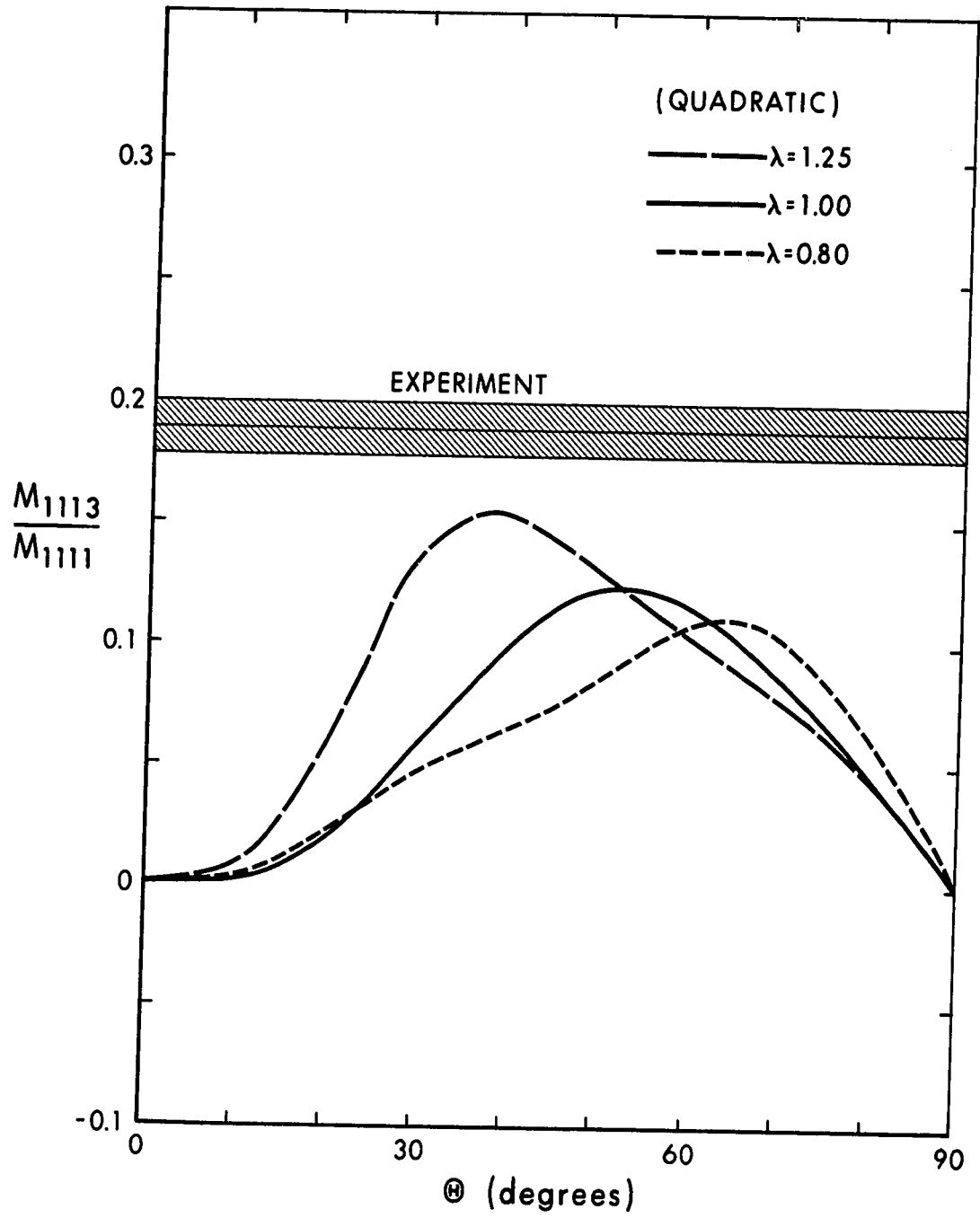
Caption IV s

Figure IV s shows the ratio of M_{3333}/M_{1111} as a function of θ for the quadratic process and $\lambda = 0.80, 1.00$ and 1.25 . Also shown is our experimental value of M_{3333}/M_{1111} for ^{23}Na in NaNO_3 . The shaded region indicates the limits of experimental error.



Caption IV t

Figure IV t shows the ratio M_{1113}/M_{1111} as a function of θ for the quadratic process and $\lambda = 0.80, 1.00$ and 1.25 . Also shown is our experimental value of $\sqrt{M_{1113}^2 + M_{1123}^2}/M_{1111}$ for ^{23}Na in NaNO_3 . The shaded region indicates the limits of the experimental error.



whether it is possible to distinguish between a linear and a quadratic process on the basis of our crystal measurements. Since the agreement between theory and experiment at 54° is considerably better in the linear than in the quadratic case, it is tempting to conclude that the relaxation mechanism is anharmonic. This conclusion must be tempered by the fact that the experimental behaviour of the ϕ -dependent term is quite clear in this case as to the validity of using the expression $M_{1113} = M'_{1113} \cos 3\phi_0$ with $\phi_0 = 18^\circ$, as in developing equations (IV 54) and (IV 59). If the $3\phi_0$ term is omitted then the agreement is better for the quadratic case than for the linear case.

It is interesting to compare our room temperature data results and Niemela's 77°K data in the light of the theoretical curves, especially those of M_{1313}/M_{1111} and M_{3333}/M_{1111} . Since it is known that thermal expansion of NaNO_3 is some ten times greater along the triadaxis than in a direction perpendicular to the triad axis (Saini and Mercier, 1934), the polar angle of the nearest neighbour oxygen atoms will decrease with increasing temperature. It follows from Figures IV o, IV p, IV r and IV s that according to our point charge calculation the values of M_{1313}/M_{1111} and M_{3333}/M_{1111} should increase with the results obtained by Niemela and ourselves. It therefore

appears that our point charge calculations are able to provide at least a semi-quantitative understanding of our data.

Finally, relatively small orientation dependence of W_2/W_1 in NaNO_3 at room temperature is perhaps not typical of the behaviour to be expected in all cases. For example, a ratio of M_{3333}/M_{1111} of near four is expected according to our simple calculation is a crystal where the nearest neighbours are located at θ close to zero. Such a ratio would imply a highly anisotropic behaviour of W_2/W_1 . An example of a case where this may be expected is sodium nitrite (NaNO_2). Indeed an investigation of the orientation dependence of the relaxation in this crystal would provide a check for the point charge model. It would thus appear in retrospect that NaNO_3 was an unfortunate choice of material for the study of the orientation dependence of W_2/W_1 because the relative dispositions of the nearest neighbour oxygen atoms around the sodium sites causes such a small anisotropy in W_2/W_1 .

References

- Abragam, A., 1961, *The Principles of Nuclear Magnetism*
(Oxford: Clarendon Press), 411.
- Abragam, A., Proctor, W. G., 1958, *Phys. Rev.*, 109, 1441.
- Andrew, E. R., 1955, *Nuclear Magnetic Resonance* (Cambridge
University Press)
- Andrew, E. R., Eades, R. G., Hennel, J. W., Hughes, D. G.,
1962, *Proc. Phys. Soc.*, 79, 954.
- Andrew, E. R., Swanson, K. M., 1957, *Proc. Phys. Soc.*, 70, 436
- Andrew, E. R., Swanson, K. M., 1960, *Proc. Phys. Soc.*, 75, 582.
- Bersohn, R., 1960, *J. Chem. Phys.*, 20, 1505.
- Bloch, F., 1946, *Phys. Rev.*, 70, 460.
- Bloembergen, N., Purcell, E. M., Pound, R. V., 1948, *Phys.*
Rev., 73, 679.
- Blume, R. J., 1962, *Rev. Sci. Inst.*, 33, 1472.
- Edmonds, A. R., 1957, *Angular Momentum in Quantum Mechanics*
(Princeton, New Jersey: Princeton University
Press)
- Goldburg, W. I., 1959, *Bull. Amer. Phys. Soc.*, 75, 337.
- Goldburg, W. I., 1961, *phys. Rev.*, 122, 831.
- Hahn, E. L., 1949, *Phys. Rev.*, 76, 145.
- Howling, D. H., 1966, *Rev. Sci. Inst.*, 36, 660.

- Hughes, D. G., 1966, Proc. Phys. Soc., 87, 953.
- Hughes, D. G., Reed, K., 1970, Rev. Sci. Inst., 41, 293
- Hughes, D. G., Reed, K., Snyder, R. E., 1970, Can. J. Phys., 48, 480.
- Kutsishvili, G. R., 1956, Publications of the Georgian Institute of Sciences IV, 1.
- Niemela, L., 1967, Ann. Acad. Sci. Fennicae A VI, No. 236.
- Pietila, A., 1968, Ann. Acad. Sci. Fennicae A. VI, No. 271.
- Pound, R. V., 1947, Phys. Rev., 72, 527.
- Pound, R. V., 1950, Phys. Rev., 79, 685.
- Pound, R. V., Knight, W. D., 1950, Rev. Sci. Inst., 21, 219.
- Redfield, A. G., 1955, Phys. Rev., 98, 1787.
- Robinson, F. N. H., 1959, J. Sci. Inst., 36, 481.
- Saini, H., Mercier, A., 1934, Helv. Phys. Acta., 7, 267.
- Schuster, N. A., 1951, Rev. Sci. Inst., 22, 254.
- Snyder, R. E., Hughes, D. G., 1970, J. Phys. C. (Solid St. Phys.), in press.
- Van Kranendonk, J., 1954, Physica., 20, 781.
- Van Kranendonk, J., Walker, M., 1967, Phys. Rev. Letters, 18, 707.
- Van Kranendonk, J., Walker, M., 1968, Can. J. Phys., 46, 2441.
- Watkins, G. D., Pound, R. V., 1951, Phys. Rev., 82, 343.

- Whittaker, E., Robinson, G., 1925, The Calculus of
Observations (Blackie and Sons Ltd.).
- Weber, M. J., Allen, R. R., 1962, Ampere colloquium, 168.
- Wikner, E. G., Blumberg, W. E., Hahn, E. L., 1960, Phys.
Rev., 118, 631.
- Yosida, K., Moriya, T., 1956, J. Phys. Soc. Japan, 11, 33.